Open Loop Stability & Control Screening of

High-Speed Slender Aircraft

by

Kevin Obrien

A Thesis Presented in Partial Fulfillment
of the Requirements for the Degree
Master of Science

Approved April 2023 by the
Graduate Supervisory Committee:

Timothy Takahashi, Chair
Werner Dahm
M. Christopher Cotting

ARIZONA STATE UNIVERSITY

May 2023

ABSTRACT

This thesis describes key Stability & Control parameters and a methodology to screening aircraft configurations for adequate handling qualities. For screening aircraft, a general-purpose Excel/ Visual Basic for Application (VBA) analysis tool was built. The analysis tool has built-in functionality to analyze aircraft utilizing a rudder for primary yaw control, collective horizontal tail for pitch, and either ailerons or differential horizontal tail for roll control. Additionally, the tool transforms aerodynamic coefficients from the moment reference point to various center of gravity locations while saving data in Stability Axis and Body Axis; it also implements pitch trim. Key stability parameters of interest are the Short Period and Dutch Roll Frequencies, Roll and Spiral time constants, *Cnβdynamic*, Lateral Control Departure Parameter (LCDP), as well as the stick-fixed Short Period and Dutch Roll Damping. Other areas of interest include pitch and lateral-directional trim as well as the implementation of an Aileron-Rudder Interconnect system. This thesis uses the tool to analyze two historical: 1) the Bell *X-2* and 2) the North American *X-15* and two theoretical: 3) the "*Sky Cruiser*" and 4) the generic High-Speed Slender Aircraft (*HSSA*), aircraft. This thesis identifies varying Stability & Control problems between these aircraft and allows one to explore potential solutions to remedy their inherent flaws.

ACKNOWLEDGEMENTS

This research was supported in part by an appointment to the Postgraduate Research Participation Program at the U.S. Air Force Institute of Technology, administered by the Oak Ridge Institute for Science and Education through an interagency agreement between the U.S. Department of Energy and AFIT.

I would like to thank Dr. Ramana Grandhi from the Air Force Institute of Technology for all of his support during this project and for hosting us at Wright-Patterson Air Force Base over the summer to conduct a majority of this research. I would also like to thank Dr. Jose Camberos from the Air Force Research Laboratory for his assistance with research on hypersonics.

TABLE OF CONTENTS

Page

Page

Page

LIST OF TABLES

Table Page

LIST OF FIGURES

Figure Page

Figure Page

Figure Page

Figure Page

Figure Page

LIST OF SYMBOLS AND NOMENCLATURE

a	=	local speed of sound,-ft/s
α	=	angle of attack, deg
b	=	span,-ft
β	=	sideslip angle
$\bar{c}$	=	reference chord (“Mean Geometric Chord”) length,-ft
C_L	=	coefficient of lift
C_l	=	rolling moment coefficient (CRM)
C_{lr}	=	rolling damping due to yaw rate
C_{lp}	=	rolling damping due to roll rate
C_m	=	pitching moment coefficient (CPM)
C_{mq}	=	pitch damping due to pitch rate
C_n	=	yawing moment coefficient (CYM)
C_{nr}	=	yaw damping due to yaw rate
C_{np}	=	yaw damping due to roll rate
C_Y	=	side force coefficient
$dC_l/dail$	=	rolling moment due to aileron
$dC_l/d\beta$	=	rolling moment due to sideslip (“Dihedral Effect”)
$dC_l/drud$	=	rolling moment due to rudder
$dC_n/dail$	=	yawing moment due to aileron
$dC_n/d\beta$	=	yawing moment due to sideslip
$dC_n/drud$	=	yawing moment due to rudder

$dC_y/d\beta$	=	side force due to sideslip
delev	=	elevator deflection,
I_{xx}	=	rolling moment of inertia, slug-ft^2
I_{yy}	=	pitching moment of inertia, slug-ft^2
I_{zz}	=	yawing moment of inertia, slug-ft^2
KEAS	=	knots equivalent airspeed, knots
KTAS	=	knots true airspeed, knots
LCDP	=	lateral control departure parameter
M	=	Mach Number
m	=	aircraft mass, lbm
n, nZ	=	load factor
p	=	roll rate, rad/s
φ/β	=	stick-fixed yaw to roll stability ratio
$\bar{q}$	=	dynamic pressure, lbf-ft^2
q	=	pitch rate, rad/s
r	=	yaw rate, rad/s
S_{ref}	=	reference area,-ft^2
τ_r	=	Roll Mode Time Constant
τ_s	=	Spiral Mode Time Constant
ω_{SP}	=	Short Period frequency,-Hz.
ω_{DR}	=	Dutch Roll frequency,-Hz.
ζ_{SP}	=	Short Period damping
ζ_{DR}	=	Dutch Roll damping

INTRODUCTION

Abzug[1], in his book *Airplane Stability & Control*, recollects that "Professor Otto Koppen would restore perspective by saying, 'remember, airplanes are not built to demonstrate Stability & Control, but to carry things from one place to another.' Perhaps Koppen went too far, because history has shown over and over again that neglect of Stability & Control fundamentals has brought otherwise excellent aircraft projects down, sometimes literally."

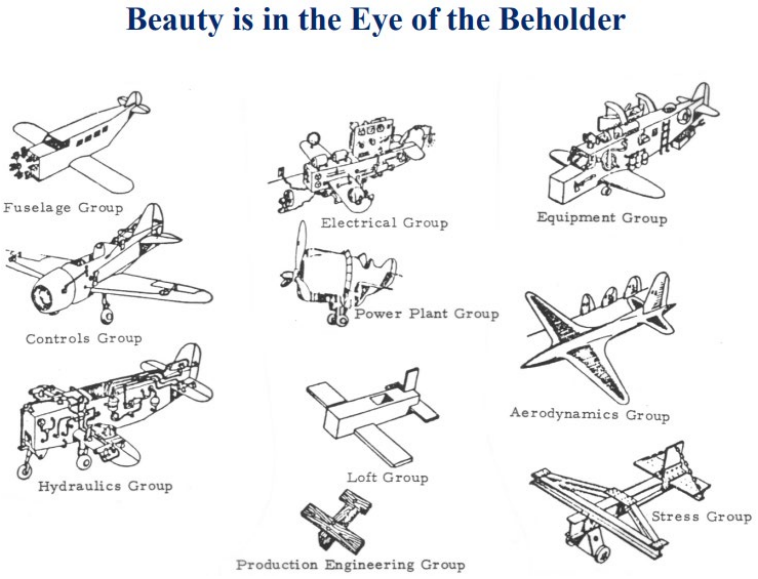

FIGURE 1: Cartoon of Dream Airplanes if each design group had full control.[1]

When designing an aircraft, many specialized design groups must be involved, from aerodynamics, structures, payloads, mass properties, stability & control, etc. Often on a project, some of these groups will not have enough influence on the design, which results in an overall subpar design. An extreme example of these ideal airplanes where a single team dominates the design is shown in FIGURE 1. [2] One key aspect of an aircraft's design is its inherent Stability & Controllability, which if left neglected can make or break an

aircraft. The goal of this thesis is to explore methods for early design screening to get a sense of how stable the aircraft will be and ways to potentially fix any glaring issues.

Stability & Control experts focus upon three main questions: 1) is the aircraft trimmable and maneuverable through a range of speeds, altitudes and load factors? 2) does the aircraft exhibit adequate response frequencies for controllability? and 3) in the case of piloted aircraft, are the handling qualities at appropriate levels to not induce excessive workload?

For an aircraft to be trimmable, it must have sufficient control power to obtain the desired pitch, roll, yaw or combination for steady level flight as well as any maneuvers (i.e. flight where $Lift \neq Weight$) from that point. To determine if an aircraft can trim in pitch, the pitch control surfaces must have enough power to maneuver to all desired angles of attack. The roll and yaw control surfaces or effectors must be sufficient to allow for good turn coordination and achieving desired bank angles without any serious adverse effects leading to departure from stable flight.

Additionally, every aircraft has rigid-body frequencies at which it responds to inputs in the control surfaces. For an aircraft to be controllable, these frequencies must be fast enough to avoid phase lag while not too fast to cause coupling with the structural natural frequencies. These frequencies are especially important with a human pilot, as phase lag can result in such delayed responses from the aircraft that the pilot themselves will induce oscillations from excessive maneuvering, resulting in the aircraft departing from stable flight.

With the goals of stability & control in mind, we can shift our focus to the specifics. The first topic to be discussed are the key screening parameters that can be used to evaluate

the preliminary stability of an aircraft. This thesis aims to incorporate much of the prior "art" and advances in stability and control through these screening parameters into a methodology for early conceptual design. Utilizing the following screening parameters, a historical and methodical approach is shown on how to address open loop stability and ways to improve certain aspects to appropriate levels for detailed design moving forward. Additionally, all the screening parameters will be examined in the context of the flight envelope, to characterize where stability and performance are good or concerning i.e., where these aircraft can realistically fly. The goal of this thesis is to provide both some historical lessons and remembrance of these screening parameters back into modern literature to aid in early aircraft design.

KEY SCREENING PARAMETERS OF INTEREST

To screen for aircraft stability, there are a variety of parameters of interest. These parameters are split into two categories, static and dynamic. The static or "stick-fixed" stability, deals with the inherent stability of an aircraft and characterizes how it responds to small disturbances. For a stable aircraft, the inherent stability should be enough to return the aircraft to its original state without any pilot input required. Dynamic stability characterizes tendencies to oscillate in response to control inputs and larger disturbances. These dynamic characteristics often deal with frequencies, damping ratios, and time constants.

Basic Stick-fixed Stability

The following key plots are the first to be constructed for any design, if the configuration of the aircraft is unstable in any of these modes, one must consider the need

for either a configuration change or an active control system to suppress any unwanted motion.

Lift-Curve Slope: The lift-curve slope is one of the key figures due to the visualization of how lift varies with angle of attack. An example lift curve slope is shown in FIGURE 2, this figure corresponds to the Bell *X-2* VORLAX model [3] that will be discussed in the following sections.

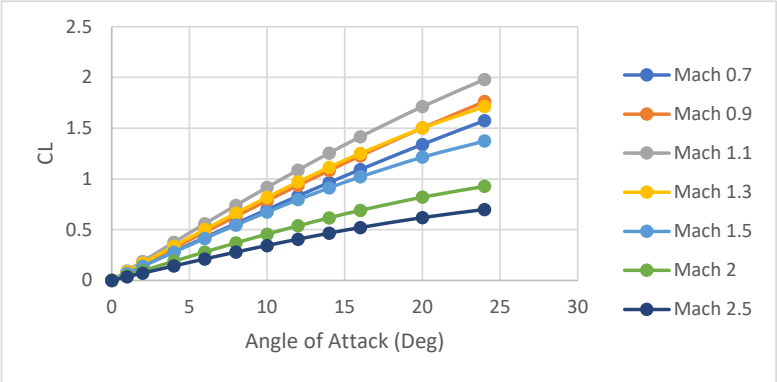

FIGURE 2: Lift Coefficient vs Angle of Attack (X-2)

For supersonic flight one key trend to notice is the shallowing of the lift curve slope. As the Mach Number increases to supersonic and the hypersonic the amount of lift the vehicle can produce drastically decreases. This is due to the upper surface losing effectiveness as the magnitude of *Cp* trends toward zero when the critical Mach Number is passed thus, the windward side (lower surface) is generating most of the lift.

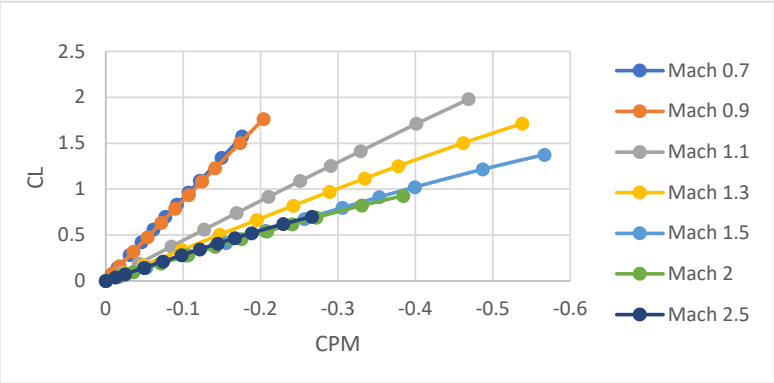

FIGURE 3: Lift Coefficient vs Pitching Moment (X-2)

Pitch Stability: To determine if an aircraft is statically stable in pitch, a lift coefficient vs pitching moment plot can be constructed. If the slope of the curve is positive, then the aircraft is determined to have positive static pitch stability. An example of this plot is shown in FIGURE 3 using data for the *X-2* model [3]. One of the key factors affecting pitch stability is the center of gravity and aerodynamic center of the vehicle. To show the relationship between the center of gravity and aerodynamic center an additional parameter called the Static Margin should be calculated.

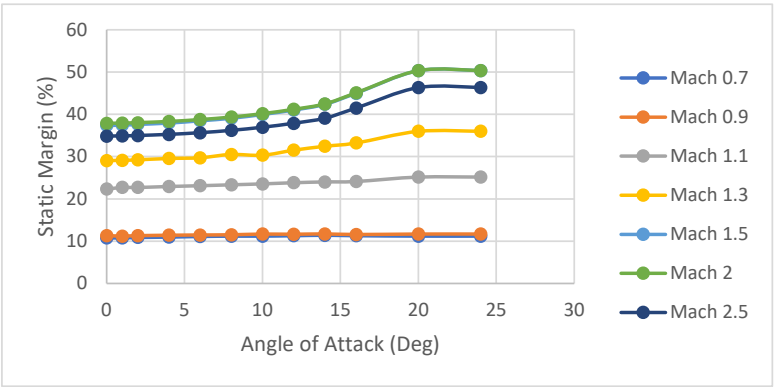

FIGURE 4: Static Margin vs Angle of Attack (X-2)

The Static Margin considers the physical distance between the center-of-gravity and a point where the pitching moment does not change as the lift coefficient increases, the aerodynamic center. This parameter gives a percentage of the mean aerodynamic chord

that the center of gravity can move and remain stable in pitch. One thing to keep in mind about this parameter is that it is implicitly dependent on the aerodynamic center, which can vary. When the aircraft goes supersonic the aerodynamic center moves from the quarter chord of the wing to the half chord resulting in a large increase in Static Margin. This is shown in FIGURE 4 for the *X-2,* where in subsonic flight the Static Margin is reasonable, around 10%, but as the aerodynamic surfaces develop supersonic leading edges, it increases to 30-40%. For high supersonic and hypersonic aircraft, another shift in the aerodynamic center will likely occur due to the body of the vehicle developing supersonic leading edges; this will push the aerodynamic center even further aft due to the combination of body and wing effects.

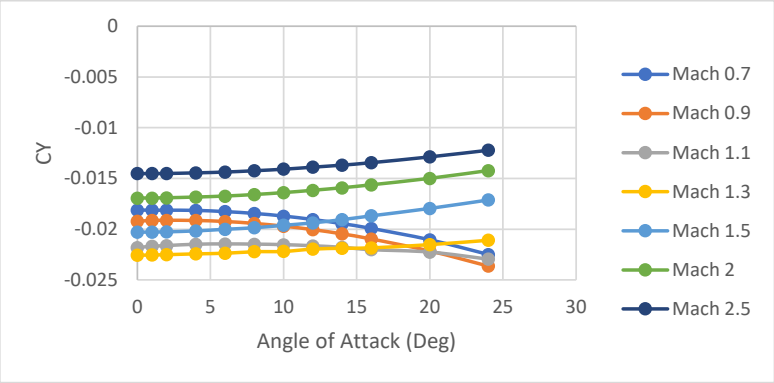

FIGURE 5: Side Force per Degree Sideslip vs Angle of Attack (X-2)

Side Force: The Side Force plot shows how much restoring force an aircraft will have when introduced to sideslip. Sideslip occurs when the aircraft is flying angled with respect to the wind. This is easily visualized when watching crosswind landings, where the aircraft appears to be “crabbed” until touchdown. An example of the side force plot is shown in FIGURE 5. Some key observable trends are that subsonic Mach curves should all trend toward a more negative side force coefficient resulting in a greater restoring force.

The supersonic Mach curves all trend toward a more positive side force coefficient resulting in less desire to trend back to the neutral point. This plot begins to foreshadow some of the lateral-directional issues that arise with high-speed slender aircraft.

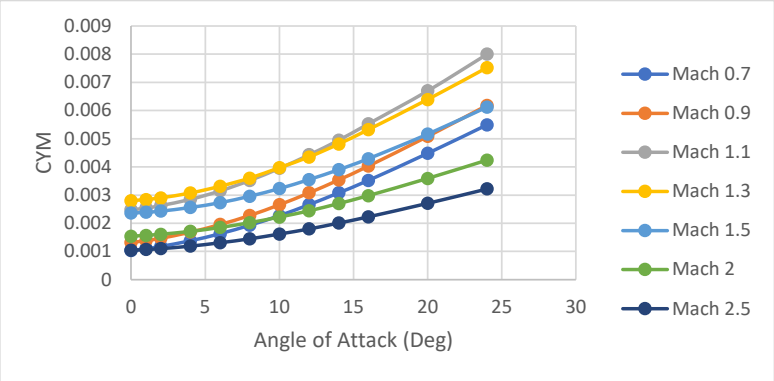

FIGURE 6: Yawing Moment per Degree Sideslip vs Angle of Attack (X-2)

Yawing Moment: To determine if an aircraft is statically stable in yaw, the yawing moment curve slope should be positive as well as all moment coefficients positive. If these two criteria are met, it indicates that the aircraft has strong static stability in yaw. FIGURE 6, shows an example of the yawing moment plot for the *X-2*. If the yawing moment coefficients are negative but the slope is positive, it indicates that the aircraft is inherently unstable in yaw.

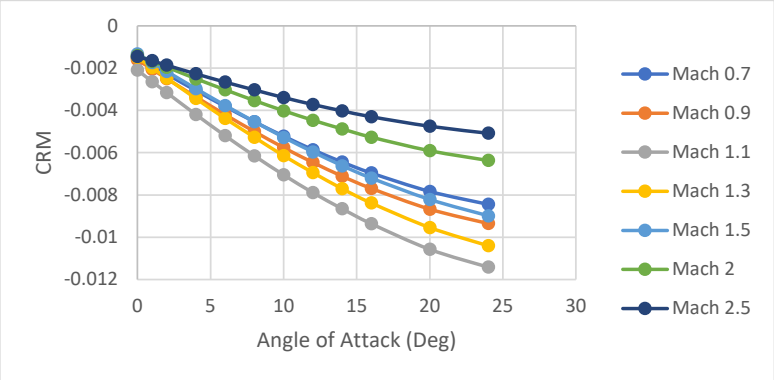

FIGURE 7: Rolling Moment per Degree Sideslip vs Angle of Attack (X-2)

Rolling Moment: If the rolling moment due to sideslip curve slope is negative, it indicates that the aircraft is statically stable in roll. The stability in roll is due to the aircraft exhibiting positive "aerodynamic dihedral." Even though aircraft have no inherent pendulum stability, positive aerodynamic dihedral promotes roll stability by enforcing a stable damped oscillation (the Dutch Roll mode discussed later) where when the aircraft rolls and yaws to the right, the inherent aerodynamics counter by rolling and yawing it back to the left and vice-versa. An example of the rolling moment plot is shown in FIGURE 7 for the *X-2*. As a vehicle increases in Mach and angle of attack the aerodynamic dihedral effect is typically reduced.

Open Loop vs Closed Loop Aircraft Design

To design an open loop aircraft, it must demonstrate inherent stability in all three axes (pitch, yaw, and roll) as discussed in Part A. In open loop systems, the pilot must manually respond to all disturbances and adjust control inputs to meet their desired flight targets. Typically, open loop aircraft have strong static stability which comes with the potential tradeoff of decreased maneuverability. If an aircraft has too much static stability, it may develop trim limits that restrict its ability to command angle-of-attack or sideslip-angle. For general aviation aircraft, good open loop stability is required to maintain ease of operation and safety. A design with "too much stability" will have trim limits that lead to problems with crosswind takeoff and landing.

For high performance aircraft, a closed loop stability augmentation system can be implemented to have both desirable "synthetic stability" along with maneuverability. A closed loop system allows for onboard computers to be utilized to assist the pilot by

automatically deflecting control surfaces to hold desired flight targets. A common example of a closed loop control system is the autopilot system on all commercial aircraft.

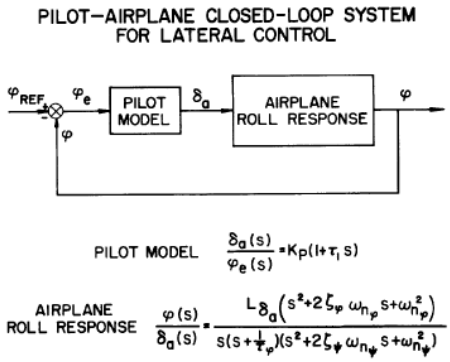

FIGURE 8: *X-15* Closed Loop System for Lateral Control [4]

With a closed loop system, open-loop stick-fixed pitch, yaw, or roll instabilities can be "programmed" away by the automatic fly-by-wire system. For many high-performance aircraft, static instability is intentionally included within the design to increase maneuverability or meet certain performance goals. To compensate for any static instability, the fly-by-wire system automatically applies control inputs to develop "synthetic stability" in the eyes of the pilot.[5] This system, typically consisting of multiple feedback control loops, first measures the aircraft motion and then applies control deflections to oppose any undesired motion. FIGURE 8 shows an example of the transfer function/control laws for the *X-15*'s closed loop feedback control system for lateral control.[4]

These fly-by-wire systems give designers extra room for tradeoffs when balancing the airframe's performance and handling qualities for the pilot. Yechout[5] gives one example of the horizontal tail size being minimized to increase the drag performance of the aircraft. This decreased tail size results in a slower stick-fixed Short Period frequency and

thus poorer open-loop handling characteristics. A feedback control system can negate these deficiencies in handling characteristics and thus reduce drag with minimal changes to other handling qualities.[5]

If the open loop stability is fundamentally unstable, there is a limitation to how much a control system can account for. The open loop stability is ultimately the deciding factor in how well a closed loop system can operate due to two primary factors: limitations in physical control surface deflections and the bandwidth of the system.

First, in order to synthesize stability parameters, there still needs to be a physical change in the system (e.g., moving a control surface). To synthesize pitch damping or modifying the Short Period Frequency for example, either elevators or some other pitch-control body flaps must be wiggled. Depending on how much a particular parameter (e.g., Cmq or $dCm/d\alpha$) needs to be synthesized, the deflections required and speed at which they are moved could become excessive. With a closed loop system, the control surface deflection budget will need to be created to accommodate three conditions; obtain trimmed flight at all flight envelope conditions, have sufficient margin for maneuverability performance targets i.e., achieving specific roll/yaw rates or angle of attack/sideslip changes, and then excess margin for the closed loop control system to wiggle. On a typical aircraft, one would expect no more than 30 degrees of deflection of any given control surface so this would become a hard limit for these three competing uses of control power. The sizing of a control surface will be highly dominated by trim requirement to ensure there is enough control power left for maneuvering and synthesis.

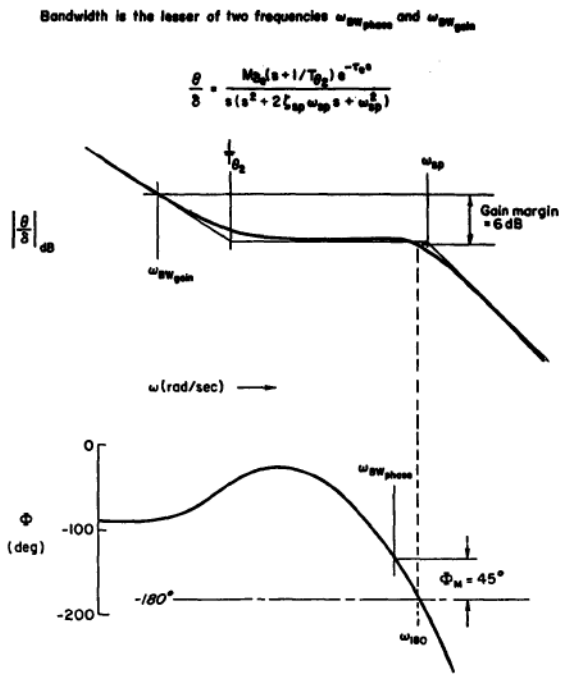

FIGURE 9: Definition of Bandwidth Frequency [6][7]

The other limitation is the Bandwidth Criterion which describes the frequency and phase response "transfer function" between control inputs and the actual physical response of the aircraft. Every system is going to have some level of lag in phase angle and over/under shoot in the response to an input. The bandwidth for the closed loop system outlines the maximum frequency at which the tracking of a particular parameter in the system can occur. For aircraft with poor or low bandwidth, the pilot will experience unwanted oscillation if rapidly correcting tracking errors due to high frequency inputs with sluggish responses from the aircraft.[6]

The Bandwidth Criterion outlines a set of criteria that limits the phase margin or gain margin of an aircraft from its neutral stability point. It states that to find the bandwidth frequency one should first determine the neutral point frequency from the 180-degree phase point on the Bode plot, shown in FIGURE 9. At this 180-degree phase point, the gain frequency is obtained by adding 6 dB. At the original magnitude the frequency at the 45-

degree phase on the plot is taken as the phase frequency. The bandwidth frequency is obtained from whichever is the smaller frequency, phase, or gain.[6] This bandwidth frequency gives the maximum frequency at which tracking can occur to maintain good handing qualities and maintain stability.

If the open loop stability is not strong enough, then the closed loop control may be strained to the point of inducing pilot induced oscillations (PIO) during rapid tracking or similar situations. MIL-STD 1797A states that "pilot-induced oscillation is sustained or uncontrollable oscillation resulting from efforts of the pilot to control the aircraft." [8] PIO typically occurs when the phase lag between the piloted inputs and system response reaches excessive phase angles and gains, resulting in the commanded maneuvering being opposite to what was intended. PIO typically occurs in areas of flight where fast transitions in vehicle dynamics occur. Examples of these transition triggers are afterburner light-off, engine unstarts, control system mode changes, strong turbulence, switching from aerodynamic control to reaction motor control, and unsymmetric stores/payload releases. [9] Additionally, if too much stability augmentation is added to achieve desired flight characteristics it can also lead to PIO problems, as seen during the development of modern aircraft like the C-17 transport, B-2 bomber, and YF-22 fighter. These aircraft suffered from "Category III – Essentially Nonlinear Pilot-Vehicle System Oscillation with Transitions", which stem from shifts in the dynamics due to the magnitude of pilot's output or internal changes in the control system and aerodynamic/propulsion configuration.[9]

The C-17 had issues with pilot induced oscillation during landing, especially crosswind, and aerial refueling. One of the main culprits of the PIO was due to the actuators not being changed during the modernization of the aircraft from a mechanical control

system to a new fly-by-wire system. The bandwidth and rates of the original actuators remained unchanged during the upgrade, resulting in the closed loop Bandwidth Criterion requirements not being met. This resulted in poor performance and the threat of PIO during high demand tasks like short-takeoff operations, aerial refueling, and low altitude operations. [10] Screening for PIO becomes a necessary step in the assurance that a closed loop system will function properly for a given aircraft.

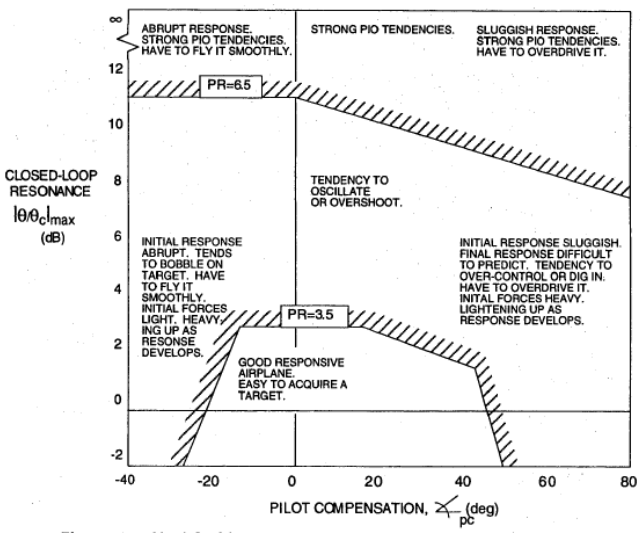

FIGURE 10: Neal-Smith Parameter Plane/Typical Pilot Comments[11]

To screen for PIO, the Neal-Smith criterion can be used to evaluate the phase compensation and resonance to determine how magnitude gains and phase lag will implicate the likelihood of PIO. [11] To help ensure that PIO risk is minimized, it is common practice to ensure that the closed loop system can perform at least one magnitude higher than what is commanded. For example, if the system needs to track at 2 Hz, then the control system and actuators should be able to drive at 20 Hz.

With some of the key ideas involved with a closed loop control system discussed, it should be noted that while closed loop systems can solve a lot of problems, they are still

limited by the open loop performance. The worse the open loop the performance is, the more work has to be done on the backend to meet the required performance goals and maintain stability. If a specific parameter needs to be modified, for example the Short Period being modified from 2 rad/s to 8 rad/s, the control system will become the dominant aspect of the airplanes' design rather than its unique geometric sizing and shape. With this in mind, it is important to remember that software can only mask so much as the aircraft must still demonstrate stick-fixed performance.

With potential solutions of closed loop control systems acknowledged, much of this thesis will focus on the design choices for adequate open loop stability. Implementation of simple open loop control laws such as aileron-rudder interconnect gains will be discussed. The design of complex closed loop control laws is not within the scope of this thesis, and thus analysis utilizing those methods will not be addressed. It is acknowledged that in many cases, the implementation of closed loop control laws will be required for high performance and high-speed slender vehicles due to poor lateral-directional stability. The design of these fly-by-wire controllers depends greatly on the detailed properties of actuators, mass properties, and computer hardware limitations all of which are difficult to pin down during initial sizing considerations.

The methodology and strategies discussed within this thesis focus upon the "Open-Loop" performance of candidate aircraft. The classic "open-loop" criteria found in MIL 8785C provides insight to the bandwidth requirements of real world aircraft. The difference between the "open-loop" performance of the aircraft and the desired closed loop bandwidth is a metric of how hard the closed-loop control system must work. The more augmentation needed; the more control power and actuator rates will be needed.

Longitudinal Short Period Frequency

The Longitudinal Short Period Frequency is a key characteristic of how the aircraft behaves or "feels" in the longitudinal direction. The Short Period is characterized as having a rocking up and down motion in the longitudinal plane like a boat bobbing over waves. As this frequency becomes faster the aircraft becomes more responsive to changes in pitch due to the pilot's control inputs.

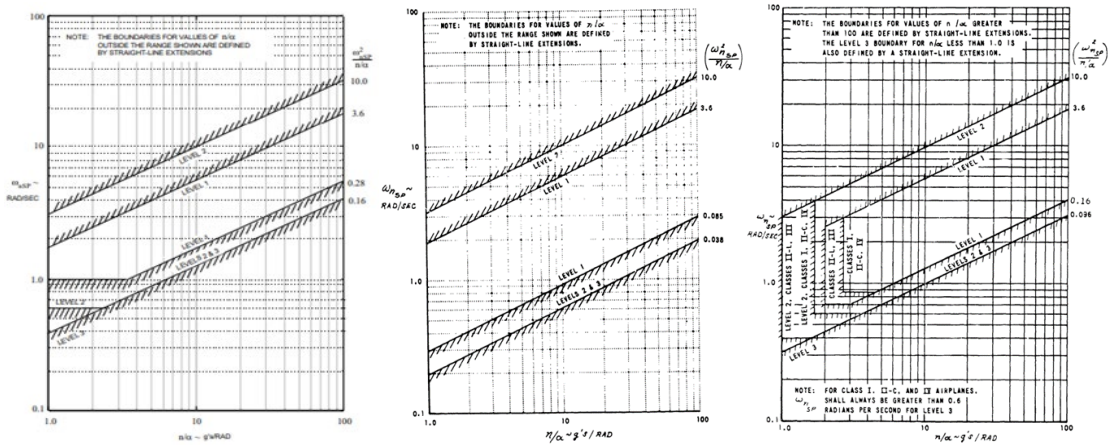

FIGURE 11: MIL STD 8785C Category A (left), B (middle), C (right) charts[12]

To help characterize the Short Period Frequency, the Military Standard (MIL STD) 8785C gives a variety of suggestions for what Short Period Frequency and pitch responsiveness should be. These suggestions are a great starting place for preliminary sizing and handling qualities. An example of handling characteristic levels defined by the MIL STD 8785C "Control Anticipation Parameter" chart is shown in FIGURE 11.[12] The suggestions in this standard are not necessarily a cookbook, but provide a reasonable starting place to ensure good handling qualities. More details on the MIL STD 8785C charts are given in the Mathematical Basis section of the paper.

Cnβdynamic

Cnβdynamic, also referred to as the control parameter, was discovered to have a key impact on the lateral-directional stability of an aircraft. It is a function of altitude, angle of attack, and Mach Number varying greatly as shown in FIGURE 12 for the *X-2*. This parameter is a root in the Dutch Roll Frequency discussed in the following section, and thus cannot be negative or it will lead to the aircraft being lateral-directional unstable. Additionally, with *Cnβdynamic's* role as a root, when it is close to zero poor lateral directional stability can occur, and thus many minimum thresholds have been proposed.

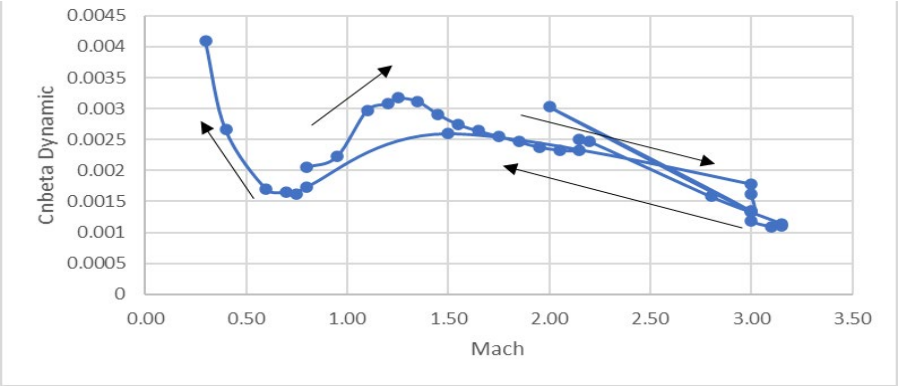

FIGURE 12: *Cnβdynamic* vs Mach Number for Replicated X-2 Flight

When looking back at lateral directional stability, Takahashi, Griffin & Grandhi [13] propose an updated version of the Weissman chart, shown in FIGURE 13 on pg. 17. The bounds on Weissman's original chart were heavily based on the few aircraft studied at the time. This results in some of the region bounds being questionable. A new A-Region bound on *Cnβdynamic* was proposed by Skow and Titiriga [14] shifting the minimal acceptable *Cnβdynamic* bound to: $Cn\beta dynamic > 0.004$. They believe the new bound seems to greatly improve confidence in the handling qualities of aircraft, as some aircraft that boarder the "A"→ "F" region are either okay or completely depart. With the "A" region

moved over, it can be ensured that the aircraft is much more departure resistant. More details on the regions are discussed in the Mathematical Basis section.

Lateral Control Departure Parameter (*LCDP*)

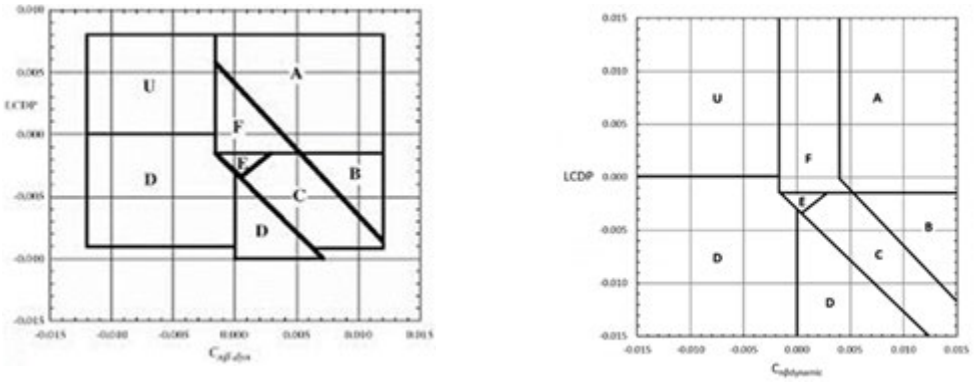

a b

FIGURE 13: Bihrle-Weissman Charts. A) After Mason [15] B) After Takahashi, Griffin & Grandhi [13]

As a long-term fall out of the Bell *X-2* crash and other early highspeed experimental aircraft, engineers developed a number of screening parameters for lateral/directional handling qualities. Day [16] recounts that "Hubert Drake, NACA HSFS Director of Research, … suggested that the probable cause for the slow divergence was adverse aileron producing adverse yaw such that the effective dihedral (roll due to yaw) was balancing or even opposing rolling moment." Over the years it began to be widely realized that the onset of control coupling could be predicted using an analytical formula. *LCDP* is the lateral control departure parameter that measures the extent of coupling between the roll and yaw effects of the ailerons and the inherent lateral and directional stability of an airframe. This parameter can be used to test the effects of the aircraft's primary roll control effectors, whether they are ailerons or differential tail control called elevons. Again, this parameter is highly dependent on angle of attack and speed, thus it must be tested for all areas within

a given flight envelope. *LCDP* and *Cnβdynamic* can be plotted together on the Bihrle-Weissman Chart as discussed previously.

Dutch Roll Frequency

The Dutch Roll Frequency is the most important lateral-directional frequency. This characteristic frequency determines how the aircraft will oscillate in roll and yaw. Depending on the natural rolling and yawing moments, the oscillation of the aircraft will present itself differently. To characterize the motion, the phi-to-beta ratio can be used as shown in Eq 1.

$$\frac{\varphi}{\beta_{airframe}} = \left| \frac{\frac{dCl}{d\beta_{airframe}}}{\frac{dCn}{d\beta_{airframe}}} \left(\frac{I_{zz}}{I_{xx}}\right) \right| \tag{1}$$

If this ratio is much greater than one, the wings will remain level and the tail will swish back and forth. If the ratio is much less than one, the aircraft will have a rocking motion in roll. When the ratio is close to one, the Dutch Roll expresses itself as a combination of the rocking and swishing motions.

Damping

As aircraft begin to fly faster another area of concern now is the damping of key rigid body frequencies. As an aircraft's speed approaches the high supersonic and especially hypersonic speeds, the damping of the Short Period and Dutch Roll modes begin to fall off to zero.[5] This is a major concern, as without damping, these oscillatory modes will begin to have a strenuous effect on the pilot as constant control will be required. If the

Short Period and Dutch Roll modes are not damped enough, it can lead to departure from stable flight. This will result in the eventual need for synthetic damping from either active aerodynamic controls or from some direct acting vectored propulsion system.

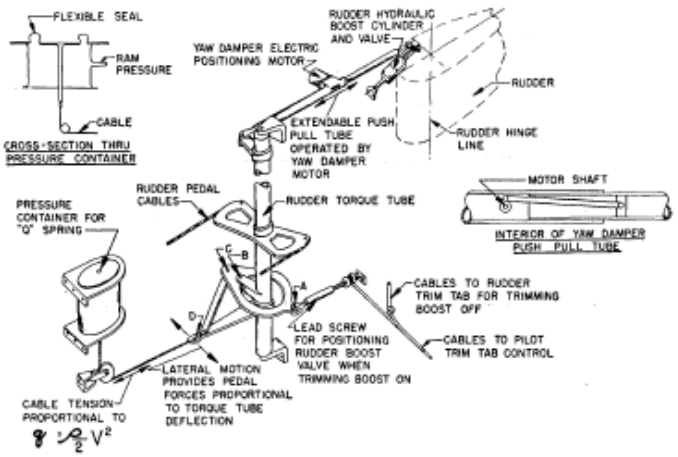

FIGURE 14: Example of a Yaw Damper on XB-47 [17]

To increase damping, control surfaces can be wiggled to synthesize and recover some damping. Throughout the years many different types of devices have been developed for creating damping, such as spring systems, bob weights, aerodynamic vanes, and servomechanical systems. A yaw damper, such as shown in FIGURE 14, can increase the Dutch Roll Damping ratio to levels where the aircrafts' tendency to have poor Dutch Roll motion can be removed.[17] This type of damper system can be utilized in pitch and roll as well with the effect of trying to suppress destabilizing oscillations.

As previously mentioned, the effectiveness of these damper systems is heavily dependent on how much control surface deflection can be budgeted for synthesis as well as how fast the surfaces can track. Depending on the aircraft configuration, the implementation of these damping systems can be difficult due to aerodynamic heating, electrical heating, mass properties, size of actuators, and size of control surfaces. Being

able to find control solutions for these high-speed slender vehicles will be essential as purely open loop performance will likely never suffice.

Inertial and Spiral-Roll Coupling

During and shortly after World War II, the speed and shape of aircraft began to rapidly change. A key example of the transformation of aircraft planforms can be seen in wing geometries, from rectangular to slightly swept, and now further to complete delta designs. This led to significant changes in the geometry and mass properties of these aircraft. The changes in shape of the aircraft and high-speed flight resulted in new undesirable stability characteristics.

These interesting mass properties eventually led to the discovery of Inertia Coupling. Inertia Coupling is a phenomenon where a disturbance in one axis of the aircraft is also felt about another. This problem began to appear in multiple of the early experimental high-speed aircraft and thus became an area of high interest, resulting in many later X-planes studying this phenomenon such as the *X-3* and *X-15*. Inertial coupling occurs once the aircraft reaches a critical frequency; the Dutch Roll motions can "crosstalk" into the Short Period pitching mode.[3] At this point, resonance occurs, and the aircraft is subjected to uncontrollable motion about all its axes.[16] Similarly, when coupling of the Roll and Spiral Modes occurs it is referred to as Lateral Phugoid coupling.

One suggested way to screen for inertial coupling is by looking at the principal mass moments of inertia. The Primary Coupling Ratio given by Equation 2 can suggest the tendency for the aircraft to experience Inertia Coupling.[16]

$$\frac{I_{xx} - I_{yy}}{I_{zz}} \tag{2}$$

As this ratio becomes more negative and approaches -1, it suggests that there is a higher tendency for the aircraft to experience Inertia Coupling. Day[16] reports some numerical values for inertial coupling prone aircraft which have been summarized in TABLE 1. It is noted that for typical passenger aircraft, this parameter is closer to zero and/or positive as I_{xx} is typically close to or larger than I_{yy}.

Table 1: Primary Coupling Ratios [16]

Aircraft	Primary Coupling Ratio
X-15	-0.94
X-3	-0.88
Space Shuttle	-0.84
YF-102	-0.81
F-100A	-0.71
X-2	-0.70

Adverse Yaw

When the ailerons are deflected, adverse yaw occurs due to differences in drag resulting in a yawing moment. This yawing moment may help self-coordinate a turn, which is called proverse yaw. If the induced yawing moment is destabilizing, however, it is called adverse yaw. Pilots (or autopilots) must correct significant adverse yaw, since if uncorrected the adverse yaw drives the vehicle to substantial sideslip angles. The lateral-directional stability of most aircraft declines precipitously beyond a critical sideslip angle, where the vertical tail begins to stall.

FIGURE 15 illustrates how excessive adverse yaw led to the *X-2* simultaneously experiencing both a lateral-directional and longitudinal departure.[18] The adverse yaw of

the *X-2* was sufficient that a sharp roll command at high-speeds led to formation of a high-sideslip angle. That high-sideslip angle, interacting with the static dihedral effect of the airframe ($dCl/d\beta << 0$) caused a lagging opposite rolling motion. Through Inertia Coupling, the energy in this nascent oscillation also cross-coupled into pitch disturbances.

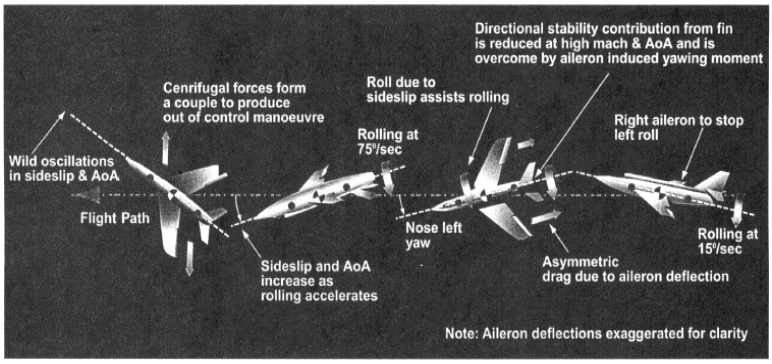

FIGURE 15: Inertia Coupling / Adverse Yaw Coupling of Bell *X-2* [18]

ADDRESSING ADVERSE YAW USING AN ARI

With the discussion of problems that can result from adverse yaw, engineers must try and find ways to limit or balance the produced adverse yaw. To limit adverse yaw engineers can use either simple or complex control blending schemes. An example of this blending may occur with noncollective aileron deflections (i.e., one aileron deflects up more than the other deflects down) as well as through coordinated rudder inputs. Very complex generalized blending schemes, where every movable surface is independently scheduled, is beyond the focus of this master's project. Note many conventional aircraft have five primary aerodynamic control surfaces: an aileron on each wing, an elevator panel on each horizontal tail fin and a single panel rudder. More complex aircraft may have twin verticals and all moving tailerons (e.g. F-18) as well as spoilerons and inboard/outboard ailerons (e.g. B-767). This results in the possibility of many alternative complex coupled

control surface schemes. However, it is felt that a good aircraft design should not have to rely on extremely complex control systems to fly, but rather should rely on their own inherent stability with slight augmentation.

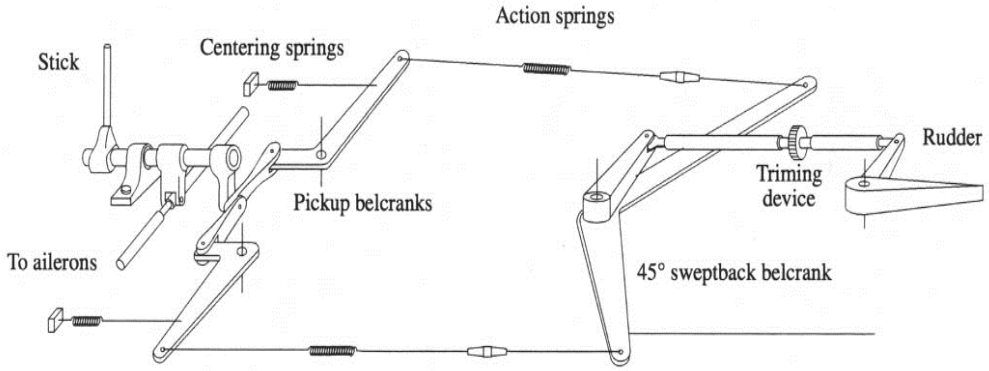

FIGURE 16: Mechanical Aileron Rudder Interconnect System as Found on a Fairchild PT-19 [19]

With this in mind the effects of a simple aileron-rudder interconnect (ARI) system will be considered. An *ARI* will treat the "aileron" as antisymmetric collective deflection of the wing mounted surfaces and the "rudder" as a deflection of the hinged surface on the vertical tail. FIGURE 16 shows an example for the mechanical ARI setup for the Fairchild PT-19.[19] The goal of the *ARI* is to utilize the primary yaw controller, here the physical rudder, to trim the induced yawing moment to zero. Additionally, an *ARI* can be used with differential horizontal tail control and the rudder, which is more common on high-speed slender vehicles. With modern computers and actuators, the *ARI* gains can be scheduled based on angle of attack and Mach number to ensure adverse yaw is minimized at all conditions.

MATHEMATICAL BASIS FOR SCREENING STABILITY & CONTROL

As discussed previously, the stability of an aircraft varies with the center of gravity position. The aerodynamic coefficients obtained for a specific moment reference point must first be moved to the appropriate center of gravity location. The need to be able to move these aerodynamic coefficients becomes crucial once further along in development, as CFD and Wind Tunnel testing will be the primary source for data replacing panel methods. CFD and Wind Tunnel testing are both expensive and time consuming thus moving the moment reference point around on each configuration is not feasible.

For all these various data collection methods, a single reference point must be used to ensure that all the data transformations are correct. To shift the aerodynamic coefficients from the moment reference point to a new *CG* location, the principals covered in statics can be used to apply moment transfers. To ensure that the moment transfers are done correctly, the free body diagrams of the force and moments on an aircraft need to be defined.

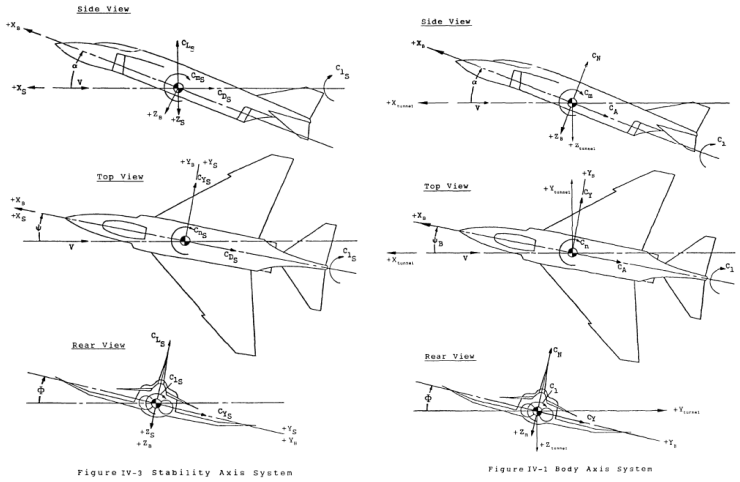

FIGURE 17: Aircraft Coordinate Systems: Stability (left), Body (right) [20]

For computing Stability & Control, two key axis systems are used: Stability Axis and Body Axis. FIGURE 17 shows the Stability Axis system on the left and the Body Axis system on the right.[20]

Table 2: Stability Axis to Body Axis Transformations [20]

$$C_{N_b} = C_{L_s}\cos(\alpha) + C_{D_s}\sin(\alpha)$$
$$C_{A_b} = -C_{L_s}\sin(\alpha) + C_{D_s}\cos(\alpha)$$
$$C_{Y_b} = C_{Y_s}$$
$$C_{m_b} = C_{m_s}$$
$$C_{l_b} = C_{l_s}\cos(\alpha) - C_{n_s}\sin(\alpha)$$
$$C_{n_b} = C_{l_s}\sin(\alpha) + C_{n_s}\cos(\alpha)$$

To conduct the moment transfers, first the axes upon which the data was obtained must be considered. Most often, the data will be given in Stability Axis which our panel method of choice, VORLAX [21], outputs coefficients in. With the data in Stability Axis, first transform the data into Body Axis as it is easier to calculate the moment transfers. Additionally, some of the lateral-directional screening parameters require the aerodynamic coefficients to be in Body Axis for computations. The transformation between Stability Axis and Body Axis is summarized in TABLE 2.

Table 3: Moment Transfer in Body Axis

$$\Delta X_{cg} = \Delta X_{cg_{new}} - \Delta X_{cg_{old}}$$
$$\Delta Z_{cg} = \Delta Z_{cg_{new}} - \Delta Z_{cg_{old}}$$
$$C_{N_{new}} = C_{N_{old}}$$
$$C_{A_{new}} = C_{A_{old}}$$
$$C_{Y_{new}} = C_{Y_{old}}$$
$$C_{m_{new}} = C_{m_{old}} + C_{N_{old}}\left(\frac{\Delta X_{cg}}{\bar{c}}\right) - C_{A_{old}}\left(\frac{\Delta Z_{cg}}{\bar{c}}\right)$$
$$C_{n_{new}} = C_{n_{old}} + C_{Y_{old}}\left(\frac{\Delta X_{cg}}{b}\right)$$
$$C_{l_{new}} = C_{l_{old}} - C_{Y_{old}}\left(\frac{\Delta Z_{cg}}{b}\right)$$

With the data now in Body Axis, the moment transformations can be applied. For the development of the Stability & Control tool, the vehicle is assumed to be axisymmetric and thus no shift in Y coordinate (along the wing) of the center of gravity will occur. With this assumption the y-axis moment transformations are not computed and left out for brevity. A summary of the moment transfer is given in TABLE 3.

Table 4: Body Axis to Stability Axis Transformations [20]

$C_{L_s} = C_{N_b}\cos(\alpha) - C_{A_b}\sin(\alpha)$
$C_{D_s} = C_{N_b}\sin(\alpha) + C_{A_b}\cos(\alpha)$
$C_{Y_s} = C_{Y_b}$
$C_{m_s} = C_{m_b}$
$C_{l_s} = C_{l_b}\cos(\alpha) + C_{n_b}\sin(\alpha)$
$C_{n_s} = C_{n_b}\cos(\alpha) - C_{l_b}\sin(\alpha)$

After completing the moment transfer, the Body Axis data can be transformed back into Stability Axis using the relations shown in TABLE 4. As mentioned earlier, some parameters will require the Body fixed data so the tool will save three different aerodynamic databases: the Center of Gravity (*CG*) centered Stability Axis data, *CG* centered Body Axis data, and original reference Stability Axis data.

The next refinement to the database involves transforming the data to be centered at the zero-pitching moment reference point. To conduct this transformation, it was elected that six collective control surface deflection cases should be sufficient along with a neutral case to create a reasonable spread of data for interpolation to find the elevator deflection that corresponds to the zero-pitching moment condition. The zero-pitching moment will be a factor of both Mach and angle of attack thus, each flight condition will have a unique pitch trim deflection. For each Mach Number and angle of attack, an interpolator is used in between the two closest control surface deflection cases run. Using the various control

surface deflection cases, an elevator deflection can be obtained that corresponds to zero pitching moment. For the cases where a larger elevator deflection is required the data is blanked due to that flight condition being unobtainable. Once the zero-pitching moment control surface case is found then the rest of the aerodynamic data can be interpolated to obtain all other aerodynamic parameters, i.e. trimmed lift, drag, rolling moment and yawing moment coefficients. The zero-pitching moment condition helps elementarily address the point of while an aircraft maybe ultimately be stable it may not be trimmable at all the angles of attack run. This problem will be shown in more detail during the detailed analysis of the selected vehicles.

To begin the detailed Stability & Control analysis more focus is now placed on describing how the aircraft's stability varies with speed and altitude i.e., the flight envelope that the aircraft is expected to operate in.

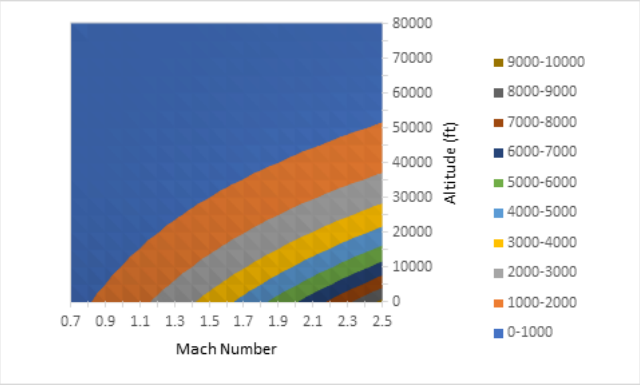

FIGURE 18: Example of Sky Map Showing Dynamic Pressure Variation

This capturing of the flight envelope is shown using "Sky Maps" – contour plotting parameters as a function of Mach and Altitude. In these plots, the speed or angle of attack is set to the *x-axis* and the altitude to *y-axis*. The parameter of interest is then plotted as a contour plot to show the trends along an operating envelope. This will allow the designer

to see how the stability of the aircraft varies with independent variables like Mach and altitude, but also buried implicit key flight parameter variables such as lift coefficient, trimmed angle of attack or dynamic pressure. An example of a Sky Map is shown in FIGURE 18. This is our preferred format to display various Stability & Control screening parameters. For each Mach and altitude pair the flight lift coefficient is calculated assuming lift equals weight at some load factor.

To start with dynamic stability, first a flight path needs to be established. This flight path must contain an altitude and a Mach Number or knots equivalent airspeed (KEAS) which will be converted to Mach Number. From an altitude and Mach Number pair the standard atmosphere model[22] can be used to obtain dynamic pressure as shown below in Equation 3.

$$\bar{q} = \frac{\bar{q}}{M^2} * M^2 \tag{3}$$

If the flight envelope is scheduled in knots equivalent airspeed (KEAS) the dynamic pressure can be solved directly using Equation 4.

$$\bar{q} = 1481 * \left(\frac{KEAS}{660.8}\right)^2 \left[\frac{lbf}{ft^2}\right] \tag{4}$$

If a turn needs to be simulated, a load factor can be obtained from an implied bank angle shown in Eq. 5. Additionally, if low g or high gee maneuvers are desired the load factor can be set that way as well. This is useful for examining ballistic like trajectories.

$$N_z = \frac{1}{\cos(\varphi)} \tag{5}$$

Using the load factor and the weight of the aircraft, the lift force required from the aircraft is calculated using Equation 6. For steady level flight a load factor of 1 is applied,

and for high atmosphere ballistic trajectory a load factor of 0.1 is used. Then using the standard nondimensional form, the flight lift coefficient is obtained with Equation 7.

$$L = N_z * W \tag{6}$$

$$C_L = \frac{L}{\bar{q} * S_{ref}} \tag{7}$$

Using this flight lift coefficient, an implied angle of attack can be obtained through interpolation. This flight angle of attack will then be used to determine a variety of dynamic stability parameters.

To use the aerodynamic database effectively, an interpolation routine must first be developed. The interpolation will need to be broken into two distinct parts. The first interpolator will need to be backwards as the only information known is the flight Mach Number and flight lift coefficient. The second interpolator will perform normal forward interpolation between angle of attack and Mach Number to obtain the desired flight aerodynamic parameters.

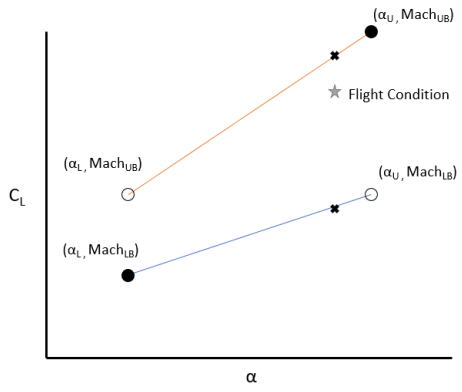

FIGURE 19: Backwards Interpolation Scheme

To perform this interpolation, first the upper and lower Mach Number bounds need to be defined. This leads to the first challenge in which at subsonic speeds, as Mach

increases the lift curve slope increases but once the leading edge becomes supersonic, the opposite is true, and the slope begins to shallow. Thus, a way to define the upper bounding curve needs to be carefully considered. To determine which Mach Number curve is the upper bounding curve it was decided that the lift curve slope, $\frac{dC_L}{d\alpha}$ should be used as there are instances when the lift curve slopes of two different Mach Numbers intersect at particular angle of attack, thus the bounds flips. FIGURE 19 gives an illistration of the backward interpolation scheme being used. Using the upper bounding Mach Number curve, the bounding angle of attack can be found. Equations 8-11 show the process for the calculation of the flight angle of attack.

$$C_{L_{\alpha_L @ M}} = C_{L_{\alpha_L @ M_L}} + \frac{(M - M_L)\left(C_{L_{\alpha_L @ M_U}} - C_{L_{\alpha_L @ M_L}}\right)}{M_U - M_L} \tag{8}$$

$$C_{L_{\alpha_U @ M}} = C_{L_{\alpha_U @ M_L}} + \frac{(M - M_L)\left(C_{L_{\alpha_U @ M_U}} - C_{L_{\alpha_U @ M_L}}\right)}{M_U - M_L} \tag{9}$$

$$\frac{dC_L}{d\alpha} = \frac{\left(C_{L_{\alpha_U @ M}} - C_{L_{\alpha_L @ M}}\right)}{(\alpha_U - \alpha_L)} \tag{10}$$

$$\alpha = \alpha_L + \frac{\left(C_L - C_{L_{\alpha_L @ M}}\right)}{C_{L_{\alpha_L @ M}} - C_{L_{\alpha_L @ M}}}(\alpha_U - \alpha_L) \tag{11}$$

With the flight angle of attack calculated, the second set of interpolations can be completed. From the flight angle of attack key parameters such as *LCDP*, *Cnβdynamic*, *dCm/dα,* rolling moment and yawing moments are calculated. The forward interpolation scheme is illustrated in FIGURE 20.

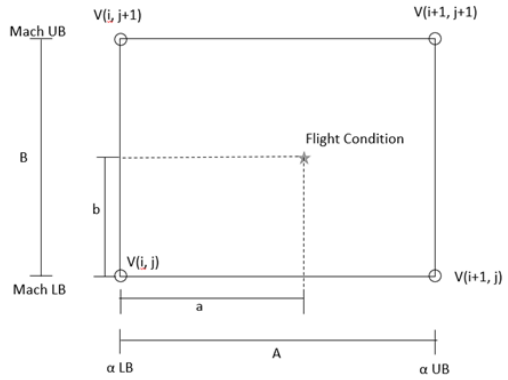

FIGURE 20: Forward Interpolation Scheme

The forward interpolation scheme process is summarized through Eqs. 12-16.

$$A = V(i+1, j) - V(i, j) \tag{12}$$

$$a = Point\ Value - V(i, j) \tag{13}$$

$$B = V(i, j+1) - V(i, j) \tag{14}$$

$$b = Point\ Value - V(i, j) \tag{15}$$

$$\begin{aligned} Point\ Value = {} & \left(1 - \frac{a}{A}\right)\left(1 - \frac{b}{B}\right)V(i, j) + \left(\frac{a}{A}\right)\left(1 - \frac{b}{B}\right)V(i+1, j) \\ & + \left(1 - \frac{a}{A}\right)\left(\frac{b}{B}\right)V(i, j+1) + \left(\frac{a}{A}\right)\left(\frac{b}{B}\right)V(i+1, j+1) \end{aligned} \tag{16}$$

If the desired flight Mach Number is equal to a Mach Number within the known database, the interpolation procedure discussed above can be simplified by just applying the simple 1D linear interpolation formula shown in Equation 17.

$$y_L = y_{1_L} + \frac{\left(x - x_{1_L}\right)\left(y_{2_L} - y_{1_L}\right)}{x_{2_L} - x_{1_L}} \tag{17}$$

With all the key parameters required for analysis now obtained, all the various screening parameters can be simply calculated. Equation 18 gives the Short Period

frequency in rad/sec and Equation 19 is used to calculate the pitch responsiveness.[23] For physical insight, recall that 6.28 rad/sec is approximately 1-Hz.

$$\omega_{SP_{rad/sec}} = \sqrt{\frac{\left(-57.3\left(\frac{dCm}{d\alpha}\right) * q * S_{ref} * \bar{c}\right)}{I_{yy}}} \tag{18}$$

$$\frac{n}{\alpha} = \frac{\left(57.3 * q * S_{ref} * \left(\frac{dCL}{d\alpha}\right)\right)}{W} \tag{19}$$

To approximate the Short Period damping, the linearized damping form is given in Eqs. 20 through 22 is used.[5]

$$M_q = \frac{Cm_q \bar{q} S_{ref} \bar{c}^2}{2I_{yy} VKTAS\left(\frac{6076}{3600}\right)} \tag{20}$$

$$\frac{Z_a}{U_1} \approx \frac{\bar{q} S_{ref}}{m * VKTAS\left(\frac{6076}{3600}\right)}\left(57.3 * \frac{dC_L}{d\alpha}\right) \tag{21}$$

$$\xi_{sp} \approx -\frac{\left(M_q + \frac{Z_\alpha}{U_1}\right)}{2\omega_{sp}} \tag{22}$$

To determine how these parameters affect the handling and control qualities of the aircraft, the MIL 8785-C Control Anticipation Parameter chart is used.[12] While this handbook/standard is not a cookbook, it does give the designer a general idea for what a good aircraft should feel like. MIL 8785-C suggests that the pitch responsiveness (gee's per incidence) and stick-fixed Short Period frequency (ω_{sp}) are important criteria to evaluate longitudinal handling qualities.

As previously mentioned, in MIL 8785-C, there are three charts broken up for the following phases of flight: Category A which "requires rapid maneuvering, precision

tracking or precise flightpath control"; Category B- is "accomplished using gradual maneuvers and without precision tracking, although accurate flight-path control may be required"; Category C- is "accomplished during gradual maneuvers and usually require accurate flight-path control."[12] The Category A chart as shown in FIGURE 21, is the primary chart used in the analysis of these experimental and high-performance aircraft due to the frequency of precise flight control being required.

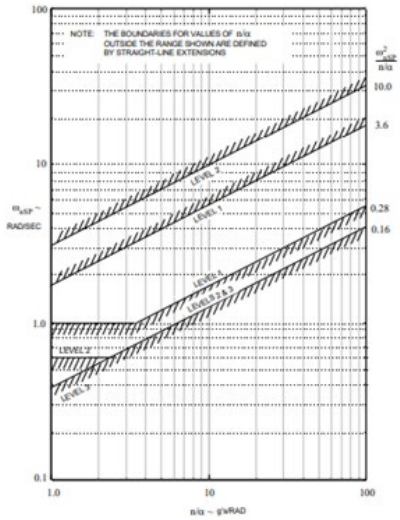

FIGURE 21: MIL STD 8785C Category A "Control Anticipation Parameter" Chart [12]

Each chart is broken up into three levels describing the pilot workload: LEVEL 1 is described as having good flying qualities suitable for the mission phase; LEVEL 2 is described as having flying quality characteristics that require more workload out of the pilot which degrades mission performance; LEVEL 3 indicates that the aircraft is still safe to operate however, the pilot workload is far too much for the mission to be completed effectively.[12] The aircraft is dangerous to fly if operated outside LEVEL 3 boundaries.

With Sky Maps being the primary format to present the screen parameters being calculated, plotting the values directly on the MIL8785-C charts becomes quite difficult as

well as not providing much context for the areas where handling qualities are bad. The Category A and Category B charts were converted into equations for use in determining the longitudinal stability and handling qualities of the aircraft in Sky Maps format. The equations and restrictions for Category A are given in TABLE 5, and for Category B are given in TABLE 6. The Short Period and Dutch Roll damping requirements are also listed.

Table 5: MIL-8785C Category A

Level	$\frac{\omega_{sp}^2}{n/\alpha}$	ω_{sp} (rad/s)	n/α	ξ_{sp} max	ξ_{sp} min	ω_{DR} (rad/s)	ξ_{DR} min
1	$0.28 < \frac{\omega_{sp}^2}{n/\alpha} < 3.6$	$\omega_{sp} > 1$	NA	1.3	0.35	$\omega_{DR} > 1$	0.19
2	$0.16 < \frac{\omega_{sp}^2}{n/\alpha} < 0.28$ $3.6 < \frac{\omega_{sp}^2}{n/\alpha} < 10$	$\omega_{sp} > 0.6$	NA	2	0.25	$\omega_{DR} > 0.4$	0.02
3	$\frac{\omega_{sp}^2}{\frac{n}{\alpha}} < 0.16$ $10 < \frac{\omega_{sp}^2}{n/\alpha}$	NA	NA	-	0.15	$\omega_{DR} > 0.4$	0

Table 6: MIL-8785C Category B

Level	$\frac{\omega_{sp}^2}{n/\alpha}$	ω_{sp} (rad/s)	n/α	ξ_{sp} max	ξ_{sp} min	ω_{DR} (rad/s)	ξ_{DR} min
1	$0.085 < \frac{\omega_{sp}^2}{n/\alpha} < 3.6$	NA	NA	2	0.3	$\omega_{DR} > 1$	0.08
2	$0.038 < \frac{\omega_{sp}^2}{n/\alpha} < 0.085$ $3.6 < \frac{\omega_{sp}^2}{n/\alpha} < 10$	NA	NA	2	0.20	$\omega_{DR} > 0.4$	0.02
3	$\frac{\omega_{sp}^2}{n/\alpha} < 0.038$ $10 < \frac{\omega_{sp}^2}{n/\alpha}$	NA	NA	-	0.15	$\omega_{DR} > 0.4$	0

15

When looking at lateral-directional stability there a many screening parameters of interest. This is due to the lateral-directional stability being the most tender and the source of most catastrophic departures. One key parameter of interest is *Cnβdynamic*, often referred to as the control parameter. This parameter is a root of the Dutch Roll frequency and thus should not be negative as that will cause the frequency to be unstable. The other major parameter of interest is called the lateral control departure parameter (*LCDP*). *LCDP* measures the coupling between the roll and yaw effects of the primary roll controller and the inherent lateral and directional stability of an airframe.[24] *Cnβdynamic* and *LCDP* are calculated for each point of interest on a given flight using equations 23 and 24. [23] For both of these parameters, the yawing and rolling moments should be in Body Axis rather than Stability Axis as denoted in the subscript.

$$Cn\beta dynamic = \left(\frac{dCn_{Body}}{d\beta}\right) * \cos(\alpha) - \left(\frac{dCl_{Body}}{d\beta}\right) * \left(\frac{I_{zz}}{I_{xx}}\right) * \sin(\alpha) \tag{23}$$

$$LCDP = \frac{dCn_{Body}}{d\beta} - \frac{dCl_{Body}}{d\beta} * \frac{\left(\frac{dCn_{Body}}{d\ aileron}\right)}{\left(\frac{dCl_{Body}}{d\ aileron}\right)} \tag{24}$$

To determine if the aircraft is prone to control coupling, the evolved Bihrle-Weissman chart (as shown below in FIGURE 22) is used.[13]

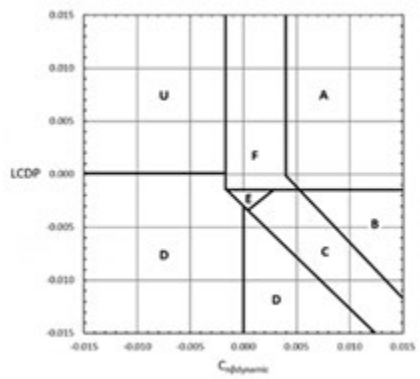

FIGURE 22: Evolved-Bihrle-Weissman Chart after Takahashi, Griffin & Grandhi [13]

By plotting *LCDP* and *Cnβdynamic*, general lateral-directional stability characteristics can be obtained. "The A region indicates that the aircraft is highly departure and spin resistant showing that the aircraft is very stable. The B region indicates that the aircraft is still spin resistant but can be subjected to roll reversals inducing departure. The C region indicates a weak spin resistance and a strong roll reversal resulting in departure. The D region indicates both strong spin tendencies and roll reversal resulting in departure. The E region is characterized as having weak spin tendency, moderate departure, and roll reversals, affected by secondary factors. The F region has weak departure and spin resistance, no roll reversal, heavily influenced by secondary factors. Lastly, the U region has high directional instability." [25] [26]

The updated version of the chart following Skow criterion is suggested for future use due to its restricted A region.[14] When comparing the two versions of the Weissman chart shown back in FIGURE 13, the updated figure removes a large chunk of the upper A-F region. Some aircraft like the *X-2* bordered the old A-F region, which was as shown in our previous paper, and thus would be fully in the F region on the updated chart.[3]

Now the dominate lateral directional frequency, the Dutch Roll, can be calculated. The stick-fixed Dutch Roll frequency is estimated using *Cnβdynamic* in hertz with Eq. 25. [23]

$$\omega_{DR_{HZ}} = \frac{1}{2\pi} * \sqrt{\frac{\left(57.3 * C_n\beta\ dynamic * q * S_{ref} * b\right)}{I_{zz}}} \tag{25}$$

The linearized Dutch Roll damping is estimated using Eqs. 26-28. [5]

$$N_r = \frac{Cn_r \bar{q} S_{ref} b^2}{2I_{zz} VKTAS \left(\frac{6076}{3600}\right)} \tag{26}$$

$$\frac{Y_\beta}{U} \approx \frac{\bar{q} S_{ref}}{m * VKTAS \left(\frac{6076}{3600}\right)} \left(57.3 \frac{dCY}{d\beta}\right) \tag{27}$$

$$\xi_{DR} \approx -\frac{\left(N_r + \frac{Y_\beta}{U}\right)}{2\omega_{DR}} \tag{28}$$

To check for Spiral-Roll mode coupling both the Roll Mode time constant and Spiral Mode time constant are now calculated. The Roll mode is estimated using Eqs. 29 and 30.[5]

$$L_P = C_{l_p} \frac{\bar{q} S_{ref} b^2}{2I_{xx} VKTAS \left(\frac{6076}{3600}\right)} \tag{29}$$

$$\tau_R \approx -\frac{1}{L_p} \tag{30}$$

The Spiral Mode, while a bit more involved, is calculated using Eqs. 31- 36.[5]

$$L_\beta = 57.3 \frac{dC_l}{d_\beta} \frac{\bar{q} S_{ref} b}{I_{xx}} \tag{31}$$

$$N_\beta = 57.3 \frac{dC_n}{d_\beta} \frac{\bar{q} S_{ref} b}{I_{zz}} \tag{32}$$

$$L_r = Cl_r \frac{\bar{q} S_{ref} b^2}{2 I_{xx} VKTAS \left(\frac{6076}{3600}\right)} \tag{33}$$

$$N_r = Cn_r \frac{\bar{q} S_{ref} b^2}{2 I_{zz} VKTAS \left(\frac{6076}{3600}\right)} \tag{34}$$

$$s \approx \frac{L_\beta N_r - N_\beta L_r}{L_\beta + N_\beta \left(\frac{I_{xz}}{I_{xx}}\right)} \tag{35}$$

$$\tau_s \approx -\frac{1}{s} \tag{36}$$

With the dynamic stability completed, basic longitudinal and lateral directional trim needs to be considered. The elevator or pitch surface deflection to trim is calculated using Equation 37. For each Mach Number and angle of attack the elevator deflection required varies drastically with many angles of attack inaccessible at high Mach Numbers due to decreased pitch performance.

$$\delta_{elevator} = \frac{C_m}{\frac{dC_m}{d_{elevator}}} \tag{37}$$

To determine the amount of sideslip that the aircraft can trim to, both the control power of the primary yaw device and roll device must be considered. To determine how effective each primary control surface is the primary roll/yaw moment ratios can be calculated.

To calculate the primary roll controller ratio, the yawing moment is divided by the rolling moment as shown in Equation 38. When the ratio is close to zero, this indicates that the ailerons are an effective roll control device with very little adverse yaw being produced.

As the ratio approaches or exceeds negative one, this shows that the aileron is producing so much adverse yaw that the aileron is acting more as a yaw controller than as the intended roll controller. Without another surface to act as the roll controller and a yaw controller to counter act the adverse yaw the aircraft will depart from stable flight. Similarly for the primary yaw controller, the rolling moment is simply divided by the yawing moment as shown in Equation 39.

$$\frac{YM}{RM_{aileron}} = \frac{dCn/d_{aileron}}{dCl/d_{aileron}} \tag{38}$$

$$\frac{RM}{YM_{rudder}} = \frac{dCl/d_{rudder}}{dCn/d_{rudder}} \tag{39}$$

To calculate the adverse yaw produced by the primary roll controller, the yawing moment produced per degree of roll control deflection is divided by the inherit stabilizing yawing moment of the aircraft as shown in Equation 40.

$$Adverse\ Yaw = \frac{dC_n/d_{aileron}}{dC_n/d_{\beta}} \tag{40}$$

The final lateral-directional trim parameter to calculate is the sideslip trim per degree of control surface deflection. The minimum sideslip that can be produced by the primary yaw device is shown in Equation 41. The minimum sideslip that can be trimmed by the primary roll device is given by Equation 42. The total minimum sideslip that the aircraft can trim to per degree of deflection is the minimum between the two cases as shown in Equation 43.

$$\beta_{yaw} = \frac{dC_n/d_{rudder}}{dC_n/d_{\beta}} \tag{41}$$

$$\beta_{roll} = \frac{dC_l/d_{aileron}}{dC_l/d_\beta} \tag{42}$$

$$\beta_{min} = \min(\beta_{yaw}, \beta_{roll}) \tag{43}$$

The last area that needs attention is the problem of solving adverse yaw with a simple aileron-rudder interconnect (*ARI*). The *ARI* must be scheduled on a Mach Number and angle of attack basis. A simple *ARI* can be defined as the ratio of the yawing moment of the primary roll controller over the primary yaw controller shown in Equation 38.

$$0 = CYM_{aileron} - C_1 * CYM_{rudder} \tag{37}$$

$$ARI(\%) = \frac{CYM_{aileron}}{CYM_{rudder}} \tag{38}$$

One thing that also must be considered is the effectiveness of the primary yaw device. In some configurations such as the Bell *X-2*, the rudder was ineffective at high-speeds and thus was locked during those portions of the flight. This would have resulted in an effective *ARI* not being possible without the rudder being unlocked.

AIRCRAFT OF INTEREST

Bell *X-2*

The first aircraft of interest is the Bell *X-2* which began development in 1947, shown in FIGURE 23. The Bell *X-2* program was a cooperative program between the Bell Aviation Corporation, the National Advisory Committee for Aeronautics (NACA) and the United States Airforce to produce two aircraft. The goal of the *X-2* program was to explore high-speed flight greater than Mach 2 as well as high altitude flight.[27] Like many high-speed aircraft of the time, the *X-2* was solely powered by a rocket engine to achieve high-speed and returned back to the runway as a glider. These rocket powered aircraft had to be

carried by a mothership to their specified launch altitudes before separating and igniting their engine resulting in takeoff not driving any of the Stability & Control.

FIGURE 23: Bell *X-2* and its B-50 Mothership

The *X-2* was a relatively long and trouble-filled program with relatively few powered flights. On the 13th powered flight, the *X-2* reached a speed of Mach 3.2 before departing from stable flight. During this departure, the *X-2* experienced severe adverse yaw which ultimately led to inertial coupling and control reversal resulting in a supersonic spin. The pilot, Milburn Apt was killed and the airframe significantly damaged.[18]

The *X-2* program did have some notable achievements with both speed and altitude records being set. On the *X-2's* final flight Apt became the first person to break Mach 3. Ivan Kincheloe, on the *X-2*'s 12th powered flight broke an altitude record of 126,200-ft.[18] As a result of the many of the stability issues encountered on this program, engineers began to conduct even more test with various other X-planes to further learn how anticipate and characterize these new stability problems.

North American *X-15*

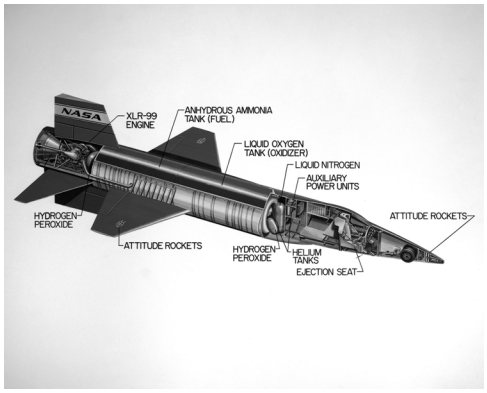

FIGURE 24: North American *X-15* [28]

The North American *X-15,* shown in FIGURE 24, stands to be one of the most successful and really only general hypersonic aircraft to ever be produced by the United States of America to this day. Like the *X-2*, the *X-15* was a rocket powered research aircraft which, intended to further expand our knowledge of high-speed and high-altitude flight. The *X-15* program studied many key topics like aerothermal heating, atmospheric reentry, reaction control systems, closed loop control systems, and more, which would all be necessary on the future Space Shuttle Orbiter program.[27]

The *X-15* program was highly successful with 199 test flights conducted between three airframes. North American won the contract in 1955 with the first flight occurring in 1959. By 1961, the *X-15* became the first aircraft to break Mach 5 and thus the first piloted hypersonic aircraft. Throughout the *X-15* program, numerous speed and altitude records were broken. In 1963, Walker set the unofficial altitude record of 354,000-ft. In 1967, Knight set the unofficial speed record of Mach 6.7.[27] The *X-15* is an interesting aircraft because of the variety of missions that it flew. It was not simply a technology

demonstrator meant to accomplish one goal but rather a research platform for a variety of projects.

Sky Cruiser

FIGURE 25: Rendering of *Sky Cruiser* [29]

The *Sky Cruiser*, shown in FIGURE 25 is a proposed aircraft designed and developed during my undergraduate aerospace engineering program as our final capstone project and published as an AIAA Conference Paper.[29] The key requirements for the aircraft were that it had be a unitary (takeoff and land on conventional runway) 14 CFR § 25 certified space tourism aircraft.[30] The aircraft consisted of a mixed propulsion system with two coverable turbofan engines mounted on top of the wing and a single rocket engine pointing out the aft end of the main fuselage.

Sky Cruiser is a rather large aircraft with a maximum takeoff weight of 131,000 lbm with a post rocket burn weight of around 66,000 lbm. *Sky Cruiser* is able to shuttle six passengers up above the 50-mile line (U.S. defined space) for 129 seconds with a peak altitude of 332,000-ft. [29] In the design of this aircraft, stability was of key concern resulting in the extremely large vertical tail. A reaction control system is included in the design for the out of atmosphere and low dynamic pressure portions of flight.

As this was an undergraduate project, much of the detailed Stability & Control methods and screening discussed so far were not applied. With the interesting shape/sizing and mission of the theoretical aircraft, revisiting in more detail was suggested.

High-Speed Slender Aircraft (*HSSA*)

FIGURE 26: NASA X-43A [31]

The High-speed Slender Aircraft (*HSSA*) is based on a generic planform that is similar to past high-speed technology demonstrators. This aircraft is based on an unpiloted, small MTOW, and small planform restrictions.

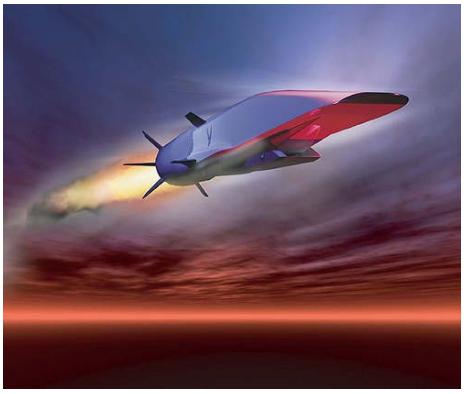

FIGURE 27: Boeing X-51 [32]

Inspiration for the *HSSA* comes from a verity of hypersonic technology demonstrators such as the NASA X-43A, FIGURE 26, program and the Boeing X-51, FIGURE 27. Both of these aircraft were primarily technology demonstrators for scramjet propulsion.[31] [32] As propulsion was the primary focus of the aircraft, it is speculated that these vehicles are limited to mainly straight and level flight with little to no maneuverability due to the minimal vertical tail area present to assist lateral-directional stability. As data on these aircraft are not public and available, an analysis of the *HSSA* will be conducted to explore some of the stability problems that may likely arise in the design of these types of aircraft.

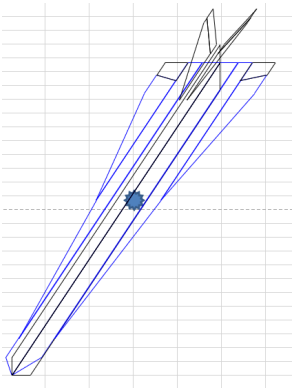

FIGURE 28: *HSSA-V1* Model

The initial design for the *HSSA*, referred to as *HSSA-V1*, shown in FIGURE 28 has noticeably small, canted verticals as many high-speed cartoons appear to have.

GENERATION OF TEST DATA

To conduct an analysis for each of the introduced aircraft, aerodynamic databases had to be created. To create the aerodynamic databases, the potential flow solver VORLAX2022a was used.[33][34] VORLAX 2022a is an updated and more efficient version

of the 1977 FORTRAN program originally written in the 1970's by Lockheed under contract for NASA.[21] For use in VORLAX, each aircraft is modeled as a series of flat plates upon which, a grid of vortices can be applied. The key aerodynamic coefficients that are obtained from VORLAX are lift, induced drag, side force, pitching moment, yawing moment, and rolling moment. VORLAX is also capable of estimating the dynamic derivatives of an aircraft as well. This code was chosen for the analysis, as it is useful for rapid database generation while remaining fairly accurate to capture trends.

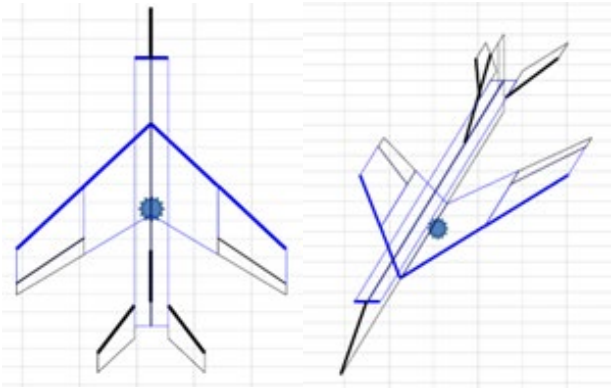

FIGURE 29: Visualization of *X-2* VORLAX Panel Model in top-down view (left) and oblique view (right)

For the creation of the Bell *X-2* panel model, detailed dimensions of the aircraft were obtained from NACA RM L57J28a.[35] see FIGURE 29. The *X-15* Model was created by my fellow graduate student Jack Griffin and Dr. Takahashi [37] [38] with improvements made to the vertical tail.

The VORLAX aerodynamic database was generated over a range of Mach Numbers and angles-of-attack for each aircraft. VORLAX is able to compute subsonic stability as well as supersonic and hypersonic through the use of adjustable leading-edge suction and the Polhemus effect.

Table 7: Aerodynamic Cases Required for Database

Case	Aero Dynamic Parameters Obtained
Base (No Control Surface Deflection)	C_L, C_D, C_Y, C_m
Base at 1 deg of Sideslip	$C_L, C_D, C_Y, C_m, \frac{dC_l}{d\beta}, \frac{dC_n}{d\beta}$
Ailerons Deflected 30 deg (No Side Slip)	$\frac{dC_l}{dail}, \frac{dC_n}{dail}$
Rudder Deflected 30 deg (No Side Slip)	$\frac{dC_l}{drud}, \frac{dC_n}{drud}$
Pitch Rate (q) dynamic derivative	C_{mq}
Yaw Rate (r) dynamic derivative	C_{nr}, C_{lr}
Roll Rate (p) dynamic derivative	C_{np}, C_{lp}

To obtain a thorough database, a total of 21 cases need to be run in VORLAX. The first seven are to obtain data for the base configuration, aileron deflection, rudder deflection, and the dynamic derivatives. These seven cases and the aerodynamic coefficients obtained from them are summarized in Table 7. For aircraft that do not have ailerons, then the aileron case is skipped. The remaining 14 cases are focused on the deflection of the horizontal tail which is split into two control effector cases.

The first case is collective horizontal tail deflection (conventional elevator) and the second is differential deflection (elevon) used in replacement of ailerons. Seven deflection cases are used to help ensure that interpolation between cases is fairly accurate, as at high-speed and angle of attack, nonlinear effects can be observed. This is done to ensure that the interpolations are good approximations as the yawing and rolling moments are highly dependent on angle of attack, Mach, and elevator deflection. Some of these trends are not linear as well so having multiple steps in deflections help ensure the nonlinearities are captured. The differential tail cases were taken at a 5-degree offset from the respective collective case. A summary of these runs is listed below in TABLE 8.

Table 8: Differential Deflection Cases Required

Collective (C_m)	Differential $\left(C_m, \frac{dC_l}{dtail}, \frac{dC_n}{dtail}\right)$	
	Left Surface	Right Surface
+25°	+30°	+20°
+15°	+20°	+10°
+5°	+10°	0°
0°	+5°	-5°
-5°	0°	-10°
-15°	-10°	-20°
-25°	-20°	-30°

For the creation of the VORLAX models, the standard Boeing sign notation was used to ensure all aerodynamic moment coefficients are consistent between vehicles. For a positive yawing moment, the trailing edge of the rudder or primary yaw device is deflected to the pilot's right. For a positive rolling moment, the pilot's left aileron or primary roll surface is deflected down. For a negative or nose down pitching moment, the elevators trailing edges are deflected downward.

ANALYSIS OF THE BELL *X-2*

Key aerodynamic properties required for calculations in the Bell X-2 analysis are summarized in Table 9.

Table 9: Key Properties of the *X-2* [16]

S_{ref} (ft^2)	258
b (ft)	8.32
$\bar{c}$ (ft)	32.2
W (lbm)	12,300
I_{xx} (lbm/ft^2)	162,000
I_{yy} (lbm/ft^2)	820,000
I_{zz} (lbm/ft^2)	937,000
I_{xz} (lbm/ft^2)	25,200

The analysis of the Bell *X-2* is going to be split up into two versions, the Original Configuration and a proposed solution with a larger vertical tail. As discussed previously, the *X-2* had extremely poor lateral-directional stability when operating at high-speeds. To try and remedy some of the lateral-directional issues, it was proposed that there were three potential options: 1) to enlarge the vertical tail/rudder, 2) to create a Mach and α scheduled Aileron-Rudder Interconnect (ARI), and/or 3) to implement differential horizontal tail control for roll.

Table 10: Bell *X-2* Vertical Tail Parameters

	Original	Enlarged Vertical
Cr (ft)	8.99	11.69
Ct (ft)	2.89	3.76
B (ft)	6.67	8.67
Sv (ft^2)	39.62	66.96
% Area Increase		69.0

First, the larger vertical tail/rudder is considered. For the larger vertical tail analysis, the dimensions of the baseline tail were scaled upwards by 30% (i.e 30% more tip and root chord as well as 30% greater exposed height). The physical dimension details for the orignal and updated vertical tails are summarized in TABLE 10. FIGURE 30 shows a comparison between the orignal vertical tail and rudder versus the scaled up version.

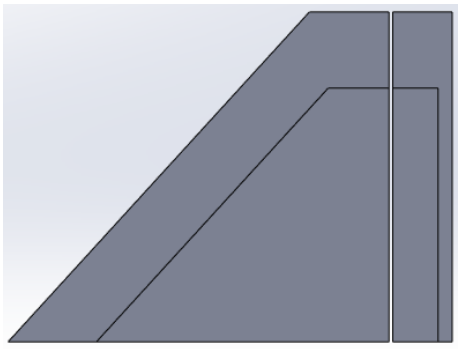

FIGURE 30: Comparison Between Large and Original Tail on *X-2*

As vertical tail size grows, there is gain in *dCn/dβ* which improves both lateral-directional stability (*Cnβdynamic*) and lateral-directional controllability (*LCDP).* One of the pitfalls in making the vertical tail larger is realized due to its effect on crosswind trim capabilities for landing. In crosswind, the larger tail can have a strong enough weathervane effect to point the aircraft in the direction of the wind due to saturated rudder and/or aileron control power. A secondary consideration of an enlarged vertical tail is its associated weight, which will drive the center-of-gravity further aft or demand nose ballast. For this paper, it was assumed that mass properties remain constant with an increase in the vertical tail.

Additionally, it is suggested that *LCDP* could be improved by adding a modern flight control system Mach-and-*α* scheduled aileron-rudder interconnect (ARI) to the *X-2*. The goal of the *ARI* is to utilize the primary yaw controller, the physical "rudder," to trim the induced yawing moment of the primary roll controller to zero. The *ARI* for this analysis will treat the ailerons as antisymmetric collective deflections and a set rudder deflection.

Lastly, with the prevalence of differential tail control being used on a significant number of high-speed aircraft, this appears to be a potential solution. Differential tail for roll control at high-speeds rather than aileron could help address the severe adverse yaw that the *X-2* experienced. Similarly, an alternative *ARI* utilizing the rudder and the differential tail is created. For the next analysis the original aileron and rudder configuration will be compared to a differential tail and rudder configuration. For each case a tentative *ARI* scheme can be scheduled throughout the flight envelope. This process is completed using pitch trimmed data.

Longitudinal Stability for Baseline Configuration

The first area of interest is the longitudinal dynamic stability which is screened for using the Short Period Frequency and the Short Period Damping ratio. A key concern when dealing with the Short Period Frequency is that if it becomes too high, there is the possibility that it will sit on top of a rigid body structural natural frequency leading to destructive resonance.

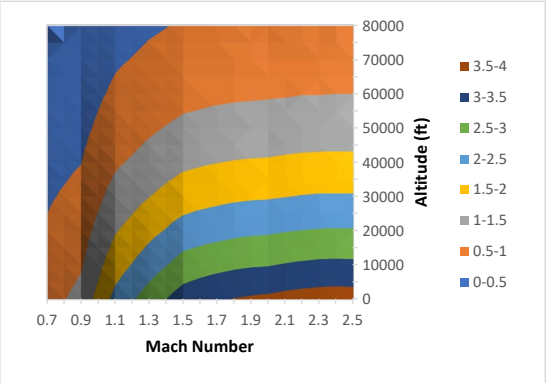

FIGURE 31: Short Period Sky Map (X-2)

From FIGURE 31, it is shown that flying supersonic at low altitude and high-speed excites the Short Period Frequency to levels of concern. This results in high-speed flight being restricted to mainly modest to higher altitudes (>40,000-ft). Throughout much of the *X-2*'s flight envelope (40,000+-ft and Mach > 1.5) the Short Period Frequencies are manageable at around 1-2 hertz.

As the altitude increases and speed increases, FIGURE 32 shows that the damping begins to fall off drastically. A modest 20% damping ratio (LEVEL 2 handling characteristics) is achieved for only a small band of lower altitude and supersonic flight. This then begs the question, how does one balance these two parameters? To keep the damping good, the pilot must fly the aircraft at relatively lower altitudes and high speeds.

This is not ideal and would result in an unrealistic restriction on the flight envelope. To solve this problem, synthetic damping will likely need to be added to the aircraft control system.

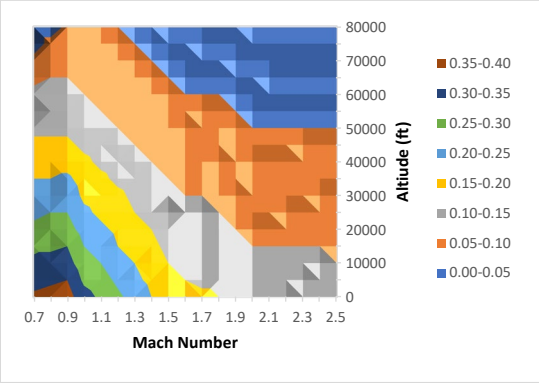

FIGURE 32: Short Period Damping Sky Map (X-2)

Altitude (ft) \ Mach	0.7	0.8	0.9	1.0	1.1	1.2	1.3	1.4	1.5	1.6	1.7	1.8	1.9	2.0	2.1	2.2	2.3	2.4	2.5
80000			2	2	2	2	2	2	2	2	2	2	2	2	2	2	2	2	2
75000		2	2	2	2	2	2	2	2	2	2	2	2	2	2	2	2	2	2
70000	2	2	2	2	2	2	2	2	2	2	2	2	2	2	2	2	2	2	2
65000	2	2	2	2	2	2	2	2	2	2	2	2	2	2	2	2	2	2	2
60000	2	2	2	2	2	2	2	2	2	2	2	2	2	2	2	2	2	1	1
55000	2	2	2	2	2	2	2	2	2	1	1	1	1	1	1	1	1	1	1
50000	2	2	2	2	2	2	2	1	1	1	1	1	1	1	1	1	1	1	1
45000	2	2	2	2	2	2	1	1	1	1	1	1	1	1	1	1	1	1	1
40000	2	2	2	2	2	1	1	1	1	1	1	1	1	1	1	1	1	1	1
35000	2	2	2	2	1	1	1	1	1	1	1	1	1	1	1	1	1	1	1
30000	2	2	2	2	1	1	1	1	1	1	1	1	1	1	1	1	1	1	1
25000	2	2	2	1	1	1	1	1	1	1	1	1	1	1	1	1	1	1	1
20000	2	2	2	1	1	1	1	1	1	1	1	1	1	1	1	1	1	1	1
15000	2	2	2	1	1	1	1	1	1	1	1	1	1	1	1	1	1	1	1
10000	2	2	2	1	1	1	1	1	1	1	1	1	1	1	1	1	1	1	1
5000	2	2	1	1	1	1	1	1	1	1	1	1	1	1	1	1	1	1	1
0	2	2	1	1	1	1	1	1	1	1	1	1	1	1	1	1	1	1	1

FIGURE 33: MIL 8785C Levels for Category A Flight (X-2) for $nZ = 1$

FIGURE 33 plots the Pitch Responsiveness and Short Period Frequency on a Sky Map derived from the Category A chart from MIL 8785-C.[12] LEVEL 1 characteristic are filled green, LEVEL 2 characteristic are yellow, and Level 3 characteristic are red. From this figure it is shown that the *X-2* has overall okay longitudinal stability over the entire flight envelope. Some discrepancies in the center of gravity location may be the cause of

the decreased performance shown here or variations in when the shift from Level 1 to Level 2 characteristics occurs.

Altitude (ft) \ Mach	0.7	0.8	0.9	1.0	1.1	1.2	1.3	1.4	1.5	1.6	1.7	1.8	1.9	2.0	2.1	2.2	2.3	2.4	2.5
80000	2	2	2	2	2	2	2	2	2	2	2	2	2	2	2	2	2	2	2
75000	2	2	2	2	2	2	2	2	2	2	2	2	2	2	2	2	2	2	2
70000	2	2	2	2	2	2	2	2	2	2	2	2	2	2	2	2	2	2	2
65000	2	2	2	2	2	2	2	2	2	2	2	2	2	2	2	2	2	2	2
60000	2	2	2	2	2	2	2	2	2	2	2	2	2	2	2	2	2	1	1
55000	2	2	2	2	2	2	2	2	2	1	1	1	1	1	1	1	1	1	1
50000	2	2	2	2	2	2	2	1	1	1	1	1	1	1	1	1	1	1	1
45000	2	2	2	2	2	2	1	1	1	1	1	1	1	1	1	1	1	1	1
40000	2	2	2	2	2	1	1	1	1	1	1	1	1	1	1	1	1	1	1
35000	2	2	2	2	1	1	1	1	1	1	1	1	1	1	1	1	1	1	1
30000	2	2	2	2	1	1	1	1	1	1	1	1	1	1	1	1	1	1	1
25000	2	2	2	1	1	1	1	1	1	1	1	1	1	1	1	1	1	1	1
20000	2	2	2	1	1	1	1	1	1	1	1	1	1	1	1	1	1	1	1
15000	2	2	2	1	1	1	1	1	1	1	1	1	1	1	1	1	1	1	1
10000	2	2	2	1	1	1	1	1	1	1	1	1	1	1	1	1	1	1	1
5000	2	2	1	1	1	1	1	1	1	1	1	1	1	1	1	1	1	1	1
0	2	2	1	1	1	1	1	1	1	1	1	1	1	1	1	1	1	1	1

FIGURE 34: MIL 8785C Levels for Category A Flight (X-2) for $nZ = 0.1$

For the high altitude semi-ballistic trajectories, the load factor is changed to $nZ = 0.1$. With this change in load factor, there are no significant changes between FIGURE 33 and 34. In FIGURE 34, the rest of the flight envelope in the bottom left corner was opened up as well as some additional points swapping from *LEVEL 2* back to *LEVEL 1*.

Lateral-Directional Stability for Baseline Configuration

When looking at the Dutch Roll Frequency one must ensure that the frequency is not too slow or too fast. MIL8785C suggests a minimum frequency of 0.4 to 1 rad/s depending on the class of the aircraft. FIGURE 35 shows that the Dutch Roll Frequencies are reasonable throughout the entire flight envelope. At low altitude and high-speed, again the frequency does get quite fast, thus coupling with the Short Period may occur.

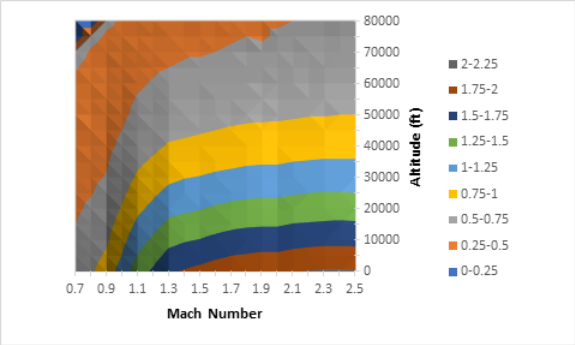

FIGURE 35: Dutch Roll Sky Map (X-2)

The Dutch Roll damping shown in FIGURE 36, appears to be highly dominated by altitude with speed having very little influence. Overall, the damping is quite light and will likely need synthetic damping to improve the handling qualities. This can be achieved by wiggling the rudder or other yaw device through the implementation of a yaw damper system.

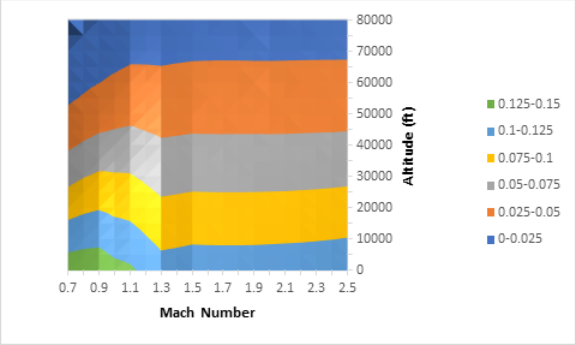

FIGURE 36: Dutch Roll Damping Sky Map (X-2)

LCDP is shown in FIGURE 37. An interesting trend that can be observed is that *LCDP* appears to be a strong function of speed with altitude having very little effect. As the speed increases *LCDP* decreases greatly going to smaller values pushing the aircraft toward the F-region or other non-spin resistant regions on the Weismann chart. For A-

Region characteristic, *LCDP* must be positive. As the value gets closer to zero, the spin-resistance of the aircraft likely suffers.

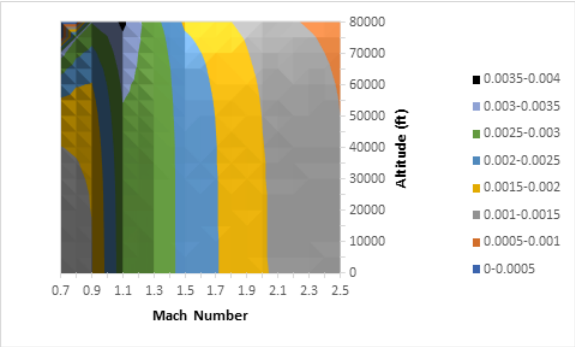

FIGURE 37: *LCDP* with Aileron Control (X-2)

Cnβdynamic is shown in FIGURE 38. From this figure it is suggested that *Cnβdynamic* is a strong function of both altitude and speed. For a large portion of the flight envelope, *Cnβdynamic* does not meet the Skow criterion, anything under the orange curve.[8] For an aircraft to be in the A-Region, *Cnβdynamic* should be greater than 0.004. This is where the *X-2* suffers as most of the flight envelope that it operated in was where *Cnβdynamic* was low. This is likely the key parameter that results in the *X-2* having poor lateral-directional stability.

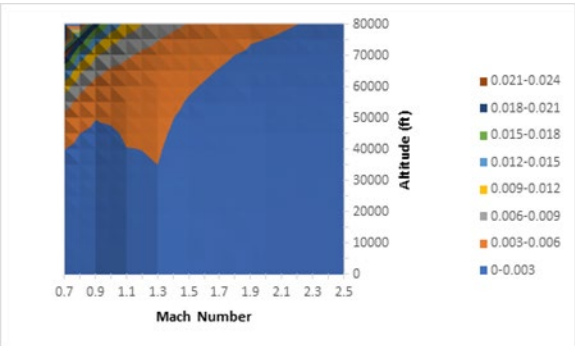

FIGURE 38: *Cnβdynamic* with Aileron Control (X-2)

The next parameters to examine are the Roll and Spiral Modes. When these frequencies lie on top of each other, there may be a chance that "Lateral Phugoid" coupling may occur.[6] Teodorescu noted the existence of this previously neglected lateral-directional oscillatory-departure mechanism generated by the roll time constant of any lateral control input exciting the Spiral Mode. He explains that this mode is extremely difficult to suppress. [38]

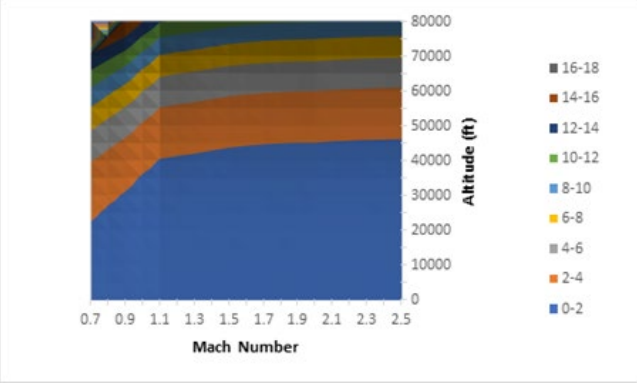

FIGURE 39: Spiral Mode Time Constant (X-2)

The Spiral Mode is shown in FIGURE 39. An interesting trend to observe is that at subsonic to transonic speeds there is strong dependence on speed. Once the aircraft is supersonic, it appears that the Spiral Mode is mainly a function of altitude. Once at supersonic speeds, the Spiral Mode time constant only increases ever so slightly.

The Roll mode is shown in FIGURE 40. A similar trend to the Spiral Mode is observed: at subsonic to transonic speeds, there is a strong dependence on altitude and speed. Once supersonic, the Roll mode appears to be only dependent on altitude and approaches a constant steady state value.

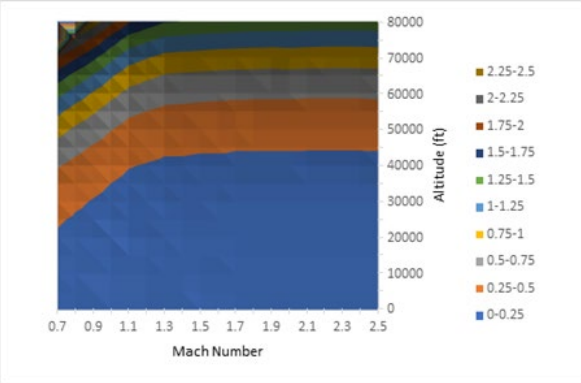

FIGURE 40: Roll Mode Time Constant (X-2)

When looking at the magnitudes of the Spiral Mode and Roll Mode it can be determined that the Spiral Mode is significantly greater than the Roll mode and thus Roll-Spiral "Lateral-Phugoid" coupling will likely never occur for the *X-2*.

Flight Envelope Limitations due to Trim and Stability Restrictions

To gain more insightful details on suitable flight envelopes for an aircraft, the presented sky maps can be further refined. There are numerous ways to restrict the data based on what the designer is focused on. If the aircraft is suspected to be prone to inertial coupling, a potential solution is to take the percent difference between the Short Period and Dutch Roll Frequencies as shown in FIGURE 41. This allows the engineer to see where in the flight envelope the frequencies lie on top of each other. When the two frequencies are close there is the potential for cross talk between the two. This cross talk will then feed into inertial coupling as discussed previously. A similar idea can be applied to the Roll and Spiral Modes to try and restrict coupling between those two modes.

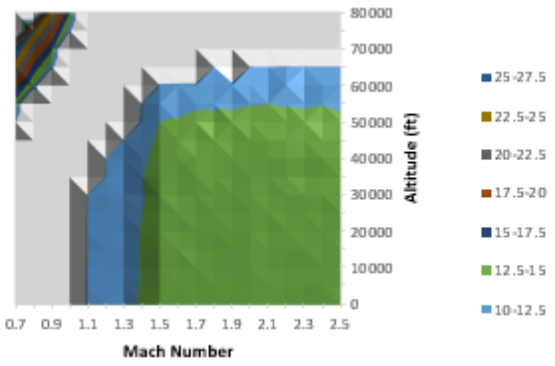

FIGURE 41: Checking Percent Difference Between Short Period and Dutch Roll Modes (X-2)

As was discussed previously, a simple restriction on *Cnβdynamic* should come from the Skow Criterion shown in FIGURE 42.[8] This allows the designer to quickly see where in the flight envelope lateral directional stability is lacking or if those regions can be avoided entirely.

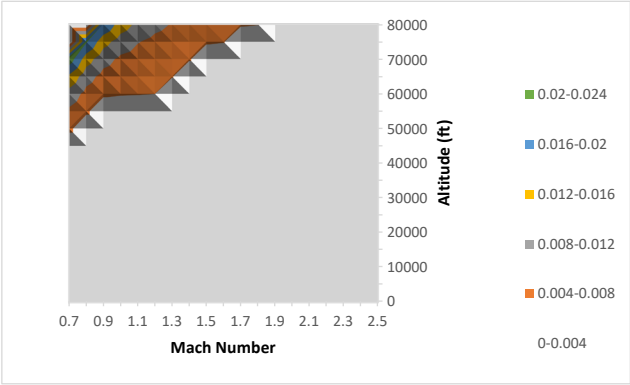

FIGURE 42: Available Flight Envelope if Bounded Skow Criteron (X-2)

When targeting ideal values for certain parameters the flight envelope may become entirely blanked out as the various screening parameters are restricting different parts of the envelope. This is easily seen in FIGUREs 41 and 42 where, if the two plots were superimposed the only desirable region is the top left corner of the envelope. This is not a feasible envelope as there is no clear arc for the aircraft to follow as it varies in speed and

altitude from subsonic to supersonic. As more and more restrictions are placed on the aircraft the more difficult it becomes to find a suitable flight envelope. This is seen in those two figures as high-speed flight is totally inaccessible if those two criteria need to be met. This results in the engineer having to decide which of the stability screening parameters are going to bound the problem as it is possible that the entire flight envelope will become inaccessible. It is felt that *CnβDynamic* and *LCDP* are the top two parameters to satisfy as lateral-directional stability is the most troublesome issue on highspeed slender aircraft.

This conclusion in the restriction of the flight envelope matches the history of the Bell X-2 program, where many stability problems were encountered resulting in the loss of the pilot and aircraft. When just considering *CnβDynamic* and inertial coupling risk, practically the entire flight envelope is full of the risk from stability. From these restrictions, it is shown that X-2 was fatally flawed and some changes to the design are required along with the implementation of a closed loop system.

Assessment of the impact of Aileron-Rudder Interconnect

To address the adverse yaw problems, a simple *ARI* scheme can be plotted as a function of Mach and altitude. Using a simple gain ratio will allow for an overall magnitude of effectiveness and feasibility to be determined. More complex control schemes could be investigated that make use of state-space analysis and transfer functions. These more rigorous/complex methods would allow for unsymmetric-differential tail or aileron, potentially opening up more feasible solutions.

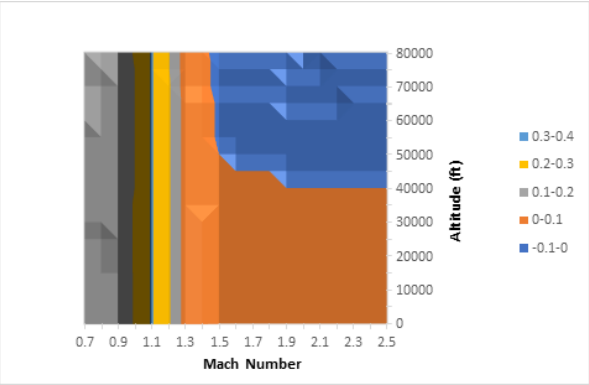

FIGURE 43: *ARI* Scheduling Required when Using Aileron for Roll Control (X-2)

For the conventional *X-2* configuration the *ARI* scheme shown in FIGURE 43 was obtained. There are a couple of interesting trends to notice. First, is that up until around Mach 1.4 the *ARI* gains are positive until switching sign and becoming more negative. For most high-speed flight and moderate altitude, a gain of around -10 % is required. Only high magnitude gains are required at high altitude flight, which is expected as aerodynamic control surfaces lose their effectiveness. This is also the area where departure from stable flight is most likely to occur. When first plotting the *ARI* obtained when using the differential tail as the primary roll controller, it was noticed that all gains were essentially zero. With the differential tail having no values of interest, it is not included here.

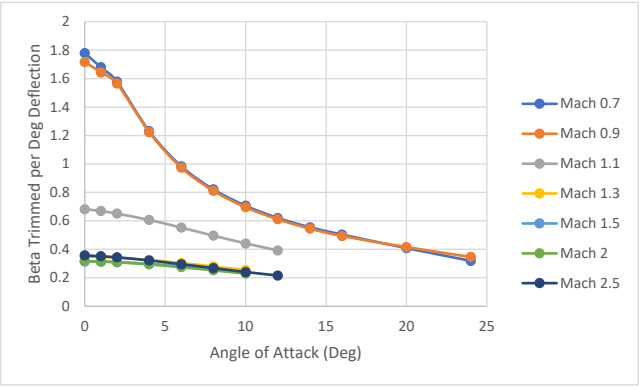

FIGURE 44: Aileron Sideslip per Degree to Trim (X-2)

However once considering the sideslip that can be trimmed, the ineffective differential tail makes sense. FIGURE 44, shows the sideslip angles that the conventional aileron configuration can trim. Assuming 30 degrees of deflection out of the rudder and ailerons, only 0.33-degree sideslip per degree of control surface deflection is required to trim to 10 degrees of sideslip. At subsonic and small angles of attack, the *X-2* can trim to around 40 degrees of sideslip.

At subsonic speeds the sideslip trim power is quite high but, it quickly decreases with increasing Mach Number. It should be noted that not all angles of attack are included with the higher Mach Number cases as the aircraft could not trim to zero pitching moment at those points. Even at the highest Mach Number run and moderate angles of attack, the conventional configuration can still trim to about 8-degrees of sideslip.

FIGURE 45 shows the sideslip angles that the differential tail configuration can trim to. From the figure it is concluded that no roll control can be established from the differential horizontal tail, as not even a degree of sideslip is trimmable. At zero degrees angle of attack, around a maximum of 10 degrees of sideslip can be achieved, with increasing angle of attack rapidly decreasing sideslip performance. In addition, using a differential tail requires some level of collective deflection for trim thus, a full 30 degrees of elevator deflection is not obtainable like the aileron case. This indicates that the horizontal tail is just too small to be effective. While differential all moving horizontal tails appear to be effective on many modern high-speed aircraft, it does not work on the *X-2* due to its small size.

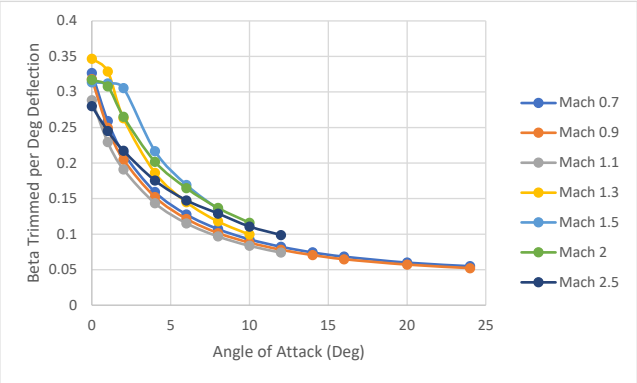

FIGURE 45: Aileron Sideslip per Degree to Trim (X-2)

Assessment of the impact of the enlarged vertical tail

Now looking at the impact on the lateral-directional stability of the *X-2* run with a larger vertical tail. With the bigger tail, the *X-2* has greatly increased lateral directional stability.

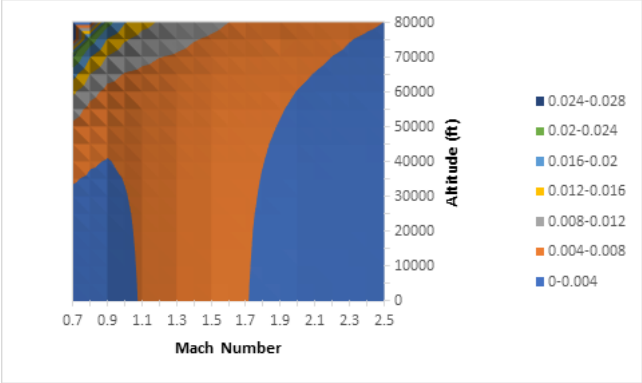

FIGURE 46: Cn Beta Dynamic of *X-2* with Large Vertical

When comparing large tail configuration *Cnβdynamic* shown in FIGURE 46, to the Baseline Configuration bounded by Skow Criterion back in FIGURE 38, it is shown that a much larger portion of the flight envelope has opened. The overall maximum value of *Cnβdynamic* increased from 0.024 to 0.028. Now a desirable pocket in the middle of the flight envelope has opened, where the *X-2* should be spin resistant. Remember on the

updated Bihrle-Weissman chart, *LCDP* needs to be positive and *Cnβdynamic* greater than 0.004.

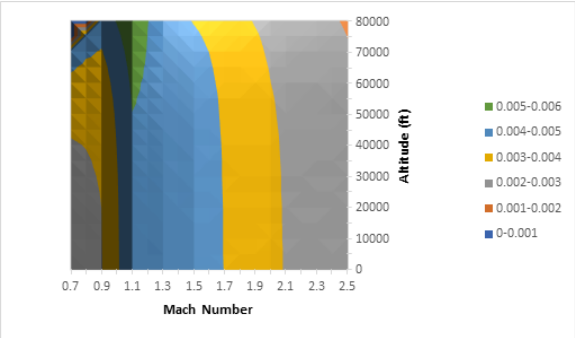

FIGURE 47: *LCDP* of *X-2* with Large Vertical Tail

When looking at *LCDP* shown in FIGURE 47, there are not really any major differences in the trends first observed in FIGURE 37. The magnitude of *LCDP* did increase by 0.002, with more of the flight envelope falling in between the values of 0.005 and 0.002 when compared to the base configuration. This further strengthened the lateral directional controllability.

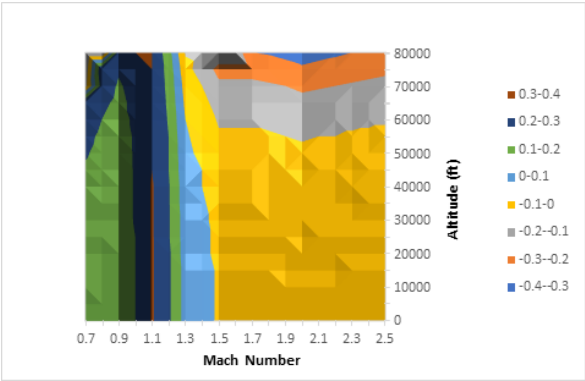

FIGURE 48: *ARI* Scheduling Required when Using Differential Tail for Roll Control (X-2)

The last parameter of interest to compare is the *ARI* gains. When comparing FIGURE 48 to FIGURE 43, the gains have been reduced slightly. For the large tail re-configured *X-2*, if an *ARI* was utilized it appears that on average the *ARI* gains would have

to have a 10% margin subtracted off, resulting in more reasonable gain percentages at high-speed and altitude.

While increasing the tail has seemed to greatly increase the lateral-directional stability one must also keep in mind the mass properties of the aircraft. With the mass properties held constant the feasibility of extending the tail to be this large is likely not possible due to weight and balance reasons. For this reason, other key parameters like the Dutch Roll Frequency and damping will not be addressed due to their high dependence on mass properties.

Conclusions from *X-2* Analysis

When looking that the longitudinal stability of the *X-2*, it can be determined that throughout the typical flight envelope the aircraft had a reasonable Short Period Frequency with the damping being quite light. When plotting the handling qualities, it was additionally found that the *X-2* had *LEVEL 1* and *LEVEL 2* regions in the flight envelope resulting in satisfactory handling qualities.

For lateral directional stability, the *X-2* suffered greatly from *Cnβdynamic*. For the Baseline Configuration only a small region of low speed and high-altitude flight met the Skow criterion. When comparing it to the larger vertical tail configuration it was found that *Cnβdynamic* was able to recover reasonably well. With the larger vertical tail configuration an ideal and routinely used portion of the flight envelope opened. Overall, the Dutch Roll frequency and *LCDP* were found to be causing no issues. There are substantial areas where the Short Period and Dutch Roll Frequencies are within 10% of each other, thus there is concern for inertial coupling. For the large vertical tail configuration *LCDP* was

strengthened pushing the *X-2* further away from the F-region. It was found that the *X-2* did not suffer from an unstable Roll Mode or Spiral Mode or a coupling of the two modes.

From this analysis some conclusions on high-speed flight can be made. For lateral-directional stability to be satisfied, high-speed aircraft really require larger than expected vertical tails. The larger vertical tails help shift *Cnβdynamic* to be greater than the Skow Criterion to ensure that the aircraft is departure resistant. As these vehicles fly faster, the damping on the frequencies become quite poor thus, synthetic damping and some type of control system is likely a necessity. The last point of concern is that as these aircraft fly faster and especially at lower altitudes, the aerodynamic frequencies become so large resulting in the possibility of exciting the structural frequencies causing vibrations or inertial coupling.

ANALYSIS OF THE NORTH AMERICAN *X-15*

For the analysis of the *X-15*, again longitudinal and lateral directional stability will be considered. Key aerodynamic properties required for calculations in the *X-15's* analysis is summarized in Table 11. [16]

Table 11: Key Properties of the *X-15* [16]

S_{ref} (ft^2)	200
b (ft)	22.36
$\bar{c}$ (ft)	8.94
W (lbm)	14,300
I_{xx} (lbm/ft^2)	116,000
I_{yy} (lbm/ft^2)	2,730,000
I_{zz} (lbm/ft^2)	2,780,000
I_{xz} (lbm/ft^2)	-20,900

With the *X-15* implementing new technologies such as a reaction control system and closed loop feedback controllers, looking at how much aerodynamic stability the *X-15* inherently has is the primary goal. One of the difficulties in the analysis of the *X-15* is translation between the panel model and the construction of the true aircraft due to the wedge control surfaces. During the period of the *X-15*'s design, it was discovered that wedge shaped airfoils/control surfaces performed well at high-speed due to the additional control power they provided. This additional control power will not be captured and thus likely the *X-15* model presented will be on the more pessimistic side in regard to rudder performance. In addition to the wedge shape, the *X-15* featured an all moving vertical tail for extra control power. The dimensions for the dorsal vertical tail are given in Table 12.

Table 12: *X-15* Vertical Tail Parameters

	Dorsal (total)	Ventral
Cr (ft)	10.27	10.27
Ct (ft)	7.60	9
B (ft)	4.66	1.49
Sv (ft^2)	41.65	14.35

	Dorsal (All Moving)
Cr (ft)	9.38
Ct (ft)	7.60
B (ft)	3.11
Sv (ft^2)	36.39

Longitudinal Analysis

The first area of analysis will be the Short Period Frequency shown in FIGURE 49. The Short Period Frequencies for the *X-15* are balanced nicely throughout the flight envelope. Between 40-60 thousand feet, the Short Period ranges from around 1.5 to .5-Hz which is responsive without being too fast or slow.

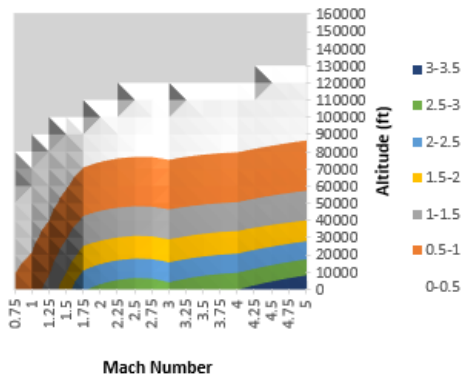

FIGURE 49: Short Period Sky Map *X-15* at $nZ = 1$

When considering the pitch responsiveness and plotting on the MIL STD 8785-C chart, the longitudinal stability appears to be mediocre with most of the flight envelope at *LEVEL 2* characteristics. FIGURE 50 shows that at even moderate altitudes (i.e., from 40,000 to 60,000-ft) the *X-15* exhibits poor longitudinal handling characteristics at low speed. This may likely be due to the placement of the center of gravity, as the aerodynamic center shifts. For higher altitudes it is expected that the handling qualities will diminish due to the low dynamic pressure.

Altitude (ft) \ Mach	0.75	1.00	1.25	1.50	1.75	2.00	2.25	2.50	2.75	3.00	3.25	3.50	3.75	4.00	4.25	4.50	4.75	5.00
160000																2	2	2
150000																		
140000																		
130000																		
120000								2	2		2	2	2	2	2	2	2	2
110000						2	2	2	2	2	2	2	2	2	2	2	2	2
100000				2	2	2	2	2	2	2	2	2	2	2	2	2	2	2
90000			2	2	2	2	2	2	2	2	2	2	2	2	2	2	2	2
80000		2	2	2	2	2	2	2	2	2	2	2	2	2	2	2	2	2
70000		3	2	2	2	2	2	2	2	2	2	2	2	2	2	2	2	2
60000	2	3	2	2	2	2	2	2	2	2	2	2	1	1	1	1	1	1
50000	2	3	2	2	1	1	1	1	1	1	1	1	1	1	1	1	1	1
40000	2	3	2	2	1	1	1	1	1	1	1	1	1	1	1	1	1	1
30000	2	3	2	1	1	1	1	1	1	1	1	1	1	1	1	1	1	1
20000	2	2	2	1	1	1	1	1	1	1	1	1	1	1	1	1	1	1
10000	2	2	1	1	1	1	1	1	1	1	1	1	1	1	1	1	1	1
0	2	2	1	1	1	1	1	1	1	1	1	1	1	1	1	1	1	1

FIGURE 50: MIL 8785C Sky Map *X-15* at $nZ = 1$

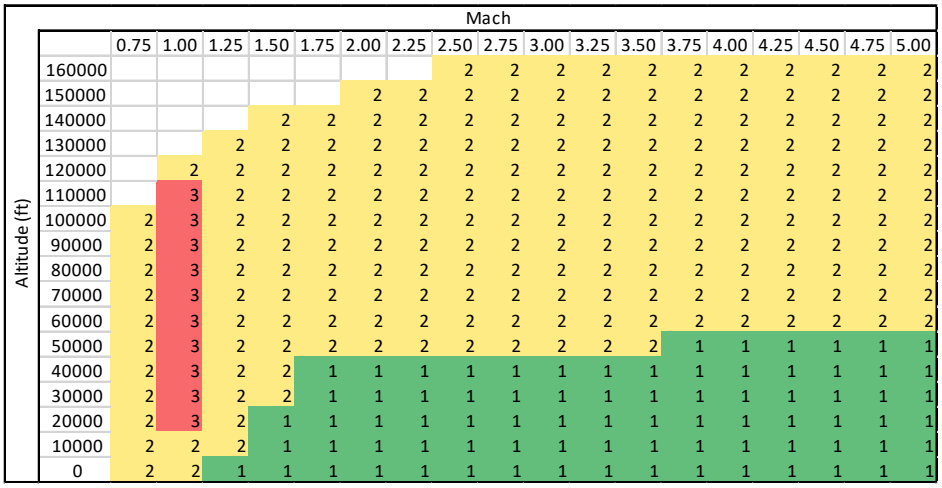

Altitude (ft) \ Mach	0.75	1.00	1.25	1.50	1.75	2.00	2.25	2.50	2.75	3.00	3.25	3.50	3.75	4.00	4.25	4.50	4.75	5.00
160000								2	2	2	2	2	2	2	2	2	2	2
150000						2	2	2	2	2	2	2	2	2	2	2	2	2
140000				2	2	2	2	2	2	2	2	2	2	2	2	2	2	2
130000			2	2	2	2	2	2	2	2	2	2	2	2	2	2	2	2
120000		2	2	2	2	2	2	2	2	2	2	2	2	2	2	2	2	2
110000		3	2	2	2	2	2	2	2	2	2	2	2	2	2	2	2	2
100000	2	3	2	2	2	2	2	2	2	2	2	2	2	2	2	2	2	2
90000	2	3	2	2	2	2	2	2	2	2	2	2	2	2	2	2	2	2
80000	2	3	2	2	2	2	2	2	2	2	2	2	2	2	2	2	2	2
70000	2	3	2	2	2	2	2	2	2	2	2	2	2	2	2	2	2	2
60000	2	3	2	2	2	2	2	2	2	2	2	2	2	2	2	2	2	2
50000	2	3	2	2	2	2	2	2	2	2	2	2	1	1	1	1	1	1
40000	2	3	2	2	1	1	1	1	1	1	1	1	1	1	1	1	1	1
30000	2	3	2	2	1	1	1	1	1	1	1	1	1	1	1	1	1	1
20000	2	3	2	1	1	1	1	1	1	1	1	1	1	1	1	1	1	1
10000	2	2	2	1	1	1	1	1	1	1	1	1	1	1	1	1	1	1
0	2	2	1	1	1	1	1	1	1	1	1	1	1	1	1	1	1	1

FIGURE 51: MIL 8785C Sky Map *X-15* at *nZ* = 0.1

Additionally, the ballistic trajectory case is examined which is shown in FIGURE 51. When comparing FIGURE 51 and 50, The flight envelope is much more open, with moderate handling characteristics all the way to 150,000-ft and high Mach Numbers.

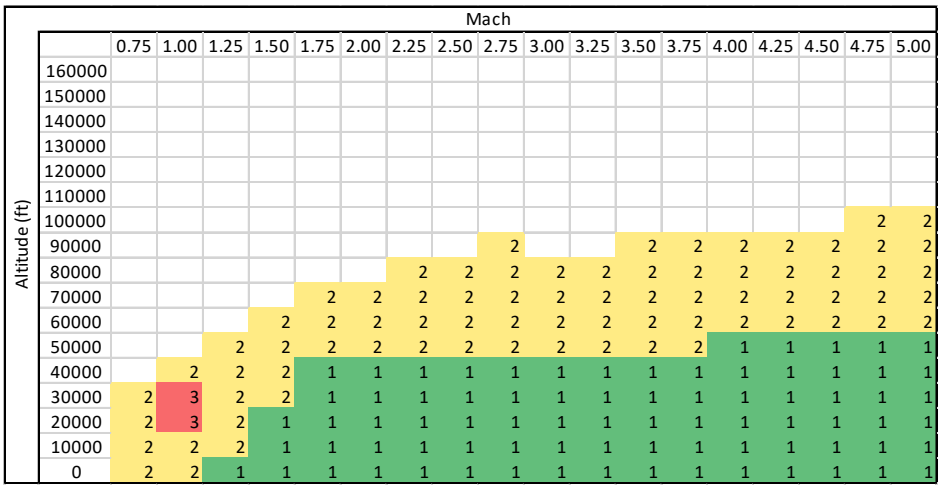

Altitude (ft) \ Mach	0.75	1.00	1.25	1.50	1.75	2.00	2.25	2.50	2.75	3.00	3.25	3.50	3.75	4.00	4.25	4.50	4.75	5.00
160000																		
150000																		
140000																		
130000																		
120000																		
110000																		
100000																	2	2
90000									2			2	2	2	2	2	2	2
80000							2	2	2	2	2	2	2	2	2	2	2	2
70000					2	2	2	2	2	2	2	2	2	2	2	2	2	2
60000				2	2	2	2	2	2	2	2	2	2	2	2	2	2	2
50000			2	2	2	2	2	2	2	2	2	2	2	1	1	1	1	1
40000		2	2	2	1	1	1	1	1	1	1	1	1	1	1	1	1	1
30000	2	3	2	2	1	1	1	1	1	1	1	1	1	1	1	1	1	1
20000	2	3	2	1	1	1	1	1	1	1	1	1	1	1	1	1	1	1
10000	2	2	2	1	1	1	1	1	1	1	1	1	1	1	1	1	1	1
0	2	2	1	1	1	1	1	1	1	1	1	1	1	1	1	1	1	1

FIGURE 52: MIL 8785C Sky Map *X-15* at *nZ* = 3

The other interesting case to look at is the banked reentry problem. If the *X-15* did not bank excessively, it would perform atmospheric skips rather than reentry. For the bank case example an assumed 70.5-degree bank angle or a load factor of nZ=*3* is used. When examining FIGURE 52, the flight envelope is heavily restricted to high-speed flight only

sub-100,000-ft. To reenter the atmosphere, it appears that the maneuver must be completed with level two handling characteristics, as *LEVEL 1* characteristics begin to appear well within the atmosphere at 40,000-ft. These *LEVEL 1* and *Level 2* characteristics indicate a lack in open loop bandwidth where the aircraft will appear to response sluggishly.

This indicates the need for a reaction control system to assist with the maneuvering of the aircraft at these high altitudes. To conduct the banking maneuver some assistance is required from the onboard thrusters to maintain control.

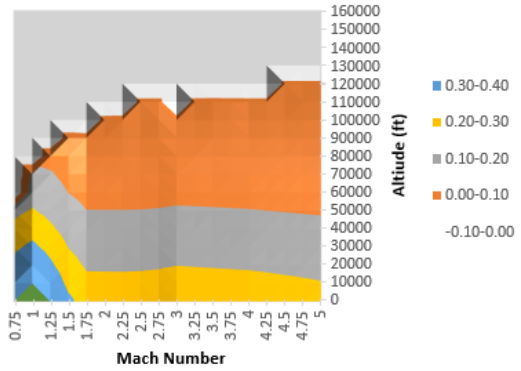

FIGURE 53: Short Period Damping Sky Map (*X-15*)

When considering the Short Period Damping on the *X-15*, shown in FIGURE 53, it appears to be relatively okay at moderate altitudes. From 40,000 to 20,000-ft, the *X-15* has around 10-20% damping with damping getting all the way up to 50% near sea level. Once again, the high-altitude issue is present with the damping approaching zero at 90,000-ft for high Mach Number and around 60,000-ft for the subsonic case. To help add in the control at the low damping points, some type of synthetic damping will be required to make maneuvering manageable, remember LEVEL 1 characteristic are at a damping ratio of 0.35 or higher.

Lateral-Directional

Starting the analysis with the Dutch Roll, shown in FIGURE 54. Throughout the entire flight envelope, the *X-15* exhibits good Dutch Roll Frequencies which are decently separated from the Short Period while still fast enough to avoid pilot induced oscillations. At high altitude the Dutch Roll performance does begin too sour as expected due to the very low dynamic pressures.

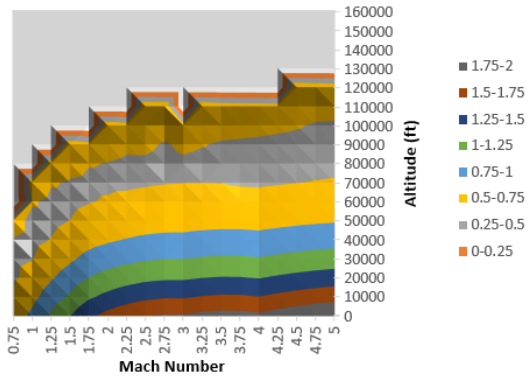

FIGURE 54: Dutch Roll Sky Map (*X-15*)

FIGURE 55 shows the Dutch Roll Damping. The Dutch Roll Damping is extremely bad, with a max damping ratio of 12% occurring at sea level and Mach 3+. For all other regions of the flight envelope, the damping is extremely light at around 2.5%.

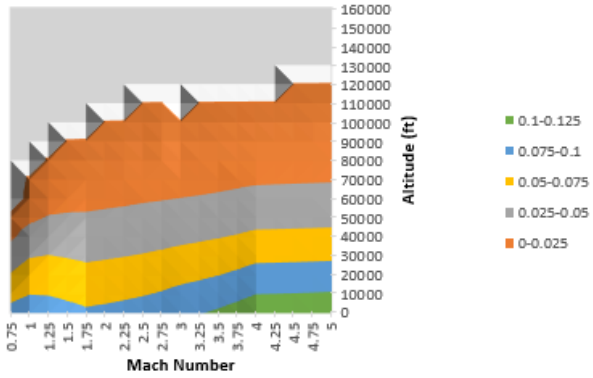

FIGURE 55: Dutch Roll Damping Sky Map (*X-15*)

When examining *Cnβdynamic*, shown in FIGURE 56, there appears to be a nice solid band where the Skow Criteron is met. With the range of *Cnβdynamic* being quite large, it makes it difficult to determine the cutoff for acceptable values.

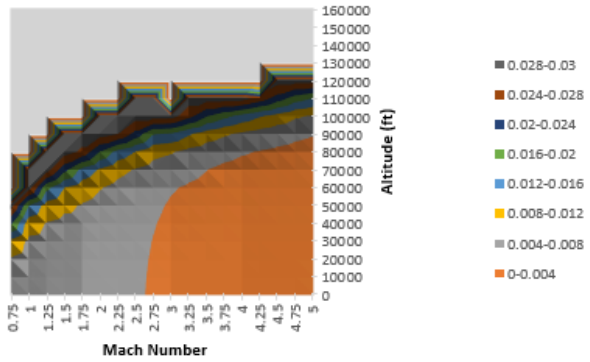

FIGURE 56: Cn Beta Dynamic Sky Map (*X-15*)

To show more clarity, FIGURE 57 shows *Cnβdynamic* with the Skow filter on. From this, it appears that the *X-15* does not necessarily suffer from a *Cnβdynamic* issue if the flight trajectory is carefully planned. Some areas of concern are low altitude and low Mach Number which appear to be right on the bound of region A.

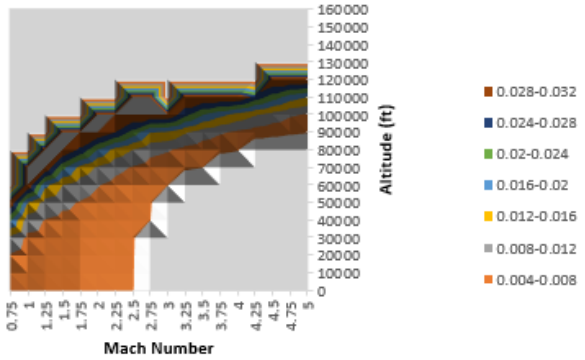

FIGURE 57: Cn Beta Dynamic Bounded by Skow Criterion Sky Map (*X-15*)

When examining *LCDP,* shown in FIGURE 58, it is shown that for all Mach and angle of attack combinations *LCDP* is positive indicating strong departure resistance.

Additionally in the figure, it is observed that when the *X-15* has subsonic leading edges, the aircraft can still pitch to the max angle of attack case. When the horizontal tail is transitioning from subsonic to supersonic around Mach 1.75, it is shown that the trim performance decreases substantially to 10 degrees angle of attack before recovering to 15 degrees.

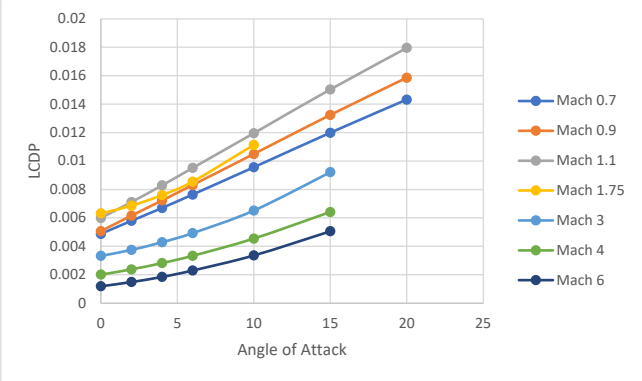

FIGURE 58: *LCDP* vs AoA (*X-15*)

The Roll mode for the *X-15* is shown in FIGURE 59. For most of the flight envelope, the Roll mode is within 2.5 seconds. Once at high altitude and high Mach Number, the Roll mode being to slow down considerably reaching around 20 seconds. This causes the aircraft to be much more unresponsive at high altitudes, further necessitating the need for the control system.

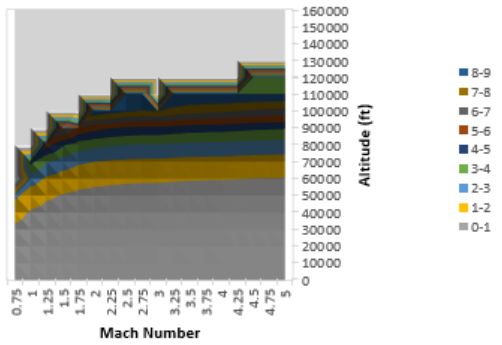

FIGURE 59: Roll Mode Sky Map (*X-15*)

Similarly for the Spiral Mode shown in FIGURE 60, the time constant is relatively short for a majority of the flight envelope. Once at the edge of the atmosphere the time constant begins to increase to extreme levels going in excess of 16 seconds.

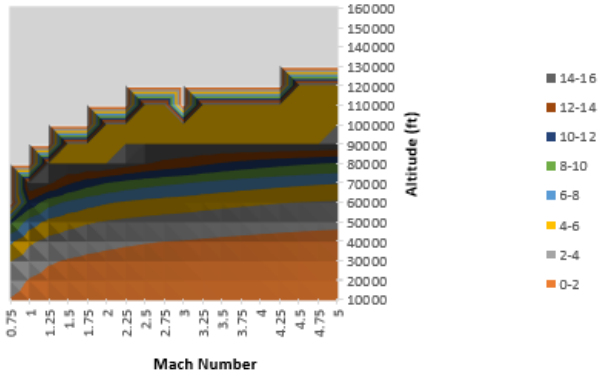

FIGURE 60: Spiral Mode Sky Map (*X-15*)

ARI Implementation

With the *X-15* being a solely differential tail vehicle, an *ARI* with differential tail is considered. The first area of interest is the sideslip trim per degree of deflection shown by FIGURE 61. For all moderate angles of attack, the *X-15* has acceptable sideslip performance.

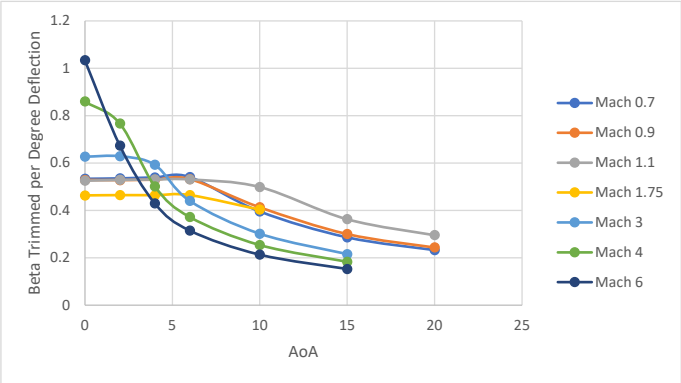

FIGURE 61: Sideslip Trim per Degree of Control Surface Deflection for *X-15*

The differential tail *ARI* gains are shown in FIGURE 62. For a simple *ARI* to work on the *X-15,* sufficiently large gains would be required. For high-speed flight, gains of 20-50% would be required, and for subsonic flight gains of more than 70% are required. When *ARI* gains are this large, the maneuverability of the aircraft diminishes significantly as most of the control power is being used to counteract the adverse yaw. With this in-mind, based on the panel method estimation of the *X-15*, a simple *ARI* would not be sufficient in major portions of the flight envelope. The increase yaw effect of the wedge tail would likely help decrease the magnitude of these gains. To remedy this, supplemental inputs from the reaction control system would likely be required for any maneuvers to correct unintended sideslip angles.

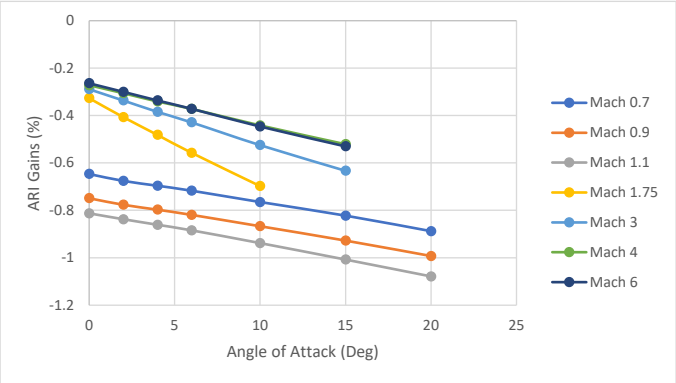

FIGURE 62: *ARI* Scheduling Required (*X-15*)

Conclusion From *X-15* Analysis

When considering the longitudinal and trim performance, it was shown that the *X-15* potentially had level two handling characteristics throughout large portions of the flight. While the center of gravity estimations may possibly exaggerate the handling qualities, this analysis captures some possibilities that were encountered. The *X-15,* while a relatively small aircraft, flew a variety of configurations that likely impacted the center of gravity on each mission. Some of these configurations included external fuel tanks, lower ventral on/off, various ablative coatings, and a model ramjet.

When looking at the various load factor configurations, it was shown that as the load factor applied increased, the obtainable flight envelope shrinks. At lift equal weight the *X-15* could fly at 100,000-ft with LEVEL 2 characteristics at Mach 2+, with a load factor of three the altitude dropped to 80,000-ft, and with a factor of 0.1 the altitude increased all the way to 150,000-ft. While the load factor impacted the altitude, the handling quality levels saw minimal to no impact as was with the X-2.

From this analysis, the *X-15* appeared to have reasonable lateral-directional performance for a majority of the flight envelope. With *LCDP* being positive, *Cnβdynamic* was the limiting factor if the *X-15* left the small band of strong lateral directional stability as shown in FIGURE 57 and 58. When coming in at Mach 2+ below 70,000-ft, the *X-15* leaves the A region and enters the F region where weak departure and spin resistance can be encountered. The *X-15* did have a closed loop roll damper system developed due to uncontrollable Mach and altitude combinations being encountered during reentry simulations. [4] With the roll damper system, the lateral directional stability was able to be strengthened to levels to ensure safety from departure. This control system was unique and different from those utilized today due to structure and relationship with its cold gas reaction thrusters.

Even with a control system installed, these aircraft can still experience departures from stability that are too much for the systems to handle. During a fatal accident in November of 1967, a*n X-15* experienced severe roll coupling issues while performing wing rocking maneuvers at 200,000+-ft. The aircraft entered a Mach 5 spin down to 120,000-ft where it entered a dive. Even with the flight control system onboard, the pilot (Michael Adams) was never able to recover the dive, and the aircraft broke apart. In this case, the combination of lateral-directional departure into excessive Short Period and Dutch Roll frequencies lead to the loss of a pilot and aircraft.

ANALYSIS OF *SKY CRUISER*

Key aerodynamic properties required for calculations in the *Sky Cruiser's* analysis are summarized in Table 13. [29]

Table 13: Key Properties of *Sky Cruiser* [29]

S_{ref} (ft^2)	1058
b (ft)	75
$\bar{c}$ (ft)	14.1
W (lbm)	74,000
I_{xx} (lbm/ft^2)	7,340,000
I_{yy} (lbm/ft^2)	28,000,000
I_{zz} (lbm/ft^2)	29,300,000

With *Sky Cruiser* being a 14 CFR § 25 certifiable aircraft, the Stability & Control of the aircraft was of upmost importance. [30] To comply with federal regulations, additional Stability & Control criteria were required in addition to the previously discussed screening parameters. The two major additional criteria were a crosswind capability of 25 knots as well as calculation of minimum control ground and air speeds in the one engine inoperative case. [30] As *Sky Cruiser* was designed during my undergrad, my initial work on Stability & Control did not include any thought of the potential for differential tail control or an aileron rudder interconnect. In this section, the baseline configuration will be analyzed in more detail with complete flight envelopes being analyzed along with an analysis of the case where differential tail control could be used in maneuvering at high speeds.

Table 14: *Sky Cruiser* Vertical Tail Parameters

	Vertical Tail
Cr (ft)	25
Ct (ft)	18
B (ft)	18
Sv (ft^2)	333

As mentioned previously, the large vertical tail is one of the most notable and controversial aspects of the design to ensure lateral-directional stability. Details for the vertical tail size are summarized in TABLE 14.

Longitudinal Stability for Baseline Configuration

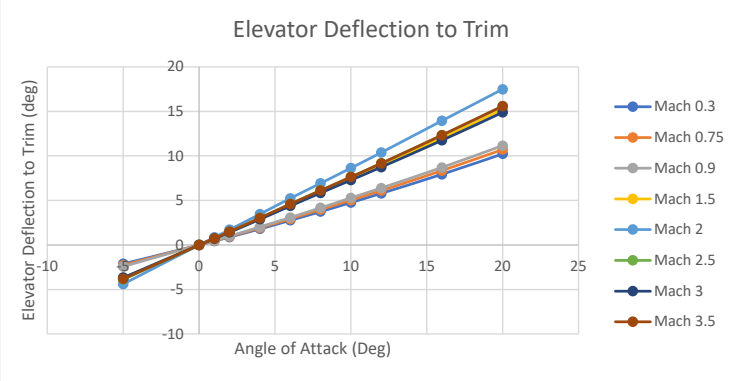

FIGURE 63: Elevator Deflection to Trim (*Sky Cruiser*)

Due to the *Sky Cruiser*'s unique mission profile, a larger all moving horizontal "T-Tail" configuration was utilized. This large horizontal allowed the aircraft to have phenomenal pitch performance as shown in FIGURE 63. At subsonic speed the elevators have two degrees of angle of attack change per one degree of deflection and at supersonic speeds it becomes approximately one to one.

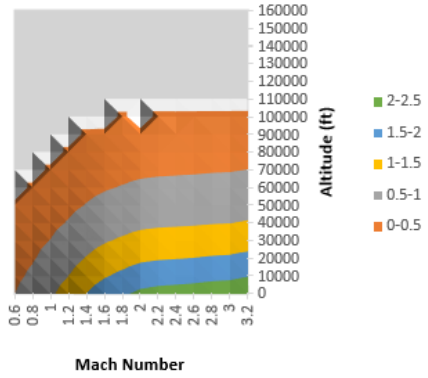

FIGURE 64: Short Period Sky Map (*Sky Cruiser*)

To ensure *Sky Cruiser* has proper longitude handling qualities, the Short Period Frequency is plotted in FIGURE 64. From the figure it is shown that as the aircraft approaches high altitude and high-speed the Short Period remains at an acceptable level of

0.5 to 1-Hz. Once out of the atmosphere, the frequency again unavoidably trends toward zero. Short Period of 2 Hz or more are encountered at high speed and low altitude which should be avoided.

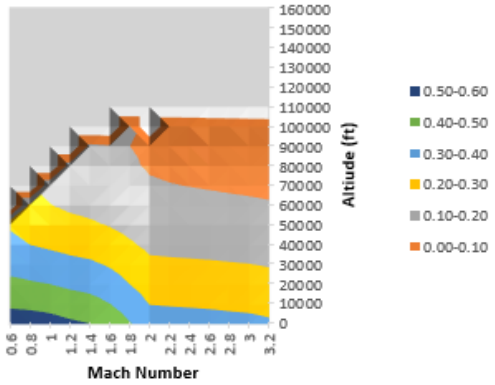

FIGURE 65: Short Period Damping Sky Map (*Sky Cruiser*)

When considering the Short Period Damping on *Sky Cruiser*, shown in FIGURE 65, it appears to be relatively good at moderate altitudes. From 60,000 to 20,000-ft, *Sky Cruiser* has around 10-30% damping with a maximum of 60% near sea level. When subsonic and at cruise altitude Sky Cruiser demonstrates LEVEL 1 damping characteristics. Once again, the high-altitude issue is present with the damping approaching zero at 90,000-ft for high Mach Numbers.

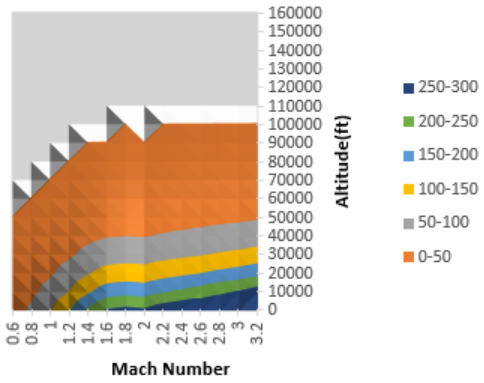

FIGURE 66: Pitch Responsivness Sky Map (*Sky Cruiser*)

Additionally, the pitch responsiveness is at reasonable levels, shown in FIGURE 66. Keep in mind, a pitch responsiveness of 50-100 results to around 1 gee per 1 – 0.6 degrees angle of attack.

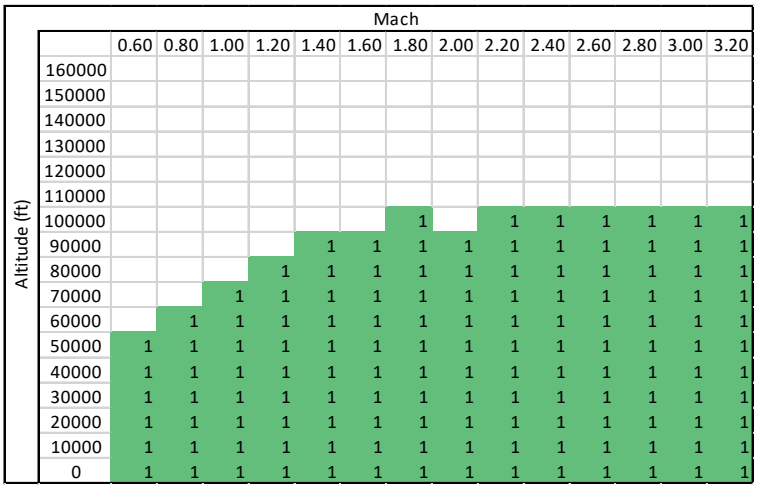

Altitude (ft) \ Mach	0.60	0.80	1.00	1.20	1.40	1.60	1.80	2.00	2.20	2.40	2.60	2.80	3.00	3.20
160000														
150000														
140000														
130000														
120000														
110000														
100000							1		1	1	1	1	1	1
90000					1	1	1	1	1	1	1	1	1	1
80000				1	1	1	1	1	1	1	1	1	1	1
70000			1	1	1	1	1	1	1	1	1	1	1	1
60000		1	1	1	1	1	1	1	1	1	1	1	1	1
50000	1	1	1	1	1	1	1	1	1	1	1	1	1	1
40000	1	1	1	1	1	1	1	1	1	1	1	1	1	1
30000	1	1	1	1	1	1	1	1	1	1	1	1	1	1
20000	1	1	1	1	1	1	1	1	1	1	1	1	1	1
10000	1	1	1	1	1	1	1	1	1	1	1	1	1	1
0	1	1	1	1	1	1	1	1	1	1	1	1	1	1

FIGURE 67: MIL STD 8785C Category B Chart nZ =1

When ploting the Short Period and the Pitch Responiveness with the guidance of MIL8785-C a Sky Map is created for the lift equal weight case or the cruise condition. FIGURE 67 shows that *Sky Cruiser* demonstrates level 1 characteristics on the category B chart at all speeds and altitudes within the atmospheric portions of the flight.

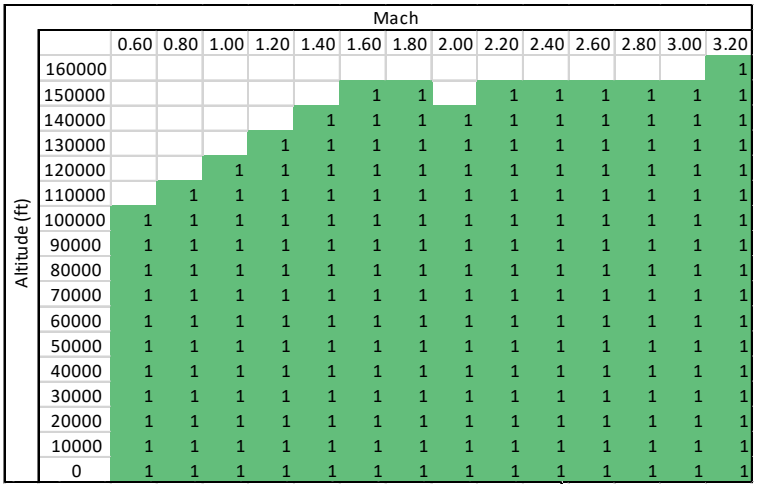

FIGURE 68: MIL STD 8785C Category B Chart $nZ = 0.1$

When taking the ballistic trajectory case, the load factor is switched from 1 to 0.1. Again, the MIL 8785C chart is used and shown in FIGURE 68. When comparing FIGURE 68 and FIGURE 67 that the flight envelope has opened up significantly when at the ballistic trajectory load factor. Now *Sky Cruiser* is showing level 1 handling characteristics up to 160,000-ft compared to the 1-gee case of 100,000-ft. Additionally, it is worth noting that through the extended flight envelope due to ballistic flight, the handling qualities are never diminished.

Lateral-Directional Stability

To ensure that the aircraft had strong lateral directional stability, much attention was given to the vertical tail. The sizing for the massive vertical tail was focused on ensuring strong placement with the A region on the original Bihrle-Weissman chart[15].

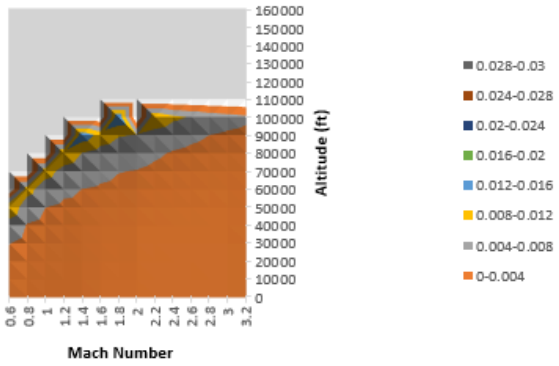

FIGURE 69: Cn Beta Dynamic Sky Map (*Sky Cruiser*)

The first aspect of the sizing was to ensure strong *Cnβdynamic* values as those are often the most crippling part of a design. During the original undergrad work, lateral directional stability was spotted directly on the Weissman-chart as shown in FIGURE 13A. In that approach, key waypoint targets were calculated for stability but not much was known about the other unused portions of the flight envelope. Using Sky maps, *Cnβdynamic* for the flight envelope can be clearly defined. FIGURE 69 shows *Cnβdynamic* throughout the trimmable flight envelope. Throughout most of the flight region *Cnβdynamic* remains strong with some weak areas at moderate speed and low altitude.

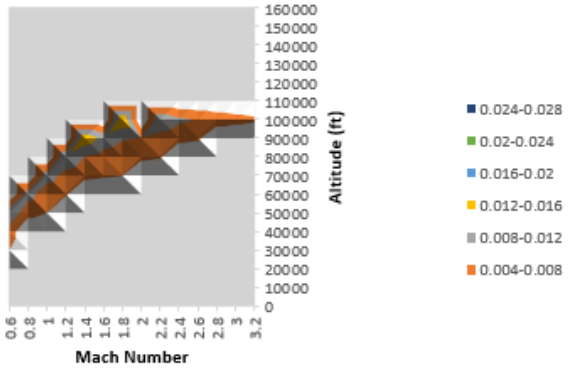

FIGURE 70: Cn Beta Dynamic Bound by Skow Sky Map (*Sky Cruiser*)

To determine the most stable flight envelope the Sky Map can be bounded using Skow's criterion. FIGURE 70 shows the bounded Sky Maps which presents a nice continuous band of flight where *Cnβdynamic* is strong. This demonstrates that a pretty good job was done on the final sizing of the vertical tail to ensure the aircraft would be lateral-directionally stable at a variety of operating conditions.

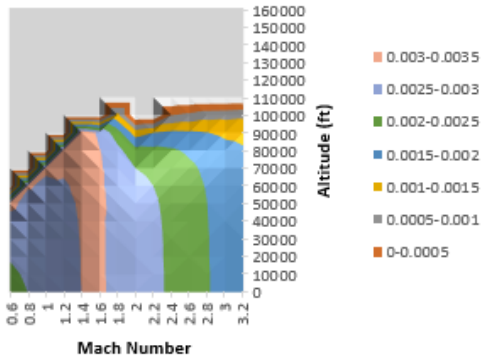

FIGURE 71: *LCDP* Sky Map (*Sky Cruiser*)

To finish characterizing the lateral directional stability characteristics a Sky Map of *LCDP* is created. FIGURE 71 shows that *LDCP* is positive throughout all atmospheric portions of the flight envelope indicating that *LDCP* has no instability problems.

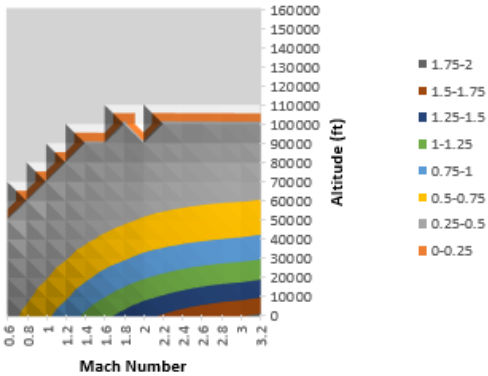

FIGURE 72: Dutch Roll Frequency (*Sky Cruiser*)

Looking at the Dutch Roll frequency presented in FIGURE 72, it is shown that throughout the flight region the frequencies are fast enough to not cause any pilot induced oscillations. At high-speeds and lower altitudes there is possible concern for coupling between the Short Period and Dutch Roll Frequencies as both become quite fast.

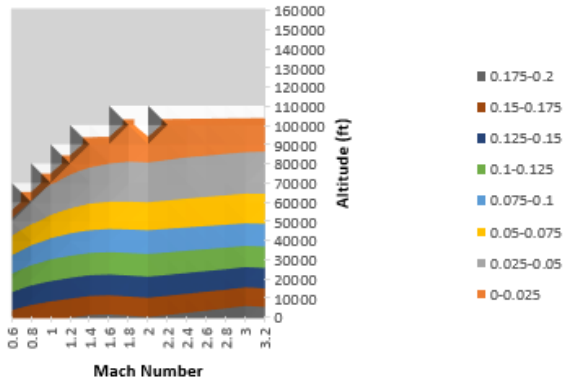

FIGURE 73: Dutch Roll Damping (*Sky Cruiser*)

When considering the Dutch Roll damping shown in FIGURE 73, it is noticed that throughout most of the flight envelope the aircraft only has around 5 to 12% damping varying around LEVEL 2 characteristics. Once above 70,000ft the damping become too and, thus synthetic damping may be an attractive option at high altitudes otherwise additional use of the reaction control system may be required.

With a poorly defined coupled mass moment of inertia, I_{xz} the Spiral Mode cannot be calculated reliably. With the Spiral Mode unable to be obtained, the screening for roll-spiral coupling cannot be completed for this aircraft, and thus will be neglected.

Introduction of an Aileron-Rudder Interconnect

While the original design of the *Sky Cruiser* utilized only ailerons for roll control it was suggested that *Sky Cruiser* could have potentially benefited from using a differential tail configuration with an *ARI* due to its large size.

To first see if differential tail control was reasonable, the amount of sideslip that can be trimmed must be sufficient. To maintain lateral-directional stability, 10 degrees of sideslip should be used as a minimum. FIGURES 74 and 75 give the sideslip trim per degree of control surface deflection for both cases.

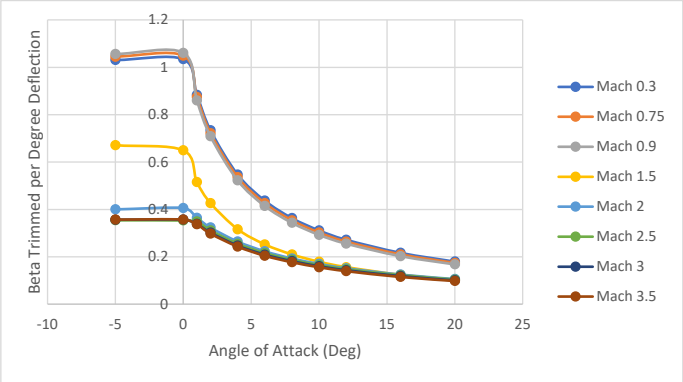

FIGURE 74: Sideslip Trim per degree for Aileron-Rudder Control

For the conventional aileron control case, it is assumed that 30 degrees of control surface deflection can be obtained from both the aileron and rudder. To get 10 degrees of sideslip with 30 degrees, the sideslip trim per degree deflection must be greater than 0.333. From FIGURE 74, the sideslip trim per degree greatly depends on speed and angle of attack. *Sky Cruiser* maintains stiff lateral-directional control all the way to approximately 15 degrees of angle of attack in the subsonic portion of flight. Once the rocket engine is ignited and the aircraft reaches high Mach Numbers, the sideslip trim performance decreases significantly to about 4.5 degrees of sideslip at high angles of attack.

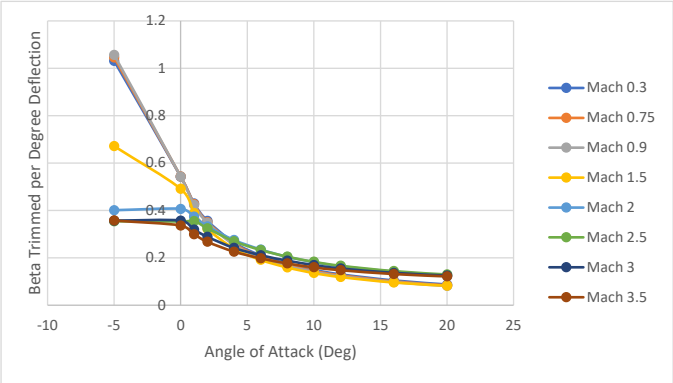

FIGURE 75: Sideslip Trim per degree for Differential-Rudder Control

When looking at the differential tail case shown in FIGURE 75, weaker sideslip performance for the subsonic portions of flight is shown. This indicates that the conventional ailerons would be required to meet the Code of Federal Regulations requirements for crosswind. One aspect to note however is the increased sideslip performance between Mach 2.5 and 3 where an extra degree of sideslip is gained. While *Sky Cruiser* was designed to use a reaction control system to maneuver the aircraft at high altitude, using differential tail could potentially reduce the *RCS* budget by allowing for aerodynamic stability to be regained more quickly.

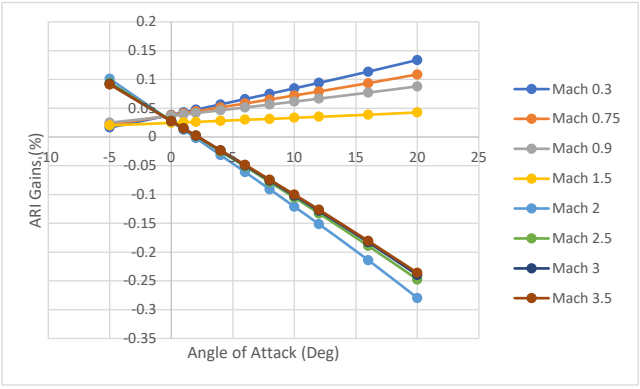

FIGURE 76: *ARI* Gains required for aileron control

With the use of differential tail suggesting that it may be useful, the associated gains must first be considered for use in an *ARI*. The *ARI* gains for the conventional configuration are shown in FIGURE 76. For subsonic flight an *ARI* can easily be implemented as only a 10% gain would be required. Once the aircraft is at high-speeds and angles of attack however, it is shown that the *ARI* gains required increase dramatically. Once the aircraft reaches Mach 2 and 15-degrees angle of attack a gain of around 25% is required, which begins to significantly saturate the controllability of the aircraft.

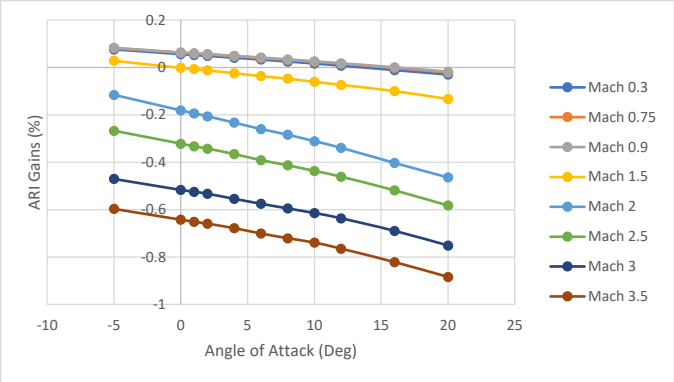

FIGURE 77: *ARI* Gains required for differential tail control

Looking at the differential case, shown in FIGURE 77, it can be seen immediately that the *ARI* gains are much more dependent on Mach Number with only slight influences by angle of attack. Up to Mach 2, the gains for the *ARI* are reasonable but, after Mach 2.5 the become excessive (greater than 35% all the way to 70%).

Since the differential tail configuration has lower gains in some of the higher angle of attack bands then the Baseline Configuration, *Sky Cruiser* could have a mixed control system as it would lead to higher performance. To check the feasibility once again, one needs to look back at the sideslip to trim plot and the elevator deflection to trim plot. Taking 5 degrees as an example angle of attack, from FIGURE 75 it is shown that the *Sky Cruiser*

will have around 0.3 degree of sideslip trim per deflection degree. Now looking at FIGURE 64, it is shown that to trim to 5 degrees, 2.5 degrees of collective deflection is required. This results in the total sideslip able to be trimmed is 8.25 degrees rather than 9 degrees due to some saturation caused by the collective deflection for trim.

Conclusions From *Sky Cruiser*

Looking at the design of *Sky Cruiser*, a couple of interesting points can be made. For large commercial high-speed aircraft, to maintain lateral-directional stability massive vertical tails appear to be required. While the weight implications this will have on the aircraft will be quite extreme, for this hybrid rocket powered and airbreathing type aircraft clever positioning of fuel tanks can overcome that problem. This does beg the question though of when does establishment of aerodynamic stability matter? With the mission of the aircraft being a spaceplane, a reaction control system is already required and thus could be used still in low dynamic pressure regions or other areas of concern. Looking at FIGURE 69, it is shown that the larger vertical tail allows the aircraft to regain aerodynamic stability at around Mach 2.1 and 90,000-ft, which is still quite high in the atmosphere. Should the tail be sized for lower altitudes such as 70,000-ft and what would the impact on the tail size be?

Additionally, from the analysis of *Sky Cruiser*, the increased control power of the large all moving horizontal "T-Tail" was shown for the implementation of a differential horizonal tail control scheme. From the analysis on the *X-2* it was shown that, while it had an all moving horizontal, there was not enough control power to use a differential tail control scheme at moderate angles of attack due to the collective trim. Comparing the

elevator power of the two aircraft it was observed that *Sky Cruiser* had around >1-degree of deflection to 1-degree angle of attack change whereas the *X-2* was around 2-degrees of deflection to 1-degree angle of attack.

ANALYSIS OF HIGH-SPEED SLENDER AIRCRAFT (HSSA)

Key aerodynamic properties required for calculations in the *HSSA's* analysis are summarized in Table 15.

Table 15: Key Properties of High-Speed Slender Aircraft

S_{ref} (ft^2)	35.0
b (ft)	5
$\bar{c}$ (ft)	7.0
W (lbm)	3,000
I_{xx} (lbm/ft^2)	9700
I_{yy} (lbm/ft^2)	193,000
I_{zz} (lbm/ft^2)	193,000

For the analysis of the *HSSA* three versions were created with varying vertical tail and control surface sizes. Without detailed mass properties all three configurations share the key properties listed in TABLE 15. The configuration of a high-speed slender vehicle is difficult due to the relatively small form factor required and operational environment. At hypersonic speeds, aerodynamic heating becomes a key concern and lots of detail is put into a thermal protection strategy.

Often times, it appears that designers try to keep control surfaces out of any of the shock boundary areas to prevent any damage from high heating. With the need for large vertical tails however, then comes the need for portions of the vertical tail to stick out requiring heavy heat resistant materials so they can survive out of the Mach cone. This then in turn, throws off the weight and balance of these configurations requiring a "neutron star"

in the nose to get them balanced. With this aspect of vehicle design addressed, the increased size of the vertical tail throughout the process will most likely breach these boundaries leading to an unrealistic final design. With this acknowledged, the trends associated with attempting to fix the lateral-directional stability with bigger verticals will be shown and their implications considered.

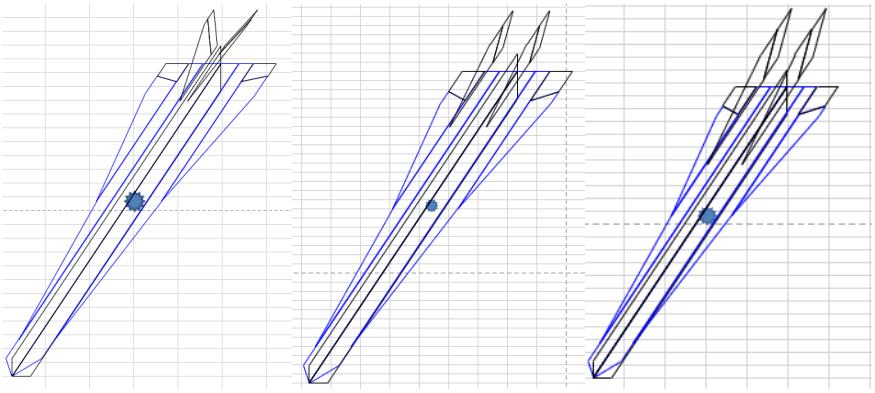

FIGURE 78: *HSSA* Versions (1-Left, 2-Middle, 3-Right)

The panel models for all three aircraft are shown above in FIGURE 78. For the second and third version, the canted twin vertices were replaced by straight verticals due to the excessive pitching moments created by the canted verticals. This will be discussed in more detail below. Key parameters of these three vertical tails are summarized in TABLE 16.

Table 16: Vertical Tail Properties of *HSSA*

	V1	V2	V3
LE Sweep (degree)	70.5	70	70
Canted Angle (degree)	36.7	0	0
Cr (ft)	2.521	3.583	5.167
Ct (ft)	0.625	1.554	2.250
bv (ft)	1.025	1	1.438
Sref (ft^2)	1.611	2.563	5.333

Configuration V1

The first version of *HSSA* shown in FIGURE 78, was thought to resemble many conceptual sketches for hypersonic vehicles. This version has canted verticals that resemble a vertical tail scale seen in many hypersonic conceptual designs.

For any rough pass on stability & Control first the basic stick-fixed stability is analyzed to determine the open loop stability. If the aircraft has poor stick-fixed stability, the design either needs to be immediately reconfigured or a discussion on a closed loop controller must begin.

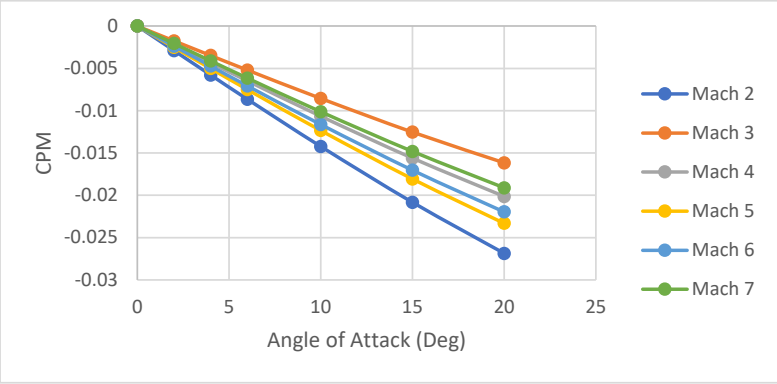

FIGURE 79: Pitching Moment vs Angle of Attack (HSSA V1)

Looking at stick-fixed pitch stability shown in FIGURE 79, the aircraft does have pitch stability. The pitching moments are strongest at the partially subsonic leading-edge case near Mach 2. Right around Mach 3, the aircraft experience a full supersonic flow, and the pitching moment drops to its weakest point.

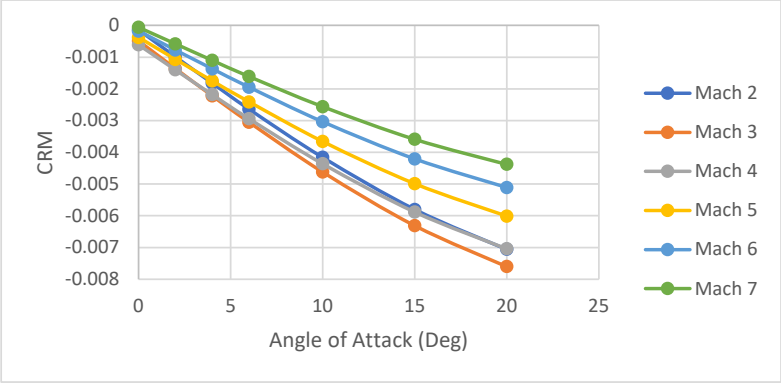

FIGURE 80: Rolling Moment vs Angle of Attack (HSSA V1)

FIGURE 80 shows the aircraft has static roll stability, indicating that the aircraft has some effective positive aerodynamic dihedral. As the vehicle increases in speed the dihedral effect begins to diminish considerably, halving in size from Mach 3 to Mach 7.

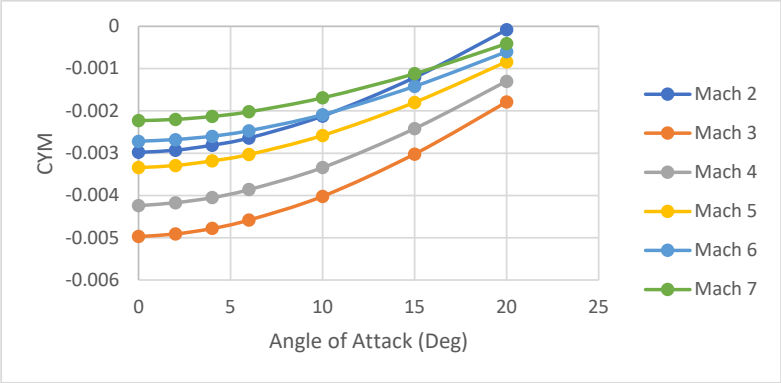

FIGURE 81: Yawing Moment vs Angle of Attack (HSSA V1)

FIGURE 81 shows a positive trend of stability in yaw, but the actual yawing moment coefficients are negative thus, the aircraft does not have inherent yaw stability. As

the angle of attack increases to around 20 degrees, the Mach 2 case almost approaches positive stick-fixed yaw stability. With the yawing moments negative, this indicates that vertical tail size is not large enough. To remedy this problem, the vertical tail size needs to be increased substantially, or a closed loop system implemented. With how unstable the yawing moment is, a closed loop system may not have the bandwidth to counter the undesirable motion, or the gains/synthetic stability required may simply be too large.

With these first three basic criteria unsatisfied, the open loop performance of the aircraft is poor. To quickly check how poor the lateral-directional stability is *Cnβdynamic* and *LCDP* are calculated.

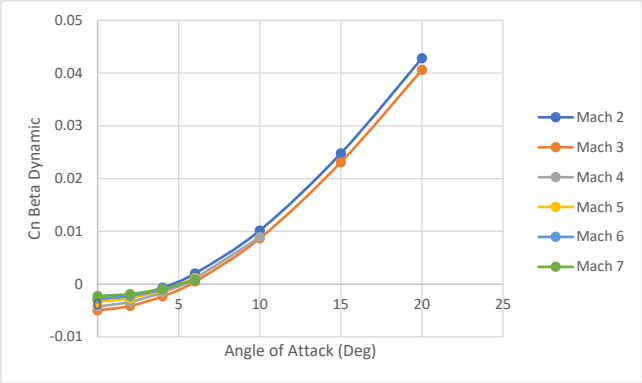

FIGURE 82: Cn Beta Dynamic vs Angle of Attack (HSSA V1)

FIGURE 82 shows *Cnβdynamic* for all possible angles of attack and Mach number. *Cnβdynamic* is negative in all cases up to 5 degrees angle of attack. It is likely not reasonable to trim to these high angles of attack just to try and obtain a reasonable *Cnβdynamic* due to propulsion as well as trim concerns. In addition, it should be noted that once around 7 degrees angle of attack, the Skow Criterion is met.

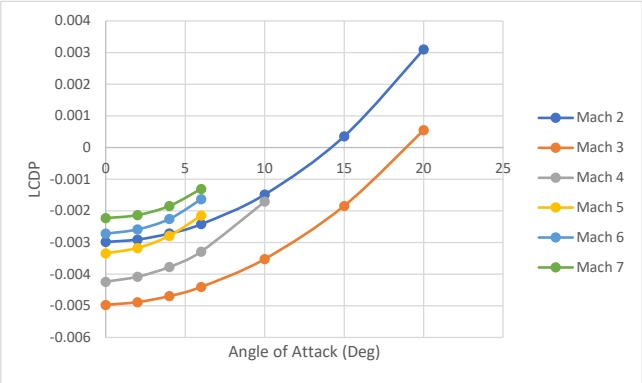

FIGURE 83: *LCDP* vs Angle of Attack (HSSA V1)

FIGURE 83 shows *LCDP* for the pitch trim configuration. The only positive cases for *LCDP* occur in the Mach 2 and Mach 3 cases at high angles of attack. All other cases result in a negative *LCDP* indicating handling characteristics that will depart from stable flight. From the Bihrle-Weissman chart discussed previously, *LCDP* and *Cnβdynamic* must be positive to even have the possibility of being within the A region.

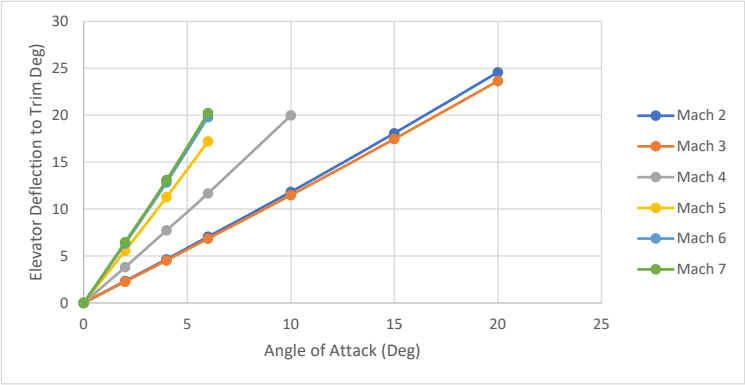

FIGURE 84: Elevator Deflection to Trim (HSSA V1)

The last area of the design to check quickly is the pitch trim performance of the elevons. From the *LCDP* plot, one can preemptively see that pitch trim performance is poor. FIGURE 84 shows the collective deflection required to achieve a desired angle of attack. From this figure one can see that the elevons were sized too small to begin with, as

they approach control saturation by around 10 degrees angle of attack on average or run out of control before then. Since differential tail control is required, this level of saturation would not allow any differential control power for roll at a trimmed collective case. With the vertical tail size not large enough for lateral directional stability, rudder sizing for sideslip is not a concern yet.

Configuration V2

The second version of the model includes a larger elevon and a much larger vertical tail and rudder combination. As mentioned previously the vertical tail design moved away from the canted configuration due to excessive pitching moments produced by the tail. The pitching moment issues of a larger canted twin vertical configuration, shown in FIGURE 85, will be briefly discussed.

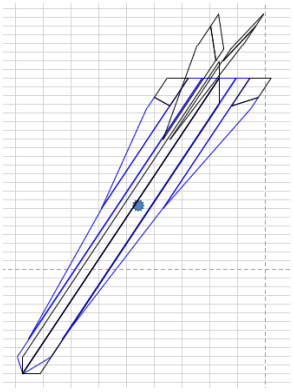

FIGURE 85: Canted Version of *HSSA-V2*

While making the vertical tail larger did help some issues, one area that was significantly impacted was the natural pitching moment of the vehicle. When comparing FIGURE 86 and FIGURE 84, even though V2 has larger elevons, the collective deflection to trim performance has barely increased, around 2 degrees of improvement.

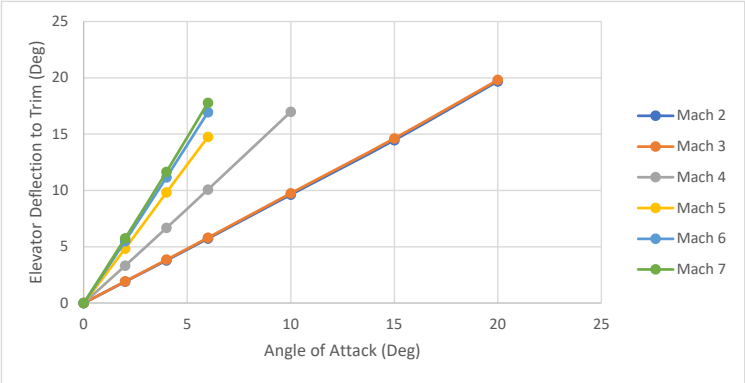

FIGURE 86: Elevator Deflection to Trim vs Angle of Attack (HSSA Canted V2)

For this analysis these two configurations share the same center of gravity location, to empathize the effect of large canted vertical tails on pitch. To get any pitch trim, the center of gravity would need to move much further back near the aerodynamic center. With these vehicle aerodynamic centers at half chord for high-speed flight, the shift back in center of gravity could be manageable. Once the aircraft exits supersonic flight however, it will experience unstable pitch due to the aerodynamic chord shifting back to the quarter chord.

With this issue noted, a more detailed analysis of a dual straight vertical tail for Version 2 was conducted, as shown back in FIGURE 78.

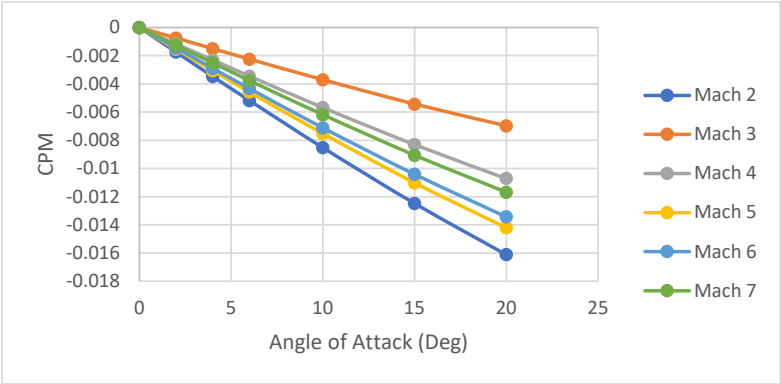

FIGURE 87: Pitching Moment vs Angle of Attack (HSSA V2)

Again, following the same procedure as before, static stability is observed again. The pitching moment curve slope is shown in FIGURE 87. When comparing V1 and V2, it is immediately obvious that there was a significant decrease in the pitching moments. This results in a much-needed decrease in pitch stability in exchange for more trim power. Overall, the pitching moment decreased by around a magnitude of 0.1. As the pitching moment slope and pitching moments are all negative, configuration V2 is statically stable in pitch.

To show the increase in trim power due to the increased elevon and reduced natural pitching moment, the elevator deflection can be plotted again. When examining FIGURE 88, it is shown that in all cases, except for Mach 6 and 7, the elevons are able to trim to the maximum angle of attack run (20 degrees). When operating at Mach 5, the collective deflection demonstrates an almost one to one degree deflection to degree of angle of attack change. This sizing for the elevons appears to be reasonable on first glance and should be sufficient for preliminary design. The lateral-directional issues must now be solved first before any more effort is spent perfecting the elevon sizing for pitch trim, maneuvering, and sideslip trim via differential control.

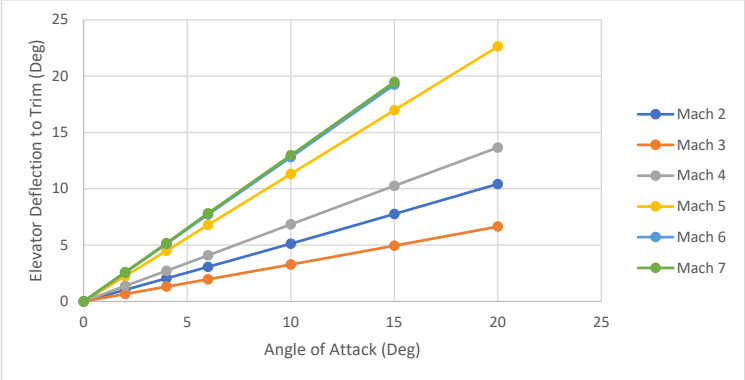

FIGURE 88: Elevator Deflection to Trim vs Angle of Attack (HSSA V2)

Overall, FIGURE 89 shows that there is very little difference in the rolling moment coefficients between the first iteration and the second iteration of the design. This is expected as little to no additional area that would contribute to the rolling moment was added to the aircraft. The increase in elevon size simply dug in to wing planform. Still the aircraft is statically stable in roll.

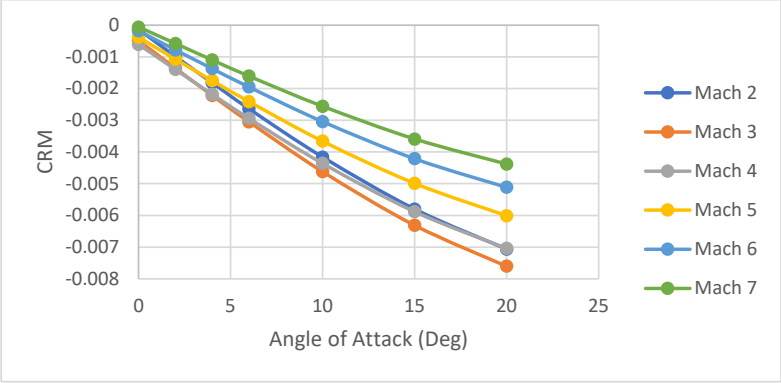

FIGURE 89: Rolling Moment vs Angle of Attack (HSSA V2)

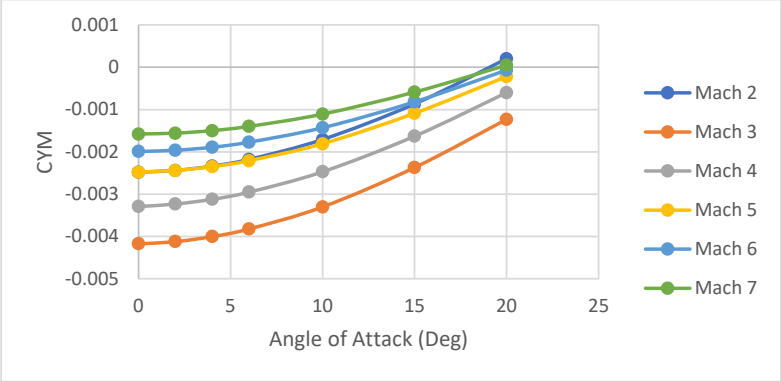

FIGURE 90: Yawing Moment vs Angle of Attack (HSSA V2)

Looking at the yawing moments shown in FIGURE 90, the positive slope trend is still present but again for most conditions, the yawing moment is negative. This indicates there is still a lack of stability in yaw still. When comparing Version 1 and Version 2, there was about a 0.001 improvement in the yawing moment. There was improvement however

at high angles of attack with slightly more coefficients switching sign to be positive. Still the *HSSA* appears to want more vertical tail area in order to have positive yawing moments.

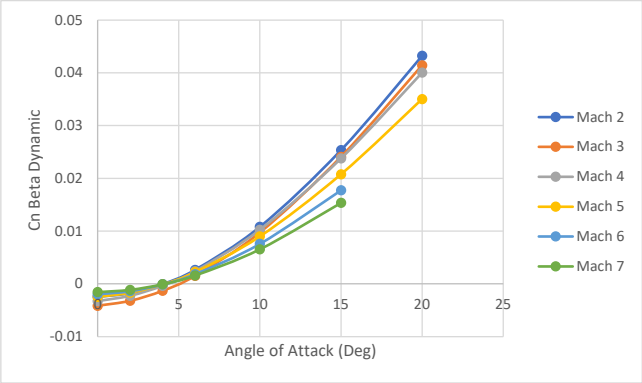

FIGURE 91: Cn Beta Dynamic vs Angle of Attack (HSSA V2)

With the strong negative signs on the yawing moments however, at low angles of attack there is still issues with *Cnβdynamic* being negative. When comparing FIGUREs 91 and 82, only slight improvements in *Cnβdynamic* (around a degree in angle of attack) were obtained, but not nearly enough to fix the issue. With *Cnβdynamic* being the root of the Dutch Roll Frequency, the aircraft will have an unstable Dutch Roll Mode leading to all kinds of issues. This must be suppressed by the closed loop system, and thus should be improved as much as possible to alleviate the stress on the control system.

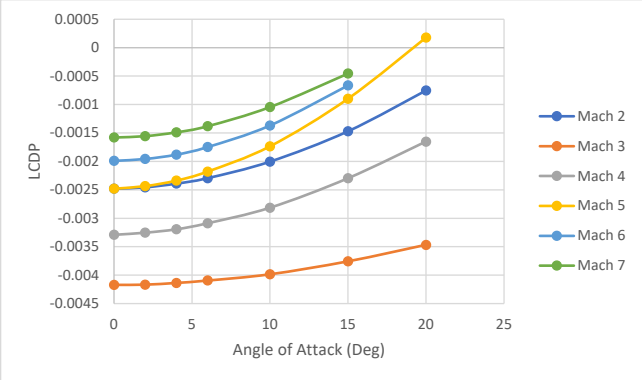

FIGURE 92: *LCDP* vs Angle of Attack (HSSA V2)

The biggest improvement from the increase in vertical tail area was *LCDP,* shown in FIGURE 92. Between Version 1 and Version 2, an additional 0.001 *LCDP* was achieved pushing the aircraft closer to lateral-directional controllability across the board. Interestingly, there was a decrease in *LCDP* performance for the Mach 2 case which was one of the best performers in Version 1.

Configuration V3

Due to the elevon sizing of Version 2 being adequate, it was decided to leave the elevon size the same and strictly increase the vertical tail to have a direct comparison point between Version 2 and Version 3. The goal for Version 3 was to roughly double the vertical tail area again, in an attempt to obtain full open loop, stick fixed stability or get the yawing moment as close to stable as possible to aid in the implementation of a closed loop feedback control system.

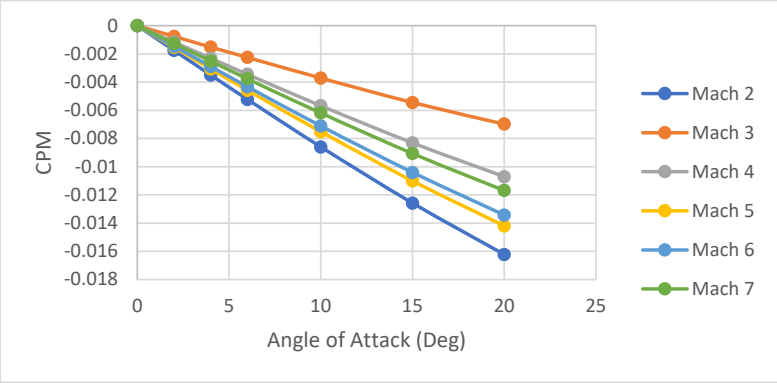

FIGURE 93: Pitching Moment vs Angle of Attack (HSSA V3)

The pitching moment curve slope is shown in FIGURE 93. When comparing V2 and V3, there is little to no change in the pitching moment. This is expected as there was little to no change in the geometry that would introduce more pitching moment area. Again,

as the pitching moment slope and pitching moments are all negative configuration V3 is statically stable in pitch.

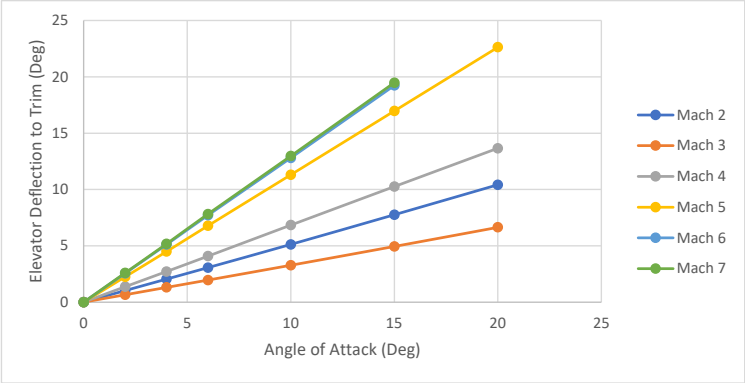

FIGURE 94: Elevator Deflection to Trim vs Angle of Attack (HSSA V3)

Additionally, when examining FIGURE 94, it is shown that there is no change in the elevator deflection to trim performance of the aircraft. Additional elevon area will be required to meet sideslip trim, especially at hypersonic Mach numbers. A collective deflection of 5 degrees is required to trim to 5 degrees angle of attack, the remaining 25 degrees of deflection may not be sufficient to achieve the desired 10 degrees of sideslip trim. This would be a further consideration if another iteration was considered.

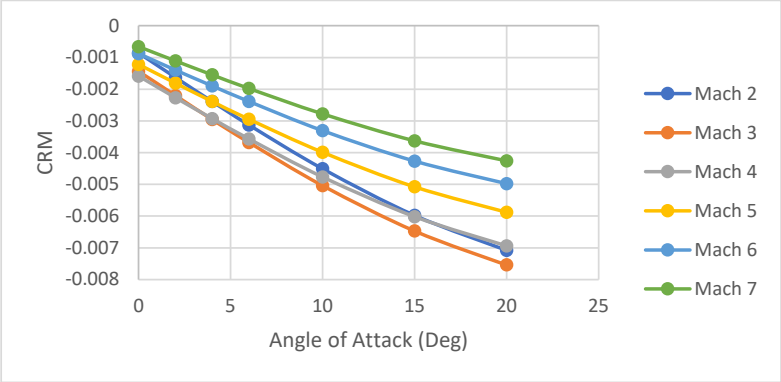

FIGURE 95: Rolling Moment vs Angle of Attack (HSSA V3)

FIGURE 95 shows once again that there is very little difference in the rolling moment coefficients between the second iteration and the third. Still the aircraft is statically stable in roll.

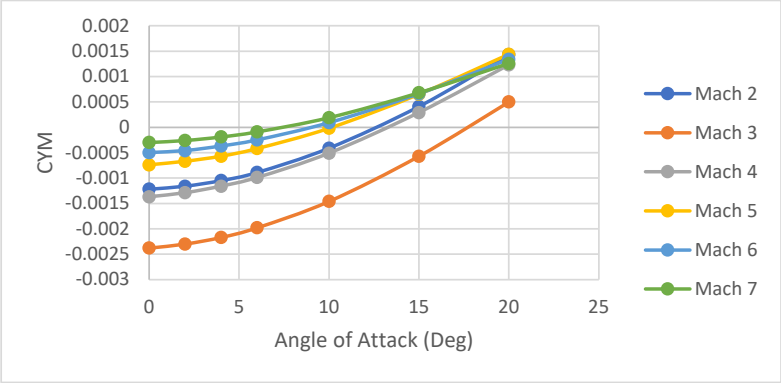

FIGURE 96: Yawing Moment vs Angle of Attack (HSSA V3)

Looking at the yawing moments shown in FIGURE 96, the positive slope trend is still present and now significantly more of the yawing moments are positive. Depending on the Mach number, positive yawing moments are achieved anywhere from 7 to 12 degrees angle of attack. When comparing Version 2 and Version 3, there was a significant 0.0015 improvement in the yawing moment. While at low angles of attack, the yawing moment is negative still thus, indicating that the aircraft does not have stick-fixed yaw stability. With the yawing moment decreasing in magnitude, it will be much more reasonable to apply a closed loop control system to fix and suppress any unstable motions at this point.

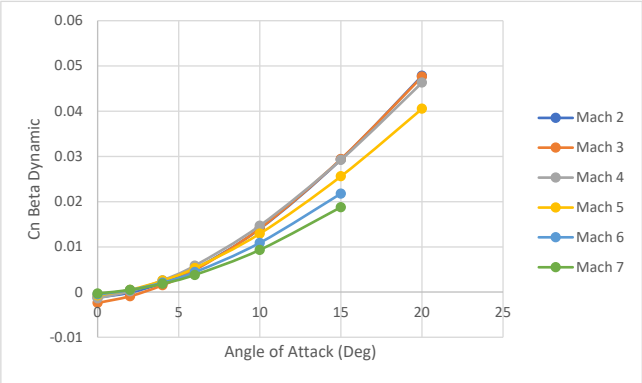

FIGURE 97: Cn Beta Dynamic vs Angle of Attack (HSSA V3)

With the presence of negative signs yawing moments at low angles of attack there are still issues with *Cnβdynamic* being negative at low angles of attack as well. When comparing FIGURES 97 and 91, there is now a clear shift to the left in *Cnβdynamic*. Now *Cnβdynamic* becomes positive at around 2.5 degrees angle of attack compared to the 5+ seen in previous versions. While the improvement in *Cnβdynamic* is good, the is still a lot more vertical surface required to satisfy the Skow criterion at low angles of attack for purely open loop control.

This leads to the conclusion that for these high-speed slender vehicles, there can never be enough vertical area on them. To have a successful maneuvering aircraft, the vehicle will likely require large amounts of vertical area in addition to a closed loop control system to aid in the weak *Cnβdynamic* values.

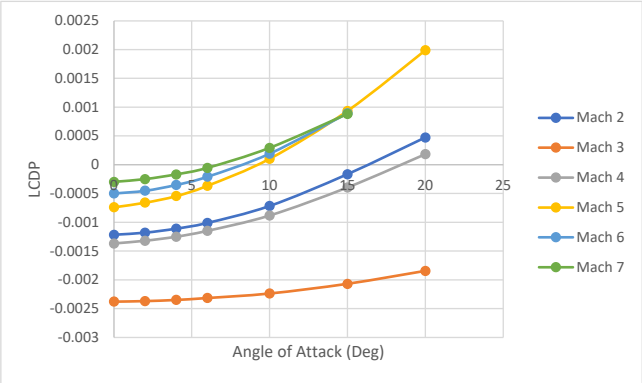

FIGURE 98: *LCDP* vs Angle of Attack (HSSA V3)

Significant increases in *LCDP,* shown in FIGURE 98, are observed again. Between Version 2 and Version 3, an additional 0.0015 *LCDP* was achieved pushing the aircraft closer to lateral-directional stability across the board. Now for hypersonic speeds, the *HSSA* experiences positive *LCDP* or departure resistant control qualities when flown at angles of attack greater than 8 degrees. For the lower Mach number, the performance was improved but *LCDP* is still unstable and will lead to the likely hood of the aircraft departing from stable flight.

Conclusion from *HSSA*

From the analysis of the *HSSA*, a few of the stability challenges of designing a high-speed slender aircraft were observed. The main issues that plague these types of aircraft are excessive pitching moments due to canted vertical, poor lateral directional stability, and hypersensitive and extreme flying conditions.

For these typically small vehicles, figuring out how to get vertical tail area is crucial and challenging. While detailed mass properties were not considered for this analysis, it is easy to see that by adding more vertical tail area more weight is going to be needed in the

nose for balance. On traditional aircraft, large vertical tails are easier to implement due to lower vertical centers of gravity from propulsion and cargo, on these slender vehicles traditionally powered by a scramjet or rocket stack the shift in vertical *CG* is much more pronounced. Additionally, when considering the geometry of the vertical tails, the extreme sweep (70 degrees +) severely limits the length and width. In order for the vertical to have a reasonable height, the base of the vertical tail becomes so long that it appears to take up the last 25% of the vehicle's fuselage. The addition of ventral vertical tails also does not assist in solving the problem as almost all lateral-directional stable is produced on the top side of the aircraft. The ventral tail also hurt the inherent rolling moment $dCl/d\beta$, by making it more positive effectively reducing the dihedral effect.

When considering the lateral-directional stability it should be noted that these vehicles will likely never have enough inherent stability to be open loop stable while sized for a practical mission. With the already sufficiently sized vertical tail on Version 3, the amount of additional area required to get the within the "A" Region of the Weissman chart just seems to be out of reach.

To ensure these vehicles can fly their intended missions, the design of a closed loop controller is almost a must. To design these controllers, however, one must consider how powerful and fast the actuators and control surfaces can be to constantly make adjustments otherwise they may contribute to departure as well due to poor bandwidth. When these controllers are put under tremendous stress, the thermal load produced can become another challenge to manage as the hypersonic vehicles already are dealing with high aerothermal heating.

DISCUSSION OF RESULTS

In this paper a variety of Stability & Control screening parameters were shown to help identify the basic handling qualities of an aircraft. The key parameters of interest are stick-fixed stability in Pitch, Yaw and Roll, the Short Period Frequency and Damping, Dutch Roll Frequency and Damping, *LCDP, Cnβdynamic*, the Roll mode, and the Spiral Mode. With these parameters, the general open loop performance of an aircraft can be gauged to determine where a closed loop system would be required as well as if the aircraft is prone to inertial coupling issues.

Key stability and control issues were examined through the various four aircraft which each explored potential solutions to their respective issues. With high-speed slender aircraft, the substantial decrease in lateral-directional performance becomes a crucial limiting factor in the open loop design of an aircraft. As shown especially for the HSSA and Bell X-2, the lack of sufficient vertical tail area and little separation from the center of gravity make *Cn β dynamic* difficult to satisfy as well as often having tender *LCDP* values.

The during the X-2's analysis, it was shown that an increase of around 70% vertical reference area was able to get the *Cn β dynamic* values under control and open up a deep pocket in the flight envelop where it should now have strong lateral-directional departure resistance. With such a large increase in the vertical tail area, the question of how much that extra area would cost needs to be asked. While the mass properties analysis is not able to be completed in this project, it is assumed that much extra tail area would heavily decrease the longitudinal performance of the aircraft due to the large increase of aft mass. In this analysis, the vertical tail size was increased to a level of strong open loop

performance, it is likely however that a middle ground between the original and enlarged tail accompanied by a closed loop system would be the ideal compromise.

The X-2 was a great example of how the screening parameter can be superimposed on one another to take a higher dimension look at stability. By combining a mix of the screening parameters one can effectively rule out large portions of a flight envelope where either improvement to the design need to be made or simple regions to avoid. In the X-2's case when combining both Skow and Inertial Coupling screening, the entire reasonable flight envelope was lost due to stability concerns. Every aircraft will have their differences and deficiencies but, by taking this approach, key screening parameters of concern can be coupled together.

These higher dimension plots could be created in a manner such that they are inspired as spiritual successor to the Weissman's plot, where instead altitude and speed are independent variables, but stability can now be split into regions defined by there deficiencies. An example of this could be Region A is characterized by strong longitudinal and lateral-directional stability, Region B has strong longitudinal but poor lateral-directional, Region C has strong lateral-directional but susceptible to inertial coupling with pitch, and Region D …, etc. This would allow the designer to not only see where the flight envelope is inaccessible but have some information about what is causing the deficiency in stability.

On Sky Cruiser, which resembles a mix between a fully slender vehicle and a conventional transport plane it was shown that again strong open loop stability was able to be obtained through a large vertical tail. In this case, due to the large rocket propellant tanks, the center of gravity placement worked with the extremely large and thus heavy tail.

A closed loop control system could have resulted in some shrinkage of the vertical tail to increase drag performance at cruise leading to ultimately a higher preforming aircraft.

Additionally, with Sky Cruiser the potential for a mixed control system of aileron for roll control at low speed and low altitudes with differential tail being used at higher Mach and higher altitudes to reduce the effect of adverse yaw was shown. The sideslip performance of the differential tail was decreased with high Mach Numbers resulting in larger gains. The cases with large gains would need to be avoid, as they would likely violate the Bandwidth Criterion leading to an ineffective closed loop system if implemented.

Lastly when examining the HSSA, the difficulty of finding enough vertical tail area on a small slender hypersonic vehicle was explored. In the first few iterations, it was shown that canted fins which appear in many cartoons appear to have significant pitching moment penalties associated with them. To get the vertical tail large enough to have reasonable $Cn_{\beta\ dynamic}$ values that can be augmented by a closed loop system, the pitch trim performance becomes so poor that the flight envelope that aircraft can trim to is significantly restricted. When switching to non-canted vertical tails, the excessive pitching moments were able to be avoided but still limitations in vertical tail area were encountered. For these vehicles it is suggested that the question to ask is how much vertical tail area can be fit on the aircraft and is the open loop performance at the point enough to be compensated by a closed loop without excessive gains or phase margins.

Ultimately, this thesis shows how open loop stability for a variety of geometrically differential highspeed slender vehicles can be approached as well as how it can be potentially scaled back when a closed loop control system is implemented for increased performance in other areas. All of these aircraft will require a closed loop control system

to ensure stability and control throughout their flight envelopes, but the goal of this paper is to get to them a point where they do not become dominated by their control laws. For an aircraft to have great closed loop performance it must also have sufficient open loop performance, as software cannot magically fix everything.

REFERENCES

[1] Abzug, M. J., & Larrabee, E. E. (2005). Airplane Stability and Control: A History of the Technologies that Made Aviation Possible. Cambridge: Cambridge University Press.

[2] Mason, W.H., Why Airplane look Like They Do," Class Notes from Virginia Tech 2009 see: https://archive.aoe.vt.edu/mason/Mason_f/SD1L3.pdf

[3] O'Brien, K.P. and Takahashi, T.T., "An Investigation of the Bell *X-2* and the Factors that Led to Its Fatal Accident," AIAA 2022-3203, 2022.

[4] Peterson, Forrest S, Rediess, Hermanm A. and Weil, Joseph, "Lateral-Directional Control Characteristics of the X-15 Airplane," NASA TM X-726, 1965.

[5] Yechout, T.R., Introduction to Aircraft Flight Mechanics, Second Edition, AIAA, 2014.

[6] Hoh, D. Hanke, Wilhelm, K. and Lange, H. H., "Bandwidth- A Criterion for Highly Augmented Airplanes," AGARD Conference Proceedings #333, 1982.

[7] Criteria for Handling Qualities of Military Aircraft, AGARD Conference Proceedings #333, August 26 1982, DTIX AD A1185969

[8] Department of Defense Interface Standard Flying Qualities of Piloted Aircraft, MIL STD-1997A, U.S. Department of Defense, Washington, D.C., August 24, 2004.

[9] Klyde, Davis H., Mcruer, Duane T. Myers, Thomas T., "Unified Pilot-Induced Oscillation Theory Volume 1: PIO Analysis with Linear and Nonlinear Effective Vehicle Characteristic, Including Rate Limiting," Flight Dynamics Directorate Wright Laboratory WL-TR-96-3028, December 1995.

[10] Iloputaife, Obi, "Minimizing Pilot-Induced-Oscillation Susceptibility During C-17 Development," AIAA 22nd Atmospheric Flight Mechanics Conference, 1997.
See: https://arc.aiaa.org/doi/abs/10.2514/6.1997-3497

[11] Bailey, Randall E., and Bidlack, Timothy J.,"Unified Pilot-Induced Oscillation Theory Volume IV: Time Domain Neal-Smith Criterion," Flight Dynamics Directorate Wright Laboratory WL-TR-96-3031, December 1995.

[12] Flying Qualities of Piloted Airplanes, MIL STD-8785C, U.S. Department of Defense, Washington, D.C., November 5,1980.

[13] Takahashi, T.T., Griffin, J.A. and Grandhi, R.V., "A Review of High-Speed Aircraft Stability & Control Challenges," submitted for publication at AIAA Aviation 2023.

[14] Skow, A.M. and Titiriga, A., "A Survey of Analytical and Experimental Techniques to Predict Aircraft Dynamic Characteristics at High Angles of Attack," AGARD *Cp*-235, 1978.

[15] Mason, W.H., "High Alpha and Handling Qualities Aerodynamics," Configuration Aerodynamics Class Notes from Virginia Tech 2018,
See: http://www.dept.aoe.vt.edu/~mason/Mason_f/HiAlphaBasicsPres.pdf

[16] Day, R.E. "Coupling Dynamics in Aircraft Design: A Historical Perspective," NASA SP-532, 1997.

[17] White, R J. , "Investigation of the Lateral Dynamic Stability in the XB-47 Airplane," Journal of the Aeronautical Science Vol. 17. Number 3, March 1950.

[18] Whitford, Ray, "Lessons Learned from the Bell *X-2* Program," SAE Transaction, Vol. 105. Section: Journal of Aerospace. Pp. 1407-1421, 1997,
See: https://www.jstor.org/stable/44650531

[19] "Chapter 17 A Couple of Bloopers!", JOURNEY IN AERONAUTICAL RESEARCH: A Career at NASA Langley Research Center, Monographs in Aerospace History, Number 12. history.nasa.gov,
See: https://history.nasa.gov/monograph12/ch17.htm

[20] Alexander, M.G., "Subsonic Wind Tunnel Testing Handbook," Wright Laboratory, WL_TR-91-3073, May 1991.

[21] Miranda, L.R., Baker, R.D., and Elliot, W.M., "A Generalized Vortex Lattice Method for Subsonic and Supersonic Flow," NASA CR 2875, 1977.

[22] Mason, W.H., "1976 Standard atmosphere Subroutine for BASIC" Department of Aerospace and Ocean Engineering, Virginia Tech, 1997

[23] Takahashi, T.T., Aircraft Performance & Sizing, Vol. II: Applied Aerodynamic Design, Momentum Press, New York, NY, 2016. 276 pages. ISBN-13: 978-1606509456

[24] Chambers, J.R. and Anglin, E.L., "Analysis of Lateral-Directional Stability Characteristics of a Twin-Jet Fighter Airplane at High Angles of Attack," NASA TN D-5361, 1969.

[25] Weissman, R., "Status of Design Criteria for Predicting Departure Characteristics and Spin Susceptibility," AIAA 74-791, 1974.

[26] Weissman. R., "Preliminary Criteria for Predicting Departure Characteristics' Spin Susceptibility of Fighter-Type Aircraft," AIAA Journal of Aircraft, Vol. 10, No. 4, April 1973.

[27] Hallion, Richard, “On the Frontier Flight Research at Dryden 1946-1981” NASA SP 4303, 1984

[28] Yvonne, Gibbs, “NASA Armstrong Fact Sheet: X-15 Hypersonic Research Program,” nasa.gov, October 2020.
See: https://www.nasa.gov/centers/armstrong/news/FactSheets/FS-052-DFRC.html

[29] Joshua, H. Heinz, O’Brien, K.P., Hatch, Tyler L and Takahashi, T.T., “Sky Cruiser – A Design Study in Space Tourism,” AIAA SciTech 2023, https://doi.org/10.2514/6.2023-1355

[30] Code of Federal Regulations, Title 14 Part 25, 2021.

[31] Conner, Monroe, “X-43A (Hyper-X),” nasa.gov, August 2017.
See: https://www.nasa.gov/centers/armstrong/history/experimental_aircraft/X-43A.html

[32] United States Air Force, “X-51A Waverider”,
See: https://www.af.mil/About-Us/Fact-Sheets/Display/Article/104467/x-51a-waverider/

[33] Souders, T.J. and Takahashi, T.T., “VORLAX 2020: Making a Potential Flow Solver Great Again,” AIAA 2021-2458, 2021.

[34] Souders, T.J. and Takahashi, T.T., “VORLAX 2020: Benchmarking Examples of a Modernized Potential Flow Solver,” AIAA 2021-2459, 2021

[35] Fournier, R.H. and Silvers, H.N. “Investigation of the Static Lateral Stability and Aileron Characteristics of a 0.067-Scale Model of the Bell *X-2* Airplane at Mach Numbers 0f 2.29,2.78,3.22 and 3.71,” NACA RM L57J28a, 1958.

[36] Griffin, J.A. and Takahashi, T.T., “Aero-Spaceplane Mission Performance Estimations Incorporating Atmospheric Control Limits,” AIAA 2022-3656, 2022.

[37] Griffin, A “Mission Code” Approach to Conceptual Design of Hypersonic Vehicles, Arizona State University, May 2022

[38] Teodorescu, B.C., "Lateral Directional Oscillatory Departure Criteria for High Angle-of-attack Flight Conditions," U.P.B. Sci. Bull., Series D, Vol. 68, No. 3, 2006.